Study of Single Phase Heat Transfer in Various Microchannels Geometries for Waste Heat Recovery Applications and Condensation of R-134a in Rectangular Microchannels at Low Mass Fluxes

By

Nouman Ali

Reg #: 00000118660

Session 2015-18

Supervised by

Dr. Majid Ali

A Thesis Submitted to the U.S. – Pakistan Center for Advanced Studies in Energy in partial fulfillment of the requirements for the degree of

MASTERS of Science in

THERMAL ENERGY ENGINEERING

U.S. – Pakistan Center for Advanced Studies in Energy (USPCAS-E)

National University of Sciences and Technology (NUST)

H-12, Islamabad 44000, Pakistan

27 March 2018

THESIS ACCEPTANCE CERTIFICATE

Certified that final copy of MS/MPhil thesis written by Mr. Nouman Ali, (Registration No. 00000118660), of U.S. – Pakistan Center for Advanced Studies in Energy (School/College/Institute) has been vetted by undersigned, found complete in all respects as per NUST Statues/Regulations, is free of plagiarism, errors, and mistakes and is accepted as partial fulfillment for award of MS/MPhil degree. It is further certified that necessary amendments as pointed out by GEC members of the scholar have also been incorporated in the said thesis.

Signature: _____

Name of Supervisor _____

Date: _____

Signature (HoD): _____

Date: _____

Signature (Dean/Principal): _____

Date: _____

Certificate

This is to certify that work in this thesis has been carried out by **Mr. Nouman Ali** and completed under my supervision in Thermal Energy Engineering Laboratory, USPCAS-E, National University of Sciences and Technology, H-12, Islamabad, Pakistan.

Supervisor: _____

Dr. Majid Ali
USPCAS-E
NUST, Islamabad

GEC member # 1: _____

Dr. Naseem Iqbal
USPCAS-E
NUST, Islamabad

GEC member # 2: _____

Dr. Adeel Waqas
USPCAS-E
NUST, Islamabad

GEC member # 3: _____

Dr. Muhammad Bilal Sajid
USPCAS-E
NUST, Islamabad

HoD-TEE _____

Dr. Adeel Javed
USPCAS-E
NUST, Islamabad

A/Principal/ Dean _____

Dr. Zuhair S. Khan
USPCAS-E
NUST, Islamabad

Dedication

I would like to dedicate this thesis to my Parents for their support and motivation

&

To my siblings for their love and care

Abstract

Utilization of waste heat from the thermal system has a considerable importance in increasing its performance due to rising trend in cost of fuel and consumption as well. Waste heat before vented into the atmosphere is captured from the exhaust of thermal system to increase the system capability by transfer to refrigerant circulating inside heat exchanger to increase the system performance. Microchannel technology provides new approach to remove larger heat flux in electronic and thermal system. Microchannels in comparison to macrochannels often higher performance due to higher surface area per unit volume ratio they provide. In heat and mass transfer applications, they provide higher heat transfer coefficient. The purpose of introducing microchannels in compact heat exchanger for the waste heat energy is to make system efficient, save cost inventory, less consumption of fuel and less harmful effect of refrigerant on environment in term of global warming potential and ozone depletion potential. The refrigerant is used inside the compact microchannel to recover the waste heat from thermal system. So, the selection and use of environment friendly refrigerants inside microchannels plays a vital role in transferring of thermal energy from refrigerant to surrounding medium. In this research work, different shapes of microchannels including circular, rectangular, square and triangular one is designed and modelled on Engineering Equation Solver program and comparison is done in between them on the basis of heat transfer as well as pressure drop during refrigerant flow at different conditions of temperatures and mass fluxes respectively. It has been found that circular channel among all other channels have higher thermal performance and effectiveness due to maximum contact area of fluids with the channel surface area. Whereas rectangular channel gives better performance followed by the circular channel and triangular channel having least value of heat transfer due to less contact area with surface and larger pressure drop because of lowest channel hydraulic diameter. The better thermal performance is achieved by dividing the total volume of system into smaller channels to increases the surface area for higher heat transfer and system should work under lower Reynold number to limit the pressure drop occurred in the system.

Keywords: *Microchannels, Heat Transfer, Pressure Drop, Engineering Equation Solver*

Contents

List of Figures

List of Tables

List of Nomenclature

Variables	Symbols	Units
Cross Sectional Area	A	mm^2
Specific Heat	C_p	$J\ kg^{-1}\ K^{-1}$
Diameter	D	mm
Mass Flux	G	$kg\ m^{-2}\ s^{-1}$
Heat Transfer Coefficient	h	$W\ m^{-2}\ K^{-1}$
Specific Enthalpy	h	$J\ kg^{-1}$
Fluid Velocity	J	$m\ s^{-1}$
Thermal Conductivity	k	$W\ m^{-1}\ K^{-1}$
Length	L	mm
Width	W	mm
Height	H	mm
Mass Flow Rate	$\dot{m}$	$kg\ s^{-1}$
Number of Channels	N	-
Heat Transfer Rate	$\dot{Q}$	W
Temperature	T	K
Overall Heat Transfer Coefficient	UA	$W\ K^{-1}$
Volumetric Flow Rate	$\dot{V}$	$m^3\ s^{-1}$
Quality	x	-
Log Mean Temperature Difference	ΔT_{LM}	K
Effectiveness	E	-

Greek	Symbols	Units
Aspect Ratio	α	-
Thickness	δ	mm
Viscosity	μ	$m^2\ s^{-1}$
Density	ρ	$kg\ m^{-3}$
Surface Tension	σ	$N\ m^{-1}$
Efficiency	η	%

Subscripts	Symbols
Average	Avg
Dimensionless	*
Heat Transfer	h
Length	l
Maximum	max
Saturation	sat
Vapor	v
Water	w
Working Fluid	f

Dimensionless Numbers

Reynold Number	Re
Prandtl Number	Pr
Nusselt Number	Nu
Froude Number	Fr
Martinelli Parameter	X
Superficial Gas Velocity	j_g
Pressure Drop	ΔP

List of Publications

Refereed Journal Publications

- Michael A. Vanderputten, Tabeel A. Jacob, **Nouman Ali**, Maria Sattar, Brian M. Fronk, (2017), "Two-Phase Flow Regimes of Condensing R-134a at Low Mass Flux in Rectangular Microchannels, "International Journal of Refrigeration, DOI: http://dx.doi.org/doi: 10.1016/j.ijrefrig.2017.08.021.

Refereed Conference Publications

- **Nouman Ali**, Hassan Nazir, Majid Ali, "Designing of Compact Rectangular Microchannel Heat Exchanger based on Thermal Resistance Network for Waste Heat Recovery Systems," 2017 International Conference on Energy Conservation and Efficiency (ICECE), UET Lahore, 22-23 November, Ref: 978-1-5386-3605-3/17©2017 IEEE.
- **Nouman Ali**, Majid Ali, Hassan Nazir, Muhammad Amin Durrani, Saba Aziz, Mohsin Tanveer, AbdulRab Asary, "Designing of Microchannel Heat Exchanger for Waste Heat Recovery Systems," 2nd International Conference on the Impact of Nanoscience on Energy Technologies, COMSAT Lahore, 25-27 October, 2017.
- Muhammad Mohsin Tanveer, **Nouman Ali**, Abdul Samad Farooq, "Heat transfer in microchannels using super critical CO_2 for solar tower applications," 2nd International Conference on the Impact of Nanoscience on Energy Technologies, COMSAT Lahore, 25-27 October, 2017

Chapter 1: Introduction

1.1 Background

Demand of energy and its utilization overall the world grows continuously as a result of depletion of fossil fuels like oil and gas, increased population, expansion of global economy and the increases demand of industrial products as well. More than ninety percent of the world thermal energy utilization by different sources are moving through system of thermal transformation. As two third of the energy is consumed and removed from energy systems in the form of low grade thermal waste. Researchers and engineers continuously searching for efficient technologies that can fulfil the demand of energy supplies, fuel consumption and reduces the environmental impact on society [1].

Historical and future predictions of world energy consumption is shown in Figure 1.1 [2]. Waste heat recovery system is the only option available that marked a significant improvements in the eradication of energy crises. The utilization of thermal energy resources plays an important role in power plant for production of power as well as for provision of heating or and cooling phenomenon. I.C (internal combustion) engines are the most important energy element in industrial sector that having thermal efficiency in between 20-40% [2]. Whereas, remaining approximately 60% thermal energy of fuel is lost into the atmosphere as a waste energy due to inefficient energy conversion and thermal losses.

Before emitting waste heat energy into atmosphere, it can be captured and utilized by designing of highly compact thermal systems to recover the maximum availability of waste thermal energy for efficient working of systems. In United States, both transportation and industrial sectors contributed 60% to energy consumption [2]. Even in both sector, the driving force is the internal combustion diesel engine. Which makes effective improvements in small changes of engine performance parameters. But also reduces its harmful impact into surroundings in the form of global warming and ozone depletion potential that is important regarding survival of human and animal lives on earth.

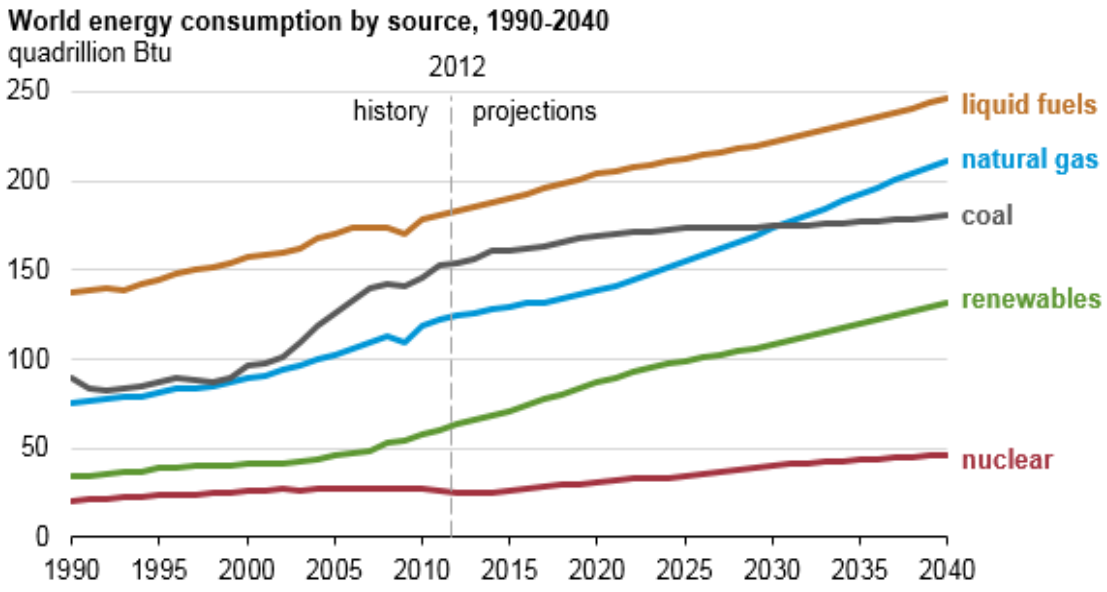

Figure 1.1: Historical and future predictions of world energy consumption [2]

The exhaust waste thermal energy from diesel engine is considered as a low grade waste energy to recover maximum thermal energy through the use of microchannels heat exchanger as shown in Figure 1.2. Recently the generation of energy along with its utilization has directly lead to significant medium or high grade waste energy. The exhaust heat from diesel engine usually have a temperature range in between 250-500°C. This has a greater potential for conversion of exhaust waste heat energy into power, heating and cooling. Waste heat energy systems are being used to recover waste heat through different types of microchannels heat exchanger like recuperator, fin tube type and plate fin type heat exchangers etc. as discussed below.

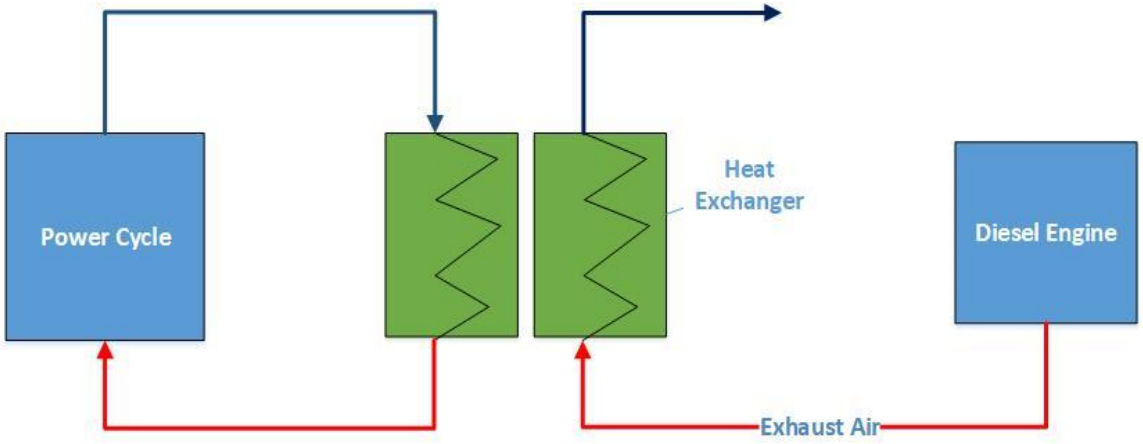

Figure 1.2: Waste heat recovery system

1.2 Heat Exchanger Classification

Heat exchangers are such devices that exchanges thermal energy at the cost of thermal contact area and driving temperature differences between two or more mediums that mediums may be the two fluids, or fluid and solid surface or two solid surfaces only. Typically they are used for application of evaporation or condensation in single phase or multiphase phenomenon. Heat exchangers are actually classified on the basis of heat transfer phenomenon, number of fluids, fluids flow arrangement and construction type as shown in Figure 1.3. However, further classification can be described on the basis compactness which is ratio of surface area to volume and non-compactness [3].

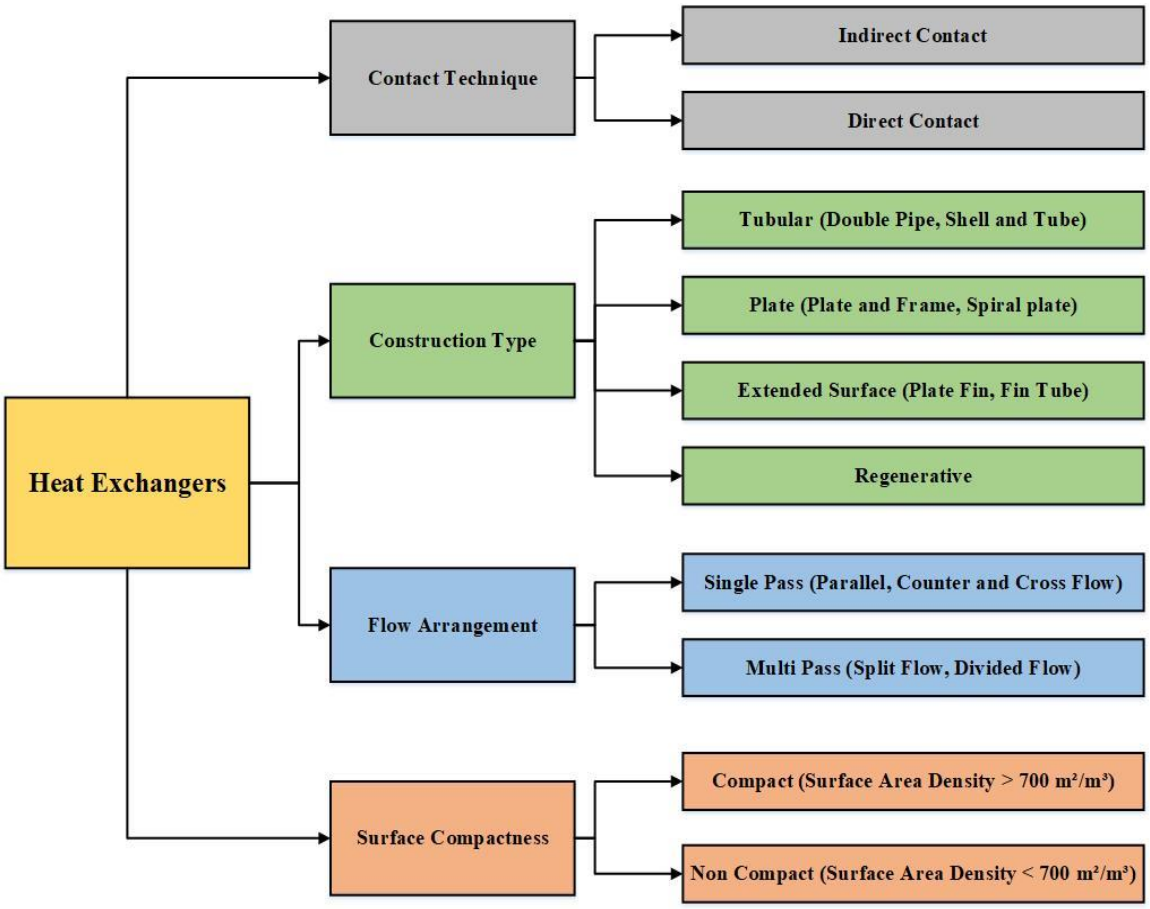

Figure 1.3: Classification of heat exchangers

According to arrangement of fluid flow like in parallel flow, fluids flow in similar direction in comparison to counter flow direction. Where both fluids exchanges heat energy and travels in opposite direction to each other. Remaining left behind is cross flow heat exchanger in which direction of fluids flow is normal to each other as shown in Figure 1.4. Such types of flow has more effectiveness regarding heat and mass transfer and its effectivity falls in between parallel and counter flow arrangement. A stream of fluid is called unmixed when it separately moves inside each channel without intermixing of fluid with each other. Which describes plate fin type unmixed-unmixed cross flow heat exchanger [4]. The exist temperature of fluid due to exchanges of heat energy in plate fin type unmixed-unmixed cross flow heat exchanger does not remain same as inlet temperature. Variation of temperature profile in crossflow heat exchanger can be visualized in Figure 1.5 [5].

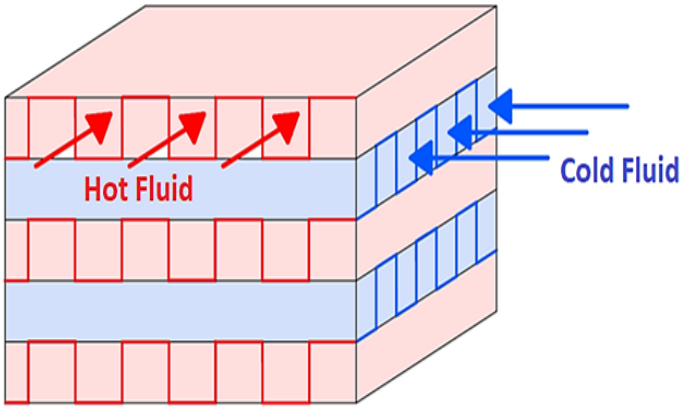

Figure 1.4: Representation of cross flow plate fin microchannel heat exchanger [5]

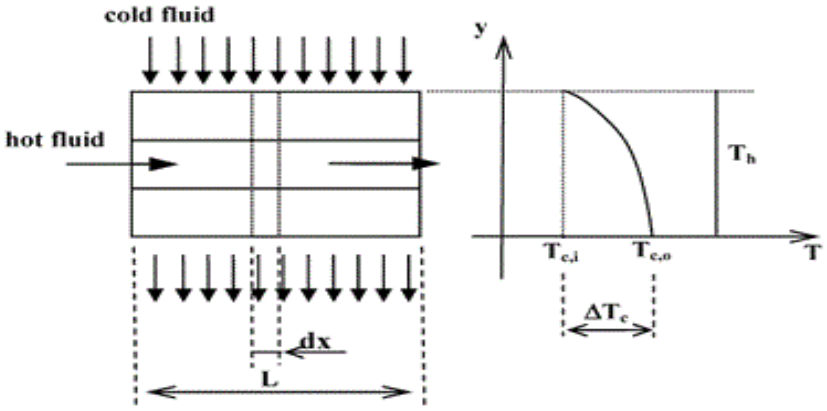

Figure 1.5: Variation of temperature profile in crossflow heat exchanger [5]

1.3 Microchannels

Before the usage of microchannels heat exchangers, conventional macrochannels heat exchangers are considered for power production and heating processes in power plants. Because of larger pressure drop and lower heat transfer inside larger channels, they are replaced by channels having hydraulic diameter lesser than millimeter usually in micrometers. Which are called as minichannels and microchannels. So with the passage of time, these conventional channels are replaced by the microchannels and minichannels for high efficient thermal systems, microchannels are abundantly used in various applications of power industries for higher heat and mass transfer and lesser pressure drop [6]. As the effect of channel hydraulic diameter also depends on effective heat and mass transfer phenomenon. Single phase convection through microchannels offers larger heat transfer coefficients as well as heat transfer area due to smaller diameter of microchannel. Transfer of higher heat in microchannels is also due to the compactness of device in term of higher area to volume ratio.

Microchannels are manufactured in wide variety of shapes like rectangular, circular, triangular and square under the consideration of various thermal system design configuration. Microchannels geometry, heat transfer as well as pressure drop are those factors that effects on flow behavior of fluid during evaporation and condensation inside channels. As the model predicted for calculating heat transfer coefficient for macrochannels not consider the effect of viscous surface tensional forces occurring in larger tubes as compare to smaller channels. Ultimately the possibility of maximum heat transfer through small internal channel flow is due to usage of curved channels instead of straight channels. As in curved channels, fluid flow interact with each other and with the wall of channel and causes of turbulence inside channels that forms vortices to transfer the higher heat between two or more mediums [7].

Sui et al. conducted research on fluid flow and its heat transfer behavior inside curved rectangular geometry of microchannels and concluded that curved rectangular shape microchannels offer greater heat transfer and lower value of pressure drop in comparison to straight microchannels as shown in Figure 1.6 [8]. Although microchannels has various applications as shown in Figure 1.7.

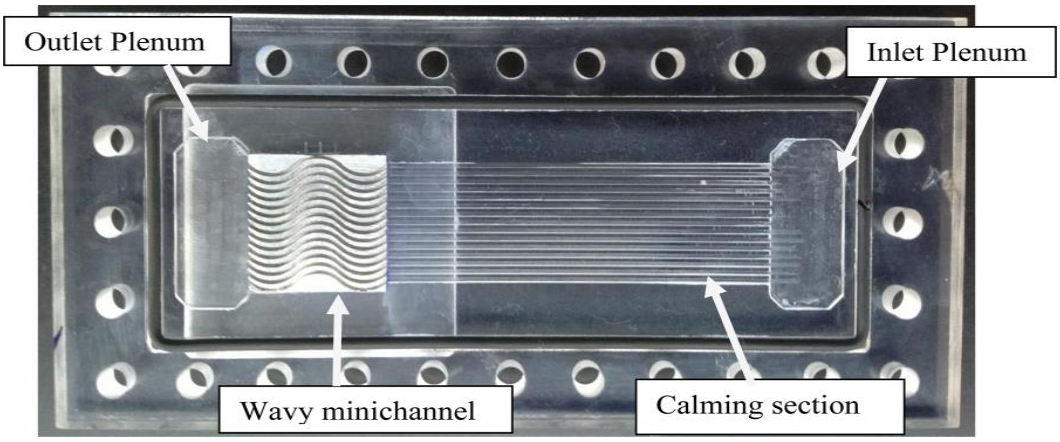

Figure 1.6: Representation of wavy and straight microchannel geometry [8]

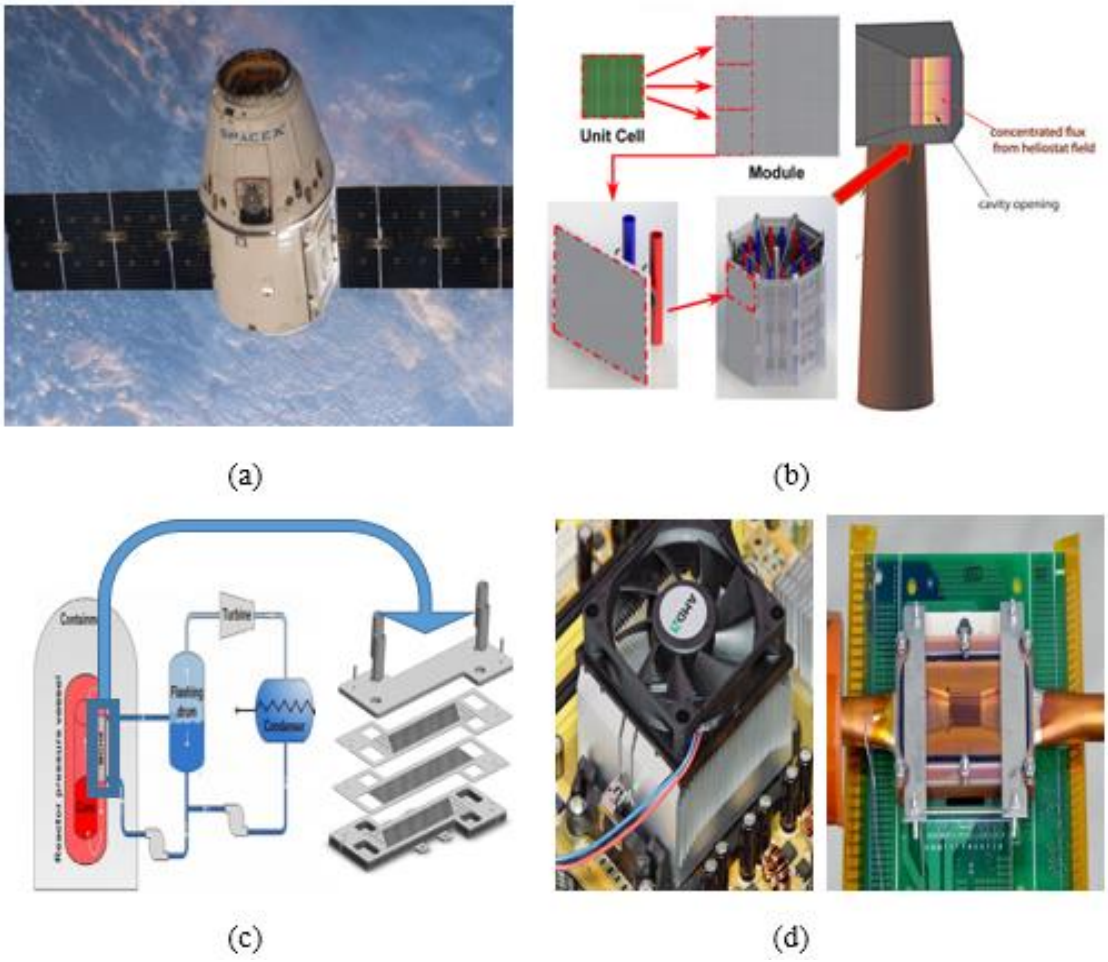

Figure 1.7: Applications of microchannels in various fields like (a) Space satellite; (b) Solar receivers; (c) Nuclear steam generators; (d) Computer systems [5]

1.4 Heat Transfer Fluids

As air-water were the initial natural refrigerants used in heat ventilation and air conditioning systems. Most of research conducted on air-water refrigerant inside mini and microchannel heat exchanger at higher mass fluxes under the adiabatic condition to visualize the various fluid flow regimes. Such mass fluxes might be applicable for cooling of high heat flux from electronics components. But they are not realistic for microchannels heat exchanger that's having higher heat duties. So, these are characterized with different refrigerants and multiple microchannels with lower hydraulic diameter and lower mass fluxes to analyze heat transfer along with pressure drop in channel geometry. R-134a replaces the HCFC, ammonia and other gases because of high impact of ozone depletion potential and higher global warming potential [9]. While R-134a has been selected for its zero ozone depletion potential. But the only issue associated with R-134a is of having modest global warming potential that is 1200.

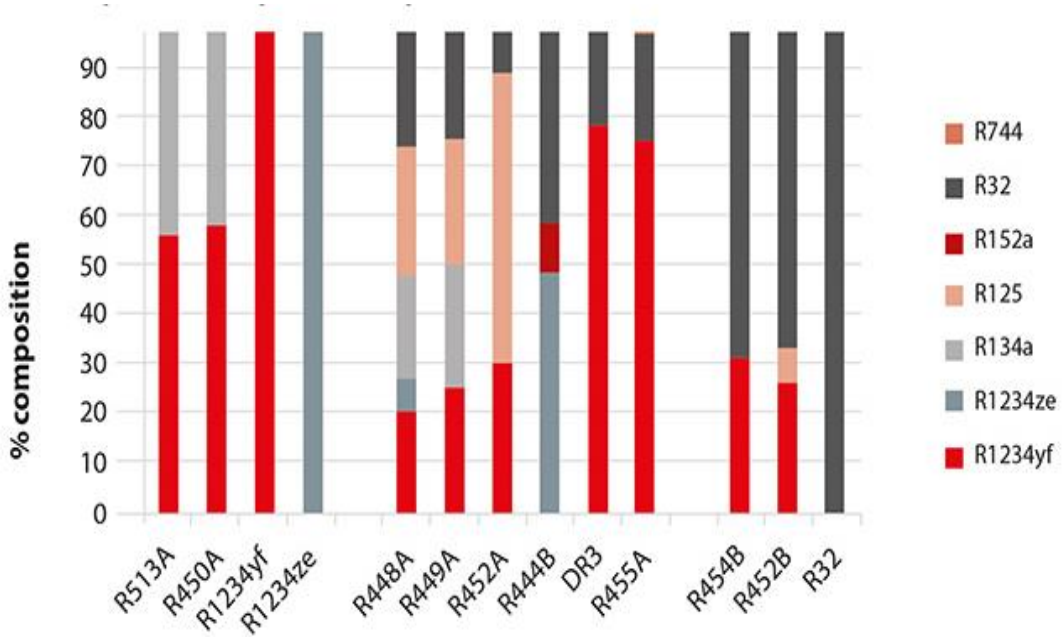

Figure 1.8: Composition of different refrigerants and their global warming effect [9]

1.5 Problem Statement

The problem is to recover the maximum availability of thermal energy from diesel engine exhaust before vented into atmosphere by using of microchannels with various shapes including rectangular, square, circular and triangular one to improve the system performance and thermal efficiency.

1.6 Goals and Objectives of Research

Major objectives of this research are as follows.

- Designing of different shapes of microchannel heat exchangers that can utilize low grade waste thermal energy.
- Mathematical modelling of heat transfer and pressure drop equations on Engineering Equation Solver program.
- Comparison of different shapes of microchannels geometries to find the best one regarding effectiveness and heat transfer.
- Determination of thermal losses by using Thermal Resistance Network.
- Validation of EES numerical results with Murat Cetin's experimental model.

1.7 Organization of Thesis

The organization of remainder thesis is as follow

Chapter 1 discuss the introduction about energy utilization, microchannels heat exchanger and their applications and heat transfer fluid along with research objectives.

Chapter 2 presents the overview of microchannels, refrigerant generations and their applications from the pioneering work to recent work, demonstrating the need for further research.

Chapter 3 discuss the methodology and mathematical modelling of heat transfer and pressure drop for determining the thermal performance and effectiveness of heat exchanger by using of Engineering Equation Solver program.

Chapter 4 presents the comparison of EES theoretical results with the experimental results of Murat model for validation and also discuss about designing of microchannel heat exchanger with various shapes of channel geometries to utilize the waste heat energy from diesel engine to improve the system's thermal performance and efficiency.

Chapter 5 discuss conclusions drawn from current dissertation along with future recommendation.

Chapter 6 presents the experimental visualization of two phase flow of condensing R-134a inside rectangular microchannels at lower mass fluxes and different saturated temperatures and the comparison with the flow map of authors.

Summary

Chapter 1 is an introductory part that introduced about recovery of waste heat by using different types of microchannel heat exchanger with an emphasis to control over the emissions generated from different sources like power plant chimneys, heat exchanger units and diesel engines. The main purpose is to utilize the environment friendly refrigerant R-134a to recover maximum availability of thermal energy into useful energy and to mitigate the negative effects of carbon-dioxide and sulphur-dioxide on the environment. Which are generated as a result of combustion processes. For which different shaped of cross flow microchannel heat exchanger are discussed and introduced to meet energy demand of country and to enhance the thermal efficiency as well as performance of the thermal systems..

References

[1] J. W. Sun, "Changes in energy consumption and energy intensity: A complete decomposition model," Journal Energy Economics, vol. 20, pp. 85–100, 1998.

[2] Seema Narayan, "An investigation of renewable and non-renewable energy consumption and economic growth nexus using industrial and residential energy consumption," Journal of Energy Economics, vol. 68, september 2017.

[3] R. K. Shah and D. P. Sekulic, "Fundamentals of heat exchanger design," Journel of Engineering, John Wiley, vol. 3, no. 9, 03 september 2011.

[4] S. K. and H. Liu, "Heat Exchangers Selection, Rating and Thermal Design, 2 nd Edition." CRC Press LLC, Boca Raton, pp. 373–396, 2002.

[5] S. G. Kandlikar, "Heat transfer and fluid flow in minichannels and microchannels." Journel of Science, Elsevier, 1st Edition, 2006.

[6] R. P. Feynman, "There's plenty of room at the bottom, miniaturization," vol. H.D. Gilbe, 1961.

[7] A. Agarwal, "Heat transfer and pressure drop during condensation of refrigerants in microchannels," Mechanical Engineering, Georgia Institute of Technology, 2006.

[8] Y.Sui, "An experimental study of flow friction and heat transfer in wavy microchannels with rectangular cross section," International Journal of Thermal Sciences, vol. 50, pp. 2473-2482 · December 2011.

[9] J. M.Calm, "The next generation of refrigerants – Historical review, considerations, and outlook," International Journal of Refrigeration, vol. 31, pp. 1123–1133, 2008.

Chapter 2: Literature Review

This research work gives literature review of microchannels geometry, single phase convection heat transfer mechanism and waste heat recovery source utilization. The hydrodynamic as well as thermal behavior of single phase convection of different refrigerants through various channels of geometry is well described in this literature study.

2.1 Earlier Studies on Microchannels (Pre-2005)

The concept of minichannels and microchannels comes from working of Tuckerman and Pease, who first time used the idea of miniaturization for the application of higher heat removal from the thermal devices. Their pioneering work on higher performance heat sinking for very large integrated system (VLSI) by using microchannels that has attracted and motivated many researchers to study on microchannel flow [1][2]. Currently, numerical modelling as well as experimental understanding of microchannels along with heat transfer of fluid flow inside channels growing rapidly. Before moving towards study of fluid flow and heat transfer inside micro and minichannels geometries, it is well to introduce the term "microchannel". On the basis of internal flow of liquids inside the channels, Kandlikar and Grande [3] explained the characteristics of channel geometry for different hydraulic diameter like

Table 2.1: Classification of microchannels Kandlikar and Grande

Classification	Hydraulic Diameter
Conventional channels	$D_h > 3mm$
Minichannels range	$3\ mm \geq D_h > 200\ \mu m$
Microchannels range	$200\ \mu m \geq D_h > 10\ \mu m$
Transition channel size	$10\ \mu m \geq D_h > 0.1\ \mu m$

Mehendale et al. [4] also classified the microchannels size on the basis of hydraulic diameter like

Table 2.2: Classification of microchannels according to Mehendale

Classification	Hydraulic Diameter
Conventional channels	$D_h > 6$ mm
Minichannels range	1 mm $\geq D_h >$ 100 µm
Microchannels range	100 µm $\geq D_h >$ 1 µm
Compact passages	6 mm $\geq D_h >$ 1 mm

Obot also classified size of microchannels on the basis of hydraulic diameter (D_h < 1 mm). Which was considered and studied by various authors like Bayraktar and Bahrami in their filed. This classification is consider as an suitable term in the modelling of microchannels heat exchanger in this paper as compare to the proposed classification of Kandlikar and Grande who studied for gases flow inside the channels [5].

Many researchers have studied single phase flow and evaporation of fluid in channels for rejecting higher heat flux from micro devices for cooling application purposes. So the single phase flow in different microchannels geometry are being used in research phase.

Wang and Peng et al. did experiments on different microchannels configuration with water and methanol fluid mixture by considering hydraulic diameter in between (311 mm > D_h > 747 mm) for 4 to 6 channels of stainless steel and determine the fully turbulent regime at Reynolds number of 1000-1500 [6].

S.V.Garimella conducted various experiments and proposed heat transfer as well as pressure drop correlations inside channel geometry. They analyzed these hydraulic diameters 444 µm, 476 µm and 500 µm of rectangular microchannels numerically on computer code. While they also investigated the heat transfer along with pressure drop at flow rates 0.08 to 0.46 kg s^{-1}. In results, they found that geometrical parameters have greater influenced on both heat transfer as well as pressure drop characteristics during flow of refrigerants inside microchannels [7].

Harms et al. worked on various experiments of microchannel systems to understand the thermal performance of refrigerant inside rectangular shaped microchannels geometry at hydraulic channel diameter (D_h = 1.923 mm) in a 25 mm × 25 mm silicon based substrate and tested two configuration of microchannels. First microchannel configuration with dimensions of 25 mm × 1 mm and the second one with 68 microchannels and dimensions 0.251 mm × 1.030 mm were used for Reynolds number range from 173-12900.

Their results described that thermal resistances was 45% lower for multiple configuration of microchannels in comparison to the singular configuration of microchannel. Whereas Nusselt number for multiple configuration of microchannel were lower than singular configuration of microchannel. At lower value of Reynold number, the agreement was not good between experimental results and local Nusselt number but at higher value of Reynolds number, there were better agreement seen in between the local Nusselt number and the experimental results by using various correlations proposed by different authors and researchers [8].

Qu and Mudawar et al. also conducted research on single phase flow of different fluids inside 21 rectangular channels of dimensions 0.231 mm × 0.731 mm with diameter (D_h = 0.351 mm) in copper based substrate to understand the heat transfer behavior and contributed towards numerical and experimental investigation. It was noted that experimental model results were in better agreement with numerical results but their conventional heat transfer with pressure drop correlations deteriorate with experimental conclusions [9].

Jiang et al. numerical visualized the effect of microchannel dimensions with heat transfer parameter to compare it with the microchannel and porous media. He concluded that the heat transfer in microchannel with porous structure is much more in comparison to the simple channels of micro heat exchanger. However the pressure drop is lower in microchannel heat exchanger with porous media [10].

2.2 Later Studies on Microchannels (Post-2005)

Shen et al. did experiments on flow of fluid in microchannels to observe the effect of heat and mass transfer with pressure drop by using various dimensions of channels. He

used 26 rectangular shaped microchannels of copper material with dimensions of 0.3 mm × 0.8 mm, 50 mm long length and hydraulic diameter of (D_h = 0.43 mm) of channel. He conducted for Reynold number from 152 to 1257 and determined that the results of heat transfer deviate and attributed towards area and surface roughness. He saw the surface roughness effect that does not effect on heat and mass transfer in the range of laminar flow. Heat transfer increases if surface roughness is effect on the heat and mass transfer that results in laminar range [11].

Wei at el. conducted so many experiments on Organic Rankine Cycle by recovering of exhaust waste heat for power plant applications. He recovered 90 kW heat energy by recovering exhaust gases at temperature of 370°C with flow rate of 4.5-6 kg s^{-1} to run evaporator heat exchanger. He concluded that the thermal system's efficiency which is increased by using the availability of maximum heat energy of exhaust gases. He concluded that thermal performance and efficiency of evaporator is increased by increasing of temperature and mass flow rates of exhaust gases [12].

Saqr et al. studied the thermoelectric heat recovery system and recovered not more than 5% of exhaust waste heat energy to generate electricity. As thermoelectric generators are typically used for small heat recovery systems. Yang et al. also studied the heat recovery process from exhaust waste heat energy systems and reached to a state that thermoelectric generating system recovering the exhaust gases heat energy not more than 4% of the potential [13]. Yang at el. conducted experiments on utilization of waste heat recovery for pipe heat exchanger. He recovered 6.5 kW of heat energy from exhaust gases at a temperature of 300ºC and determined the pressure drop of 25 Pa and 0.46 value of effectiveness of heat exchanger because of lower temperature coolant fluid [14].

Mathew and Hegab together theoretically worked on calculating the thermal performance and its behavior inside microchannel heat exchanger in parallel flow direction under provision of constant heat. They developed equations that determined the heat transfer behavior between different fluids and also predicted effectiveness and axial temperature of the working fluid inside microchannel heat exchanger by considering laminar flow constraint. Their model actually only valid for parallel flow heat exchanger but not for counter flow or cross flow heat exchanger. Their model also be used when each fluids at axial location have unequal or equal amount of constant flux [15]. They

also stated that effectiveness depends on heat capacity ratio. Effectiveness will be higher when hot stream has lower capacity of thermal energy. The decrease in heat capacity ratio at given number of heat transfer units (NTU) increases the effectiveness of fluid inside microchannels [16].

Tsuzuki et al. researched on microchannel heat exchanger with the use of S-shaped fins to decrease the formation of pressure drop due to turbulence of fluid inside channel geometry. Tsuzuki et al. did numerical work on ANSYS FLUENT to develop a correlation of Nusselt number and also proposed correlation of heat transfer determination for the copper based microchannel heat exchanger. Whose dimensions are $1240\times68\times4.75$ mm³ and two fluids used inside channel geometry, one fluid is cold water and other one is hot CO_2. Their results were in error of only 3% in comparison to the numerical results. Only 5% difference were in between experimental and correlations [17]. As the Reynold number on the water side was less and higher on CO_2 side due to formation of vortices that creates turbulence and causes of higher pressure drop in channel. Tsuzuki et al. also concluded from his research that the S-shaped fin configuration has higher value of pressure drop about one-seventh of zigzag configuration but the heat transfer results in both configuration were approximately same [18].

In previous years, Mushtaq et al. did conductive numerical research on different sizes of channels in a counter flow direction. Results shows that decreases the channels size leads to increases the pressure drop as well as effectiveness of microchannel heat exchanger. As new correlations such as Reynold number and Nusselt number are going to developed under considerable research for prediction of effectiveness of different shapes of microchannel heat exchanger regarding different flow arrangements [19][20].

Mavridou et al. studied and analyzed single phase cross flow plate and fin tube heat exchanger with single pass arrangement by using channel geometry of triangular shape. They also find out the different plate fin configuration arrangement along with the use of open cell metal foam with two pore sizes including 10 ppi (parts per inch) and 40 ppi. They concluded from their results that for the similar heat output values, 40 ppi metal foam and the design of plate fin heat exchanger had lower volume and lighter weight in comparison to shell and tube heat exchanger and all other simple plate fin

configuration. But the challenged associated with the metal foam is the increases of pressure drop as compare to plate fin configuration without metal foam usage [21].

Kang and Tseng et al. contributed their research work in microchannels area by designing cross flow rectangular based microchannel heat exchanger. Assumptions for fluids taken are incompressible, uniform steady and laminar flow. However the dimensions regarding width and height of channel geometry are 200 μm and 32 μm [22]. They determined the effect of effectiveness, heat transfer as well as pressure drop inside the rectangular shaped channel to compare their theoretical solutions with the experimental one and as a result they reach to a point that both the heat transfer rate as well as pressure drop at the same value of effectiveness much affected by average mean temperature of both hot and cold fluid. In result, effect of heat transfer and pressure drop inside channels at different values of effectiveness were significant. They also changed the geometry dimensions as well as material of channels from silicon to the copper to see the effect on thermal behavior between the cold and hot fluids. They varied various parameters such as inlet temperatures, flow rates and pressure difference and measured temperature difference of 10ºC at same value of effectiveness 0.33. They got heat transfer rate greater than 2700 for various mean temperature values. They concluded that a small rise in average mean temperature of working fluid may causes of increases in thermal performance and decrease in pressure difference. By experimentation results, it also described that small value of effectiveness can give greater heat transfer rate. They also changed the geometrical parametric dimensions of their heat exchanger to see the positive and negative aspects of heat transfer inside microchannels [22]. They observed the increase of heat transfer rate from 2.7 kW to 22 kW by increasing size of microchannel heat exchanger twice without any variation in fin configuration. Whereas pressure drop increases four times.

Cetin, Murat et al. designed rectangular channel based microchannel heat exchanger to observed heat transfer along with pressure drop characteristics inside rectangular channel geometry. They used water and air as a refrigerant with six rows for water flow channels and seven for air flow channels. From the experimental setup results, they observed heat transfer coefficient, Nusselt number, Reynold number by using correlation specifically for rectangular channels and also calculated NTU (Number of

Transfer Units), effectiveness, overall efficiency of microchannel heat exchanger system, heat transfer and the difference of pressure between entrance and exist side of rectangular based microchannels. They compared their experimental results with the commercial heat exchanger and their results shows that their microchannel heat exchanger produce cooling performance of 681 W through a volume of 677.6 cm^3. Which is higher than commercial heat exchanger whose cooling performance is 0.702 kW with volume of 2507 cm^3 [23].

Christopher Ward et al. experimentally designed a microchannel waste heat recovery system. Whose dimensions were 21cm × 15 cm × 8 cm and made with diffusion brazing stainless steel alumina. They used exhaust gases at temperature of 500ºC from 13.4 kW of generator to passes these gases through microchannels to measure heat transfer inside channels. They got 11.1 kW of heat energy with an effectiveness of 0.87 at design point. They also reach to the point that if it coupled with ORC (Organic Rankine Cycle) then it will give 35% more performance [24].

James S. Yih et al. conducted research on microchannel cross flow heat exchanger and examined the geometry thermally under the laboratory conditions. The heat exchanger they designed was actually referred as Heat Recovery Unit (HRU) as shown in Figure 2.1, which was designed to recover maximum availability of thermal energy from the diesel engine to heat the furnace oil. They measured the geometrical parameters of microchannels by developing two methods. The first method was based on image processing of microscope photographs and second method was based on analysis of measurement of profilometer. The results showed that on average basis, air channels were smaller in area of cross section approximately 11% on comparison to design. As area of cross sectional of oil were 8% smaller. The hydraulic diameter of both channels were approaching the design. They did thermal testing of microchannel unit included effectiveness, pressure drop of both fluids and heat transfer behavior as well. Their experimental results were in better agreement with the predicted models. However measured pressure drop values of oil and air were much higher. The small variation was attributed to the ideal representation of model of microchannel area. Although they measured 12.3 kW of heat duty and effectiveness of heat exchanger was 97.8%. They also used film anemometer to measure and collect the velocity measurements of air to

examine it flow through air channels at exist of the heat recovery unit. Which showed the flow maldistribution and the temperature was determined and analyzed for the stable thermal loaded conditions [25].

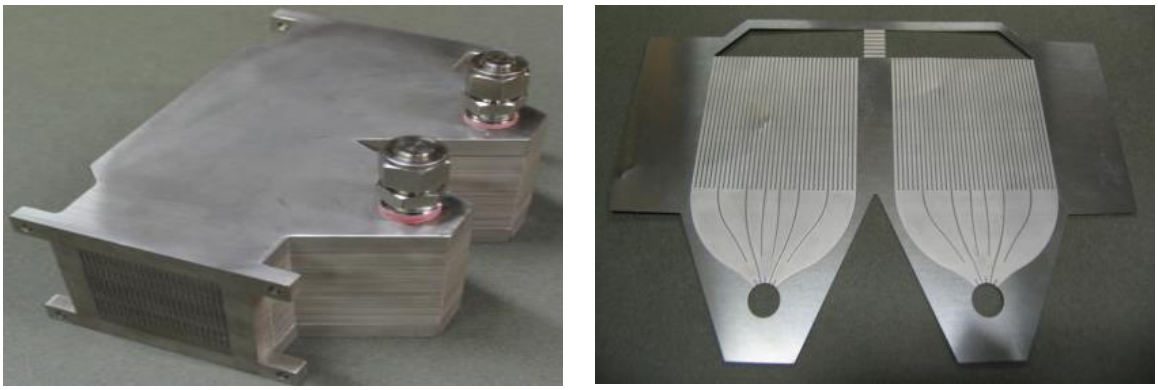

Figure 2.1: Heat recovery unit on right and channels internal view on left side [25]

B.S Gawali and D.A. Kamble conducted their research on geometrical parameter of channels to measure the heat transfer under forced convection single phase flow condition. They numerically analyzed the hydraulic diameter of channel with the computer based code. They set base area for cooing chip 35 cm × 50 cm, length of microchannel 50 cm, height 400 μm, 450 μm, 500 μm, 600 μm and spacing were 300 μm, 350 μm, 250 μm respectively. Hydraulic diameter was varied from 444 μm to 476 μm with mass flow rate of deionized water varied from 0.08 to 0.46 kg s^{-1}. The experimental model results showed that the maximum pressure difference was about 0.12 bar at flow rate 0.27 kg s^{-1} to 0.46 kg s^{-1} for hydraulic diameter 444 μm. They concluded that hydraulic diameter parameter is dominant in all rectangular channels for channel confinement [26].

2.3 Refrigerant Generation

The selection and usage of less harmful and environmental friendly refrigerant is very important in microchannels study regarding impact on external environment in the form of global warming potential and ozone depletion potential too. Before 19^{th} century, initial natural refrigerants were water and air used in refrigeration and automobile industries at larger scale before the innovation of new refrigerants. But from 1880 to 1930s, Ammonia, methyle chloride and sulphur dioxide replaces the air water mixture in industrial applications that came under the category of first generation. Unsafe and

flammability were the only problems associated with these refrigerants due to which these were neglected. /With the Second generation from 1931 to 1990s with the invention of chlorofluorocarbon, R-12 and R-11 that had no issues just like refrigerants of above generation. They easily compressed in the liquid form to transfer to chemical industries for process engineering and also used in automobile industries. These refrigerants became unstable and lost its structural bonding due to the falling of ultra violet radiations. So, with the passage of time, these refrigerants then replaced by HFCs and HCFCs of third generation that initiated from 1990 to 2010s [27]. Such refrigerant had similar advantageous characteristics over the previous one but these refrigerants had high impact on global warming potential. Which was not consider suitable for industrial uses so that's way research carried out until the exploration of new refrigerants in the market to replace the previous one. Whereas, generation fourth started from 2010 to till now, which is introduces new refrigerants in the market like R-22, R-121, R-134a and R-113 etc. R-22 have lower value of ozone depletion potential as well as global warming potential. R-134a refrigerant has been recognized and considered as a better refrigerant over ammonia, CFC and HCFC in industrial applications due to low impact on global atmosphere and minimum ozone formation [27]. But furthermore, zeotropic mixtures of different refrigerants are also under consideration in research field that will be used in research and industries later on. The refrigerant properties came under various generations are shown in Figure 2.2.

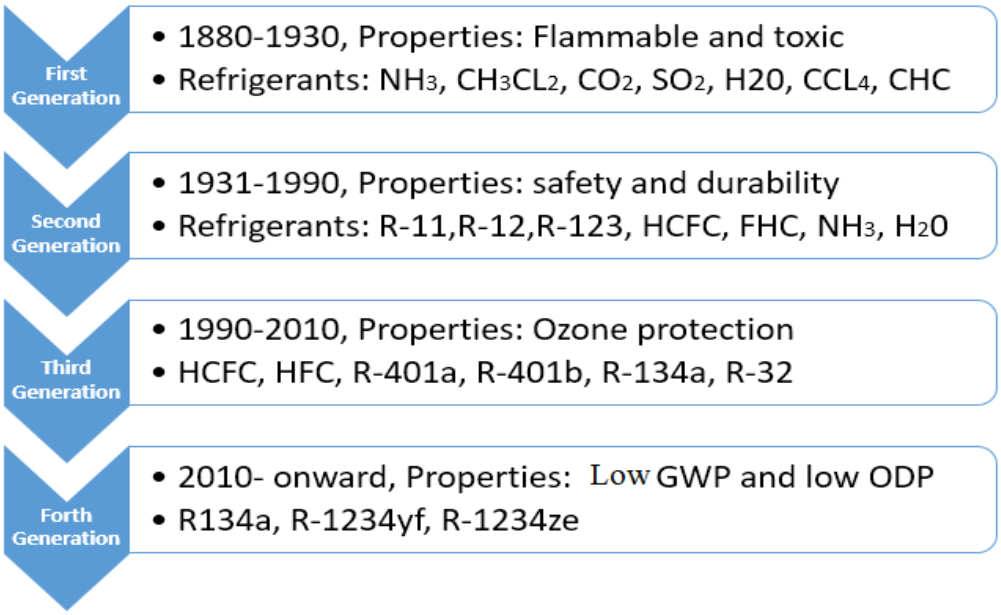

Figure 2.2: Refrigerant progression based on their GWP and ODP [27]

Summary

Chapter 2 gives an overview of microchannels and minichannels concept. It discussed the earlier and later on study of utilizing microchannel technology for different applications. From concept of microchannels miniaturization, Tuckerman and Pease comes to mind, who gave idea of using microchannels for the very first time for removing of higher heat flux from thermal systems and then this study proceeds to next generation till the recovery of waste heat systems. The main focus was to recuperate thermal energy by introducing the efficient refrigerant to overcome environmental issues which is the main issue of today era through microchannels. For which many authors have done extensive research by introducing the empirical correlations of Reynold number, Nusselt number, heat transfer coefficient and pressure drop for microchannels.

References

[1] D. B. Tuckerman and R. F. W. Pease, “High-performance heat sinking for VLSI,” IEEE Electron Device Lett., vol. 2, no. 5, pp. 126–129, 1981.

[2] D.B. Tuckerman, “Heat transfer micro-structures for inte-grated circuits,” Lawrence Livermore National Lab Ca, Feb. 1984.

[3] S. G. Kandlikar and W. J. Grande, “Thermohydraulic performance enhancement and fabrication technology evaluation of single phase flow in microchannels for high heat flux chip cooling,” vol. 7632, 2010.

[4] R. K. Mehendale, S. S., Jacobi, A. M., and Shah, “"Fluid flow and heat transfer at micro and meso-scales with applications to heat exchanger design," Journel of Applied Mechanics, vol. 53, pp. 175–193. 2000.

[5] N. T. Obot, ‘Toward a Better Understanding of Friction and Heat/Mass Transfer in Microchannels–A Literature Review,” Journel of Microscale Thermophys, vol. 6, pp.155-173, 2003.

[6] B. W. and X. Peng, “B. Wang and X. Peng, ‘Experimental investigation on liquid forced convection heat transfer through microchannels,’ International Journal of Heat and Mass Transfer, vol. 37, pp. 73-82, 1994.

[7] S.V.Garimella, “Single-phase flow and heat transport and pumping considerations in microchannel heat sinks, Journel of Heat Transfer, vol. 25, pp. 15–25, 2004.”

[8] M. K. and F. G. T. Harms, "Developing convective heat transfer in deep rectangular microchannels," International Journal of Heat and Fluid Flow, vol. 20, pp. 149-157, 1999.

[9] W. Q. and I. Mudawar, "Experimental and numerical study of pressure drop and heat transfer in a single-phase micro-channel heat sink," International Journal of Heat and Mass Transfer, vol. 45, pp. 2549-2565, 2002.

[10] P. Jiang, M. Fan, G. Si, and Z. Ren, “Thermal and hydraulic performance of small scale microchannel and porous media heat exchangers,” vol. 44, 2001.

[11] J. Z. and Y. C. S. Shen, J. Xu, "Fluid flow and heat transfer with rough wall surface," Energy Conversion and Management, vol. 47, pp. 1311-1325, 2006.

[12] W. Cai, "Hydrogen production from ethanol steam reforming in a micro-channel reactor," International Journal of Hydrogen Energy, vol. 35, pp. 1152-1159, 2010.

[13] Saqr and M. Musa, "Thermal design of automobile exhaust based thermoelectric generators, Objectives and challenges. International Journal of Automotive Engineers, vol. 9, pp. 155−160 2008.

[14] Jinho Yang, "Potential applications of thermoelectric waste heat recovery in the automotive industry," IEEE. 24th International Conference on Thermoelectric, Clemson, Clemson, South California, pp. 170-174, 2005.

[15] H. H. B Mathew, "Experimental investigation of thermal model of parallel flow microchannel heat exchangers subjected to external heat flux," International Journel of Heat and Mass Transfer, vol. 55, pp. 2193-2199, 2012.

[16] H. H. B Mathew, "Application of effectiveness-NTU relationship to parallel flow microchannel heat exchangers subjected to external heat transfer," International Journel of Thermal Sciences, Vol. 30, pp. 1-10, 2009.

[17] T. L. N. Tsuzuki, Nobuyoshi, Motoaki Utamura, "Nusselt number correlations for a microchannel heat exchanger hot water supplier with S-shaped fins," Applied Thermal Engineering, vol. 29, pp. 3299–3308, 2009.

[18] N. Tsuzuki, Y. Kato, K. Nikitin, and T. Ishizuka, "Advanced microchannel heat exchanger with S-shaped fins," J. Nucl. Sci. Technol., vol. 46, no. 5, pp. 403–412, 2009.

[19] M. I. Hasan, "Investigation of a Counter Flow Microchannel Heat Exchanger Performance with Using Nanofluid as a Coolant," Journal of Electronics Cooling and Thermal Control, vol. 2, no. 3, pp. 35–43, 2012.

[20] H. H. Mushtaq I. Hasan, A.A. Rageb, M. Yaghoubi, "Influence of channel geometry on the performance of a counter flow microchannel heat exchanger," International Journel of Thermal Sciences, vol. 48, pp. 1607–1618, 2009.

[21] S. Mavridou, "'Comparative design study of a diesel exhaust gas heat exchanger for truck applications with conventional and state of the art heat transfer enhancements,'" Applied Thermal Engineering., vol. 30, pp. 935–947, 2010.

[22] S. C. Kang, S. W. Tseng, "Analysis of effectiveness and pressure drop in micro

cross-flow heat exchanger," Applied Thermal Engineering, pp. 877–885, 2007.

[23] A. G. Çetin, Murat, "Design and experimental investigation of a microchannel heat exchanger," Mechanical Engineering, Middle East Technical University, 2010.

[24] Ward, Christopher, "Design and performance of a small scale waste heat recovery unit," Mechanical Engineering, Oregon State University, USA, December 5, 2011.

[25] Yih, James S., "The geometric characterization and thermal performance of a microchannel heat exchanger for diesel engine waste heat recovery," Mechanical Engineering, Oregon State University, USA, Nosvember 29, 2011.

[26] B. S. Gawali and D. A. Kamble, "Analysis of rectangular microchannel under forced convection heat transfer condition," International Journal of Engineering Science and Technology, vol. 3, no. 2, pp. 2041–2043, 2011.

[27] J. M.Calm, "The next generation of refrigerants – Historical review, considerations, and outlook," International Journal of Refrigeration, vol. 31, pp. 1123–1133, 2008.

Chapter 3: Methodology and Modelling

3.1 Methodology

This chapter explains the basic heat transfer equations used for analyzing physical thermodynamic and thermal hydraulic effect of fluids inside different microchannels geometries like rectangular, square, triangular and circular microchannels. EES (Engineering Equation Solver) program is used to determine the microchannel heat exchanger performance and to solve different complex heat transfer equations by taking average mean temperature of fluid that lead towards the surface area calculations for microchannel heat exchanger. However geometrical configuration is used to determine the channel hydraulic diameter of different microchannel geometries. Initially heat transfer from hot working fluid to cooling fluid will be measured along with its effectiveness ratio. Then overall heat transfer coefficient is calculated by thermal resistance network that consists of combining effect of conductive and convective resistances. Conductive resistance is just like a sandwich between two convective resistances as shown in Figure 3.4. Some dimensionless numbers are introduced to calculate the local convective heat transfer coefficient like Nusselt number, Reynold number, Prandtl Number, Stanton number and Colburn number by using specific correlations for different microchannels geometries that proposed by various authors. Finally, heat duty, pressure drop, heat capacity rate ratio, effectiveness ratio, NTU (number of transfer units), system efficiency is determined. The extensive methodology is shown in Figure 3.1.

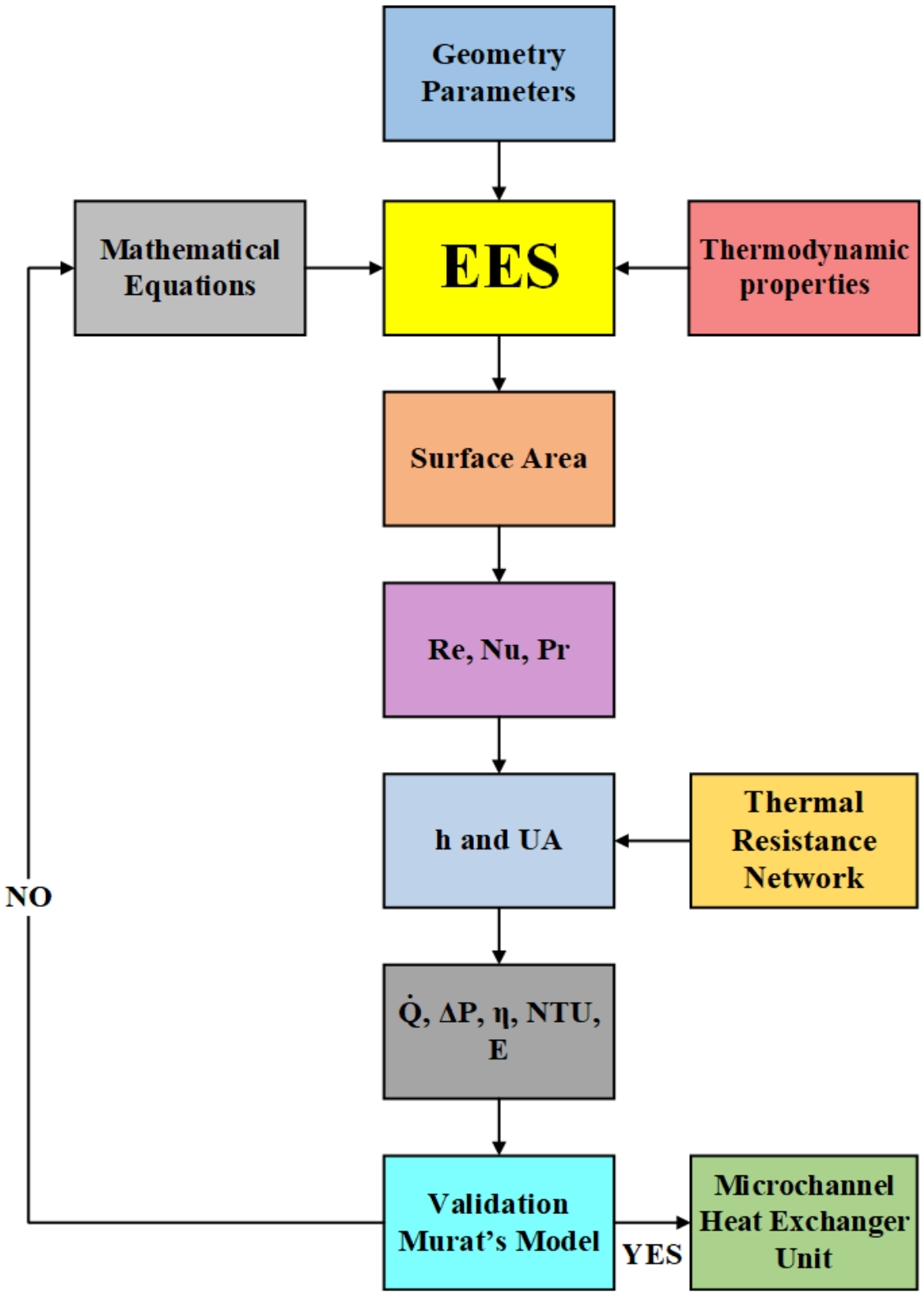

Figure 3.1: Methodology for single pass cross flow microchannel heat exchanger

3.2 Waste Heat Recovery System

The objective of microchannel heat exchanger design is to utilize waste thermal energy from the exhaust of Kubota SQ-14 diesel engine before vented to atmosphere in order to power a cooling cycle as represented in Figure 3.2. Inside the microchannel heat exchanger geometry, heat energy is transformed from exhaust gases to the heat transfer refrigerant R-134a. Which will circulated through Organic Rankine Cycle to produce the power output through expander. Which in turn rotate the shaft to create shaft work. This shaft work is used in driving the compressor in a vapor compression cycle of refrigeration cycle.

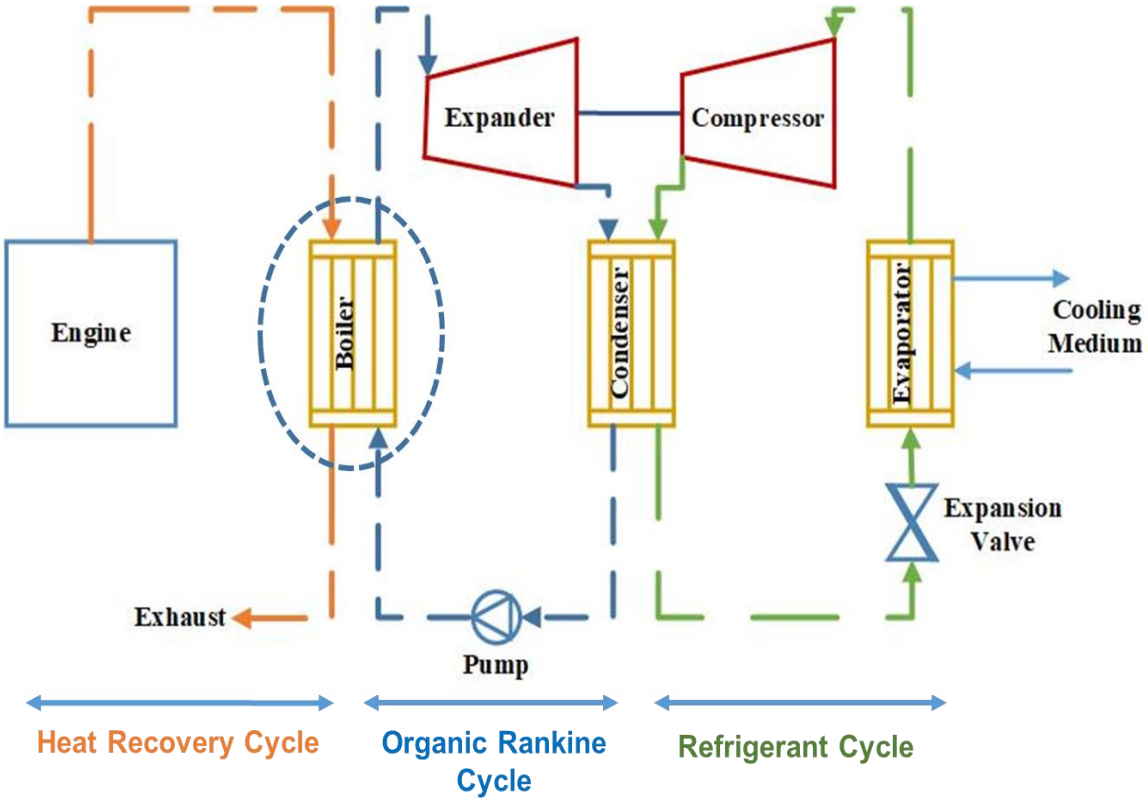

Figure 3.2: Recovery of waste heat energy through microchannel heat exchanger

3.3 Mathematical Modelling

3.3.1 Heat Transfer Modelling

For modelling of heat transfer and pressure drop, initially input data is required in the form of geometrical configuration of microchannel heat exchanger, temperature along with mass flow rate of fluids to analyze their heat transfer as well as pressure drop behavior. So, the data points are acquired from Kubota SQ-14 Diesel Engine. Which is modeled on Engineering Equation Solver (EES) program to understand the phenomenon of thermal performance under steady state condition with no phase change taken as an assumption, the heat transfer in microchannel geometry is determined from energy balance for refrigerant R-134a flows inside channels as well as for exhaust gases that moves on opposite side of channels in cross flow direction as shown in Equation (3.1)-(3.3). The total amount of thermal energy leaving from the exhaust gases is the cumulative sum of energy received by refrigerant R-134a as well as the energy lost to the surrounding atmosphere. $\dot{Q}_h$ represents heat loss from exhaust gases to refrigerant and surrounding as well. As the energy gain or lost in overall system is a combination of flow rate with constant specific heat as well as the change in temperature under steady state condition with no phase change and negligible kinetic as well as potential changes.

$$\dot{Q}_h = \dot{m}_h \times C_{p_h} \times (T_{h1} - T_{h2}) \tag{3.1}$$

$$\dot{Q}_c = \dot{m}_c \times C_{p_c} \times (T_{c2} - T_{c1}) \tag{3.2}$$

$$\dot{m}_h \times C_{p_h} \times (T_{h1} - T_{h2}) = \dot{m}_c \times C_{p_c} \times (T_{c2} - T_{c1}) - \dot{Q}_h - \dot{Q}_c \tag{3.3}$$

Where $\dot{m}_{h,c}$ is the mass flow rate of given fluids, Subscripts c and h shows the cold and hot streams. Whereas numbers 1 and 2 represents inlet and outlet condition respectively. When the heat transferred from hot fluid towards the cold one then the enthalpy of the cold fluid increases with the decrease in enthalpy of hotter fluid. As the mean temperature difference in between the hotter and colder fluid varies with heat transfer area of microchannel heat exchanger during analysis.

$$\Delta T_{in} = T_{h1} - T_{c2} \tag{3.4}$$

$$\Delta T_{out} = T_{h2} - T_{c1} \tag{3.5}$$

ΔT_{LM} is a log mean temperature difference can be calculated as the function of fluid's inlet and exit temperatures for cross flow heat exchanger is expressed by Equation (3.6).

$$\Delta T_{LM} = \frac{\Delta T_{in} - \Delta T_{out}}{ln\left(\frac{\Delta T_{in}}{\Delta T_{out}}\right)} \tag{3.6}$$

As temperature effectiveness P as in Equation (3.7) is a ratio of actually heat transfer to the heat that will be transferred if the same temperature of cold fluid was increased to the temperature of hot fluid. R is called as heat capacity rate ratio obtained by dividing heat capacity of cold fluid to hot one as shown in Equation (3.8). A is a total heat transfer area for hot and cold side. Which is unknown parameter calculated via the *UA-LMTD* method as shown in Equation (3.9) [1].

$$P = \frac{T_{c2} - T_{c1}}{T_{h1} - T_{c1}} = \frac{\Delta T_c}{\Delta T_{max}} \tag{3.7}$$

$$R = \frac{C_c}{C_h} = \frac{T_{h1} - T_{h2}}{T_{c2} - T_{c1}} = \frac{\Delta T_h}{\Delta T_c} \tag{3.8}$$

$$\dot{Q} = U \times A \times F \times \Delta T_{LM} \times N \tag{3.9}$$

F is non-dimensional correction factor that's the function of heat capacity rate ratio R, temperature effectiveness ratio P and the unmixed fluids flow arrangement. F has a value less than unity for cross flow configuration [1]. It is available in graphical form as shown in Figure 3.3.

$$F = \emptyset(P, R, flow\ arrangement) \tag{3.10}$$

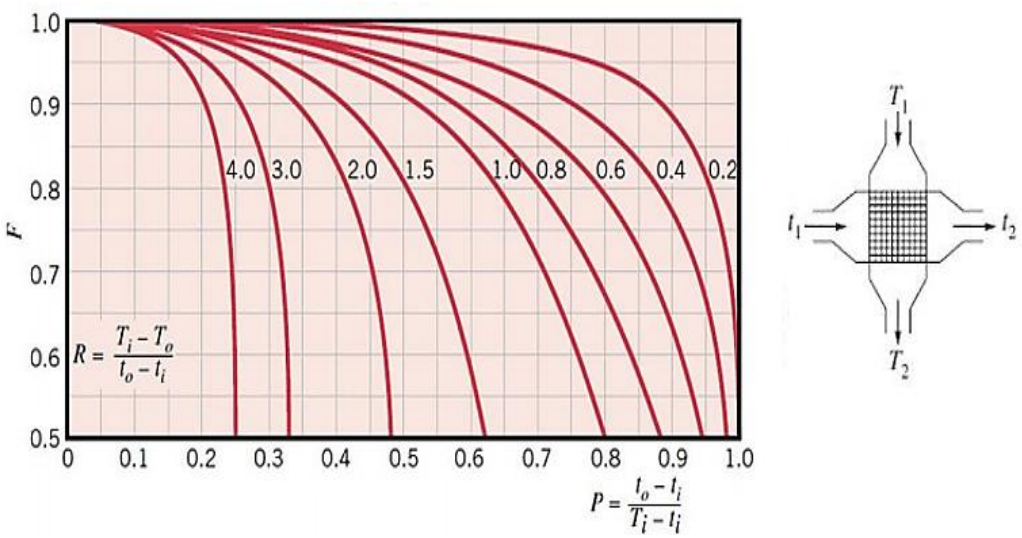

Figure 3.3: LMTD correction factor F with both unmixed fluids for cross flow heat exchanger [1]

3.3.2 Thermal Resistance Network

U is an overall heat transfer coefficient obtained by cumulative sum of convective as well as conductive thermal resistances as shown in Figure 3.4 with the following steps. Initially convection takes place from hot fluid to the wall of the channel, conduction phenomenon occurs in the middle section through the separation wall and then again convection to the cold fluid happen from the conduction separation wall [2].

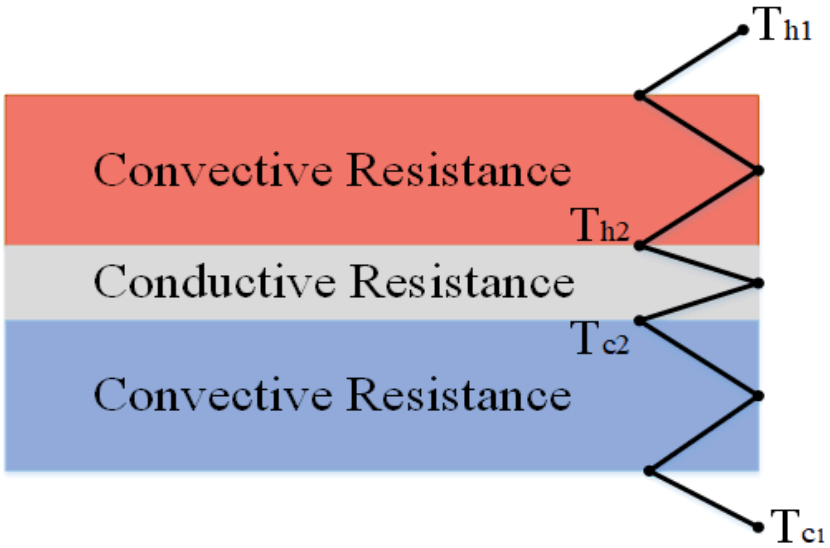

Figure 3.4: Representation of Thermal Resistance Network [3]

$$R_t = R_h + R_w + R_c + R_{f,h} + R_{f,c} \tag{3.11}$$

$$R_t = \frac{1}{UA} \tag{3.12}$$

$$R_h = \frac{1}{(\eta_{o,h}.A.h)_h} \tag{3.13}$$

$$R_c = \frac{1}{(\eta_{o,c}.A.h)_c} \tag{3.14}$$

$$R_w = \frac{\delta_w}{k_w.A_w} \tag{3.15}$$

$$R_{f,h} = \frac{R_{fh}}{\eta_{o,h}.A_h} \tag{3.16}$$

$$R_{f,c} = \frac{R_{fc}}{\eta_{o,c}.A_c} \tag{3.17}$$

$$UA = \left(\frac{1}{(\eta_{o,h}.A.h)_h} + \frac{1}{(\eta_{o,c}.A.h)_c} + \frac{\delta_w}{k_w.A_w} + \frac{R_{fh}}{\eta_{o,h}.A_h} + \frac{R_{fc}}{\eta_{o,c}.A_c}\right)^{-1} \quad (3.18)$$

From Equation (3.11) to (3.18), R_h and R_c shows hot and cold fluids convective resistances. Whereas $R_w, R_{f,h}$ and $R_{f,c}$ represents wall resistance and fouling resistances of respective fluids. The fouling factors are taken as a reference from TEMA (Tubular Exchanger Manufacturers Association) code [4] because of difficulty in predicting the fouling factor due to present of so many variables that changes fouling behavior alternatively. *N* shows the minimum number of channels required in the test section is estimated by Equation (3.19) [5].

$$N = \frac{(V \times \rho_l)}{(G \times W \times H)} \quad (3.19)$$

G is the required mass flux to maintain the flow of fluids inside channel is shown in Equation (3.20) and hydraulic diameter for non-circular geometry is expressed by Equation (3.21). For determination of convection heat transfer coefficient for hot and cold side of fluids, a dimensionless Reynold number and Nusselt number proposed by Kays and Crawford introduced correlation of Nusselt number for rectangular microchannel under fully developed laminar flow condition as shown in Equation (3.22) and (3.23) [6]. Nusselt number correlation for triangular channel from Kandlikar is given in Equation (3.24) and Siedel and Tate's Nusselt number correlation for circular channel is given in Equation (3.25). If Re < 2300 then flow inside the channels will be steady and fully developed laminar otherwise turbulent flow. Whereas the Nusselt number correlation used depends upon the channel's aspect ratio that is a ratio of shorter length of microchannel to the longer length. E.g. $\alpha = \frac{w}{H}$. It's varied with increasing height and reducing of width of channel. Whereas Stanton number, Prandtl number and Colburn factor are also used to see the behavior of heat transfer as given by Equation (3.26) to (3.28).

$$G = \frac{\dot{m}_{ref}}{\mathrm{A}} \quad (3.20)$$

$$D_h = \frac{4 \times \mathrm{A}}{P} = \frac{4 \times (free\ flow\ area)}{perimeter} \quad (3.21)$$

$$Re = \frac{G \times D_h}{\mu} \tag{3.22}$$

$$Nu_{Rectangular} = \frac{h \times D_h}{K_f} = [8.235 \times (1 - 1.883\alpha_c + 3.767\alpha_c^2 - 5.814\alpha_c^3 + 5.361\alpha_c^4 - 2\alpha_c^5)] \times \left(\frac{\mu_b}{\mu_w}\right)^{-0.14} \tag{3.23}$$

$$Nu_{Triangular} = 0.943(\alpha_{ch}^5 + 5.358\alpha_{ch}^4 - 9.251\alpha_{ch}^3 + 11.931\alpha_{ch}^2 - 9.803\alpha_{ch} + 3.375) \tag{3.24}$$

$$Nu_{Circular} = \left\{1.86\left(Re^{\frac{1}{3}}\right)\left(Pr^{\frac{1}{3}}\right)\left(\frac{D}{L}\right)^{\frac{1}{3}}\right\}.\left(\frac{\mu_h}{\mu_w}\right)^{(0.14)} \tag{3.25}$$

$$St = \frac{h}{G \times c_p} \tag{3.26}$$

$$Pr = \frac{v}{\alpha} = \frac{\mu \times C_p}{K} \tag{3.27}$$

$$J = St \times Pr^{\frac{2}{3}} = \frac{Nu \times pr^{\frac{-1}{3}}}{Re} \tag{3.28}$$

3.3.3 Pressure Drop Modelling

Pressure drop is used to measure the pressure difference between inlet and outlet of microchannel system. Different correlations of pressure drop for different geometries has been developed. As Pressure drop in a smooth rectangular channel for laminar and steady flow can be calculated by using Equation (3.29). Frictional factor f *is* used in pressure drop correlation is taken from Hagen-Poiseuille Equation that is valid only if Re less than 2300 otherwise Blasius Friction factor in Equation (3.31) (in a range of 3,000 < Re < 100,000) will be used for turbulent condition [7][8].

$$\Delta P = \frac{(f \times L \times \rho \times u^2)}{2 \times D_h^2} \tag{3.29}$$

$$f = \frac{64}{Re} \tag{3.30}$$

$$f = 0.079 \times Re^{-0.25} \tag{3.31}$$

η_f in Equation (3.32) shows fin efficiency for plate fin microchannel heat exchanger, the purpose of using these fins to increases the total surface area for heat transfer rate.

$$\eta_{f=}\frac{tanh(m\times I_1)}{m\times I_1} \tag{3.32}$$

Where m in Equation (3.33) is a characteristic factor, b is the height fin, δ is thickness of fin, K_f is conductivity of material used that is Aluminum 3003-O. As the overall surface performance in term of efficiency of fin is expressed by η_o in Equation (3.35). ε is a effectiveness ratio as shown in Equation (3.36) that describes the actual heat transfer occurs in the system to the maximum possible heat transfer or in other words it explain the thermal performance and capability of a microchannel system that how much it is effective in transferring of heat energy from hot to the cold fluid. NTU (number of transfer units) [9] Which actually shows a ratio of thermal conductance to minimum heat capacity rate as given in Equation (3.37).

$$m = \left[\frac{2h}{K_f\times\delta}\left(1+\frac{\delta}{L_f}\right)\right] \tag{3.33}$$

$$I_1 = \frac{b}{2} - \delta \tag{3.34}$$

$$\eta_o = \left[1-\left(1-\eta_f\right)\times\frac{A_f}{A_t}\right] \tag{3.35}$$

$$\varepsilon = \frac{\dot{Q}}{\dot{Q}_{max}} = \frac{C_h\times(T_{h1}-T_{h2})}{C_{min}\times(T_{h1}-T_{c1})} = \frac{C_c\times(T_{c2}-T_{c1})}{C_{min}\times(T_{h1}-T_{c1})} \tag{3.36}$$

$$NTU = \frac{U\times A_t}{C_{min}} \tag{3.37}$$

3.4 Geometrical Properties and Configuration

3.4.1 Rectangular and Square Geometry

The geometrical configuration determination for cross flow finned microchannel heat exchanger is somehow complex due to plain fins in geometry. These fins can be considered in any shape. Square or rectangular shape fins has rounded corner geometry in practical as compare to sharp corner that can be visualized in Figure 3.5 and 3.6. In which cold stream is named by refrigerant R-134a and hot stream is named as exhaust air that's are coming into square or rectangular shaped microchannels in cross flow direction to

transfer heat mechanism. The primary as well as secondary surface area of rectangular geometry is shown in Figure 3.7 followed by Equation from (3.38) to (3.48).

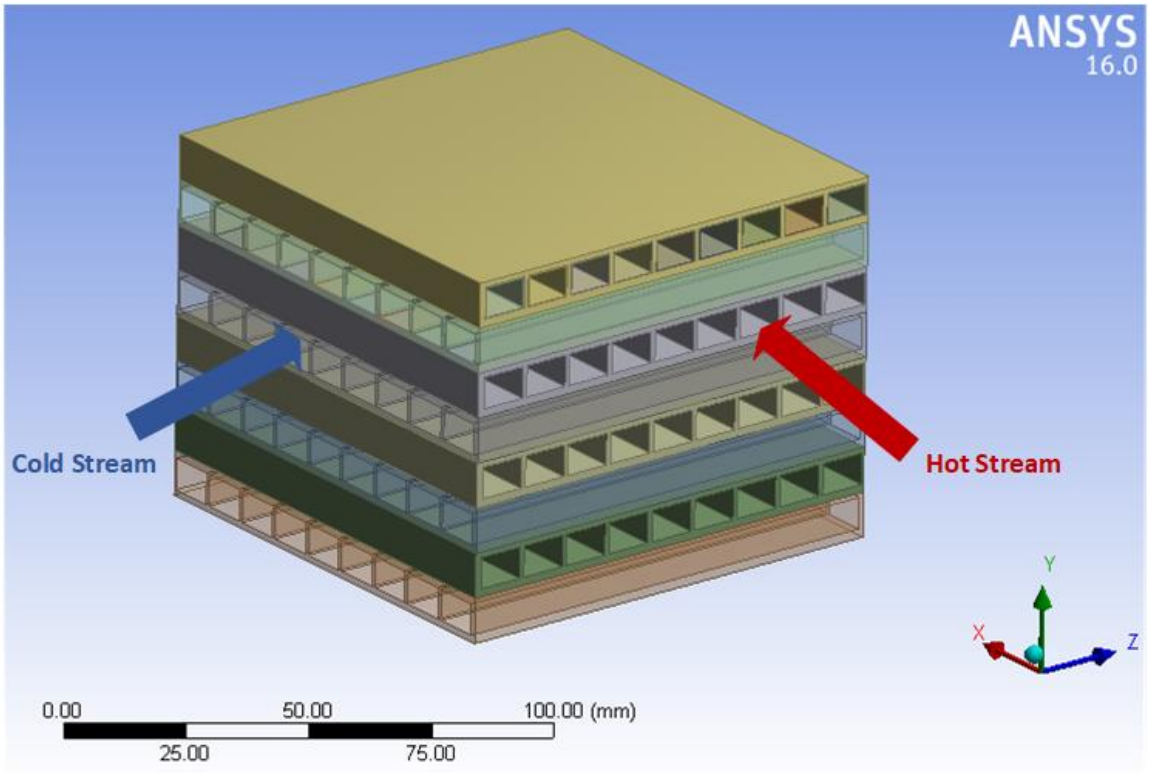

Figure 3.5: Representation of cross flow rectangular plate fins heat exchanger

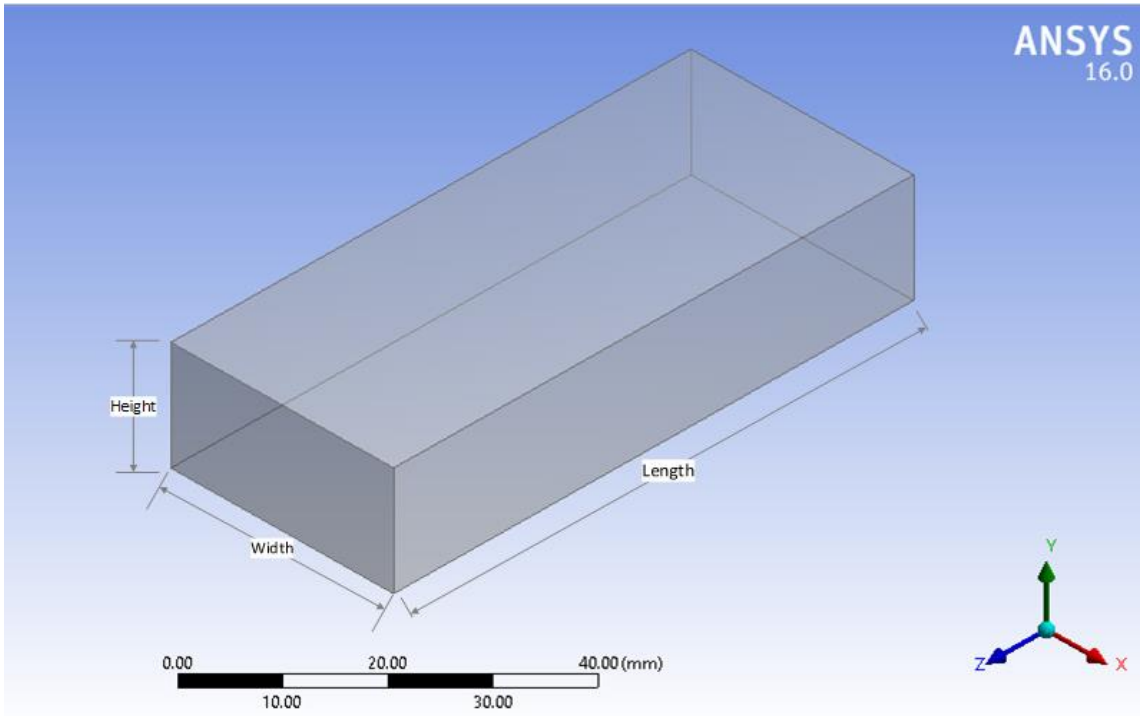

Figure 3.6: Representation of cross flow rectangular plate fins heat exchanger

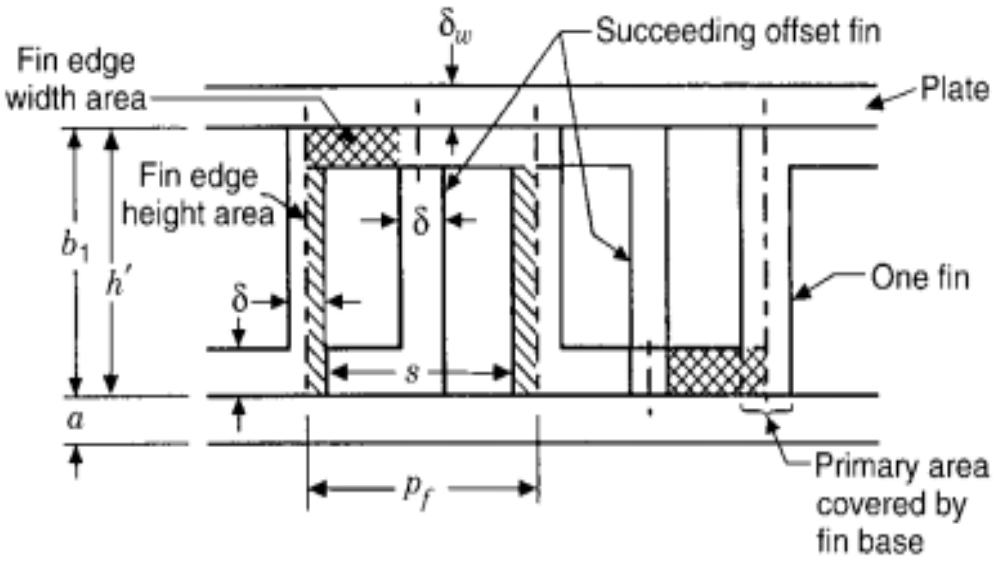

Figure 3.7: Geometrical representation of rectangular fin heat exchanger [1]

As the surface area for determination of thermal performance for both hot and cold streams, consists of two surface area (fins), primary surface area A_p and secondary area A_S of fins. Four components, which are required to measure the primary surface area of fin heat exchanger:

(a) Plate total area

(b) Primary surface area of plate covered by the fin base

(c) Area of header bar for fluid 1 in L_2 direction at the nearest end of fins

(d) Area of plates and header bars at fluid 1 inlet for fluid 2, outlet core face

Whereas secondary surface area of fin contains

(a) Area of fin height

(b) Area of fin edge height

(c) Area of fin edge width

Although sum of component 1, 3 and 4 minus 2 gives primary surface area of fin. Above available components of primary surface area combines to give total area plate

$$\textit{Total area of plate} = 2\times L_1\times L_2\times N_p \tag{3.38}$$

$$\textit{Primary surface area of plate covered by the fin} = 2\times \delta \times L_f\times n_f = 2\times \delta \times L_f\times L_2\times N_p \tag{3.39}$$

Whereas n_f is the total number of fins, L_f is the flow length of fin, N_f shows the number of fins per unit length in direction of L_2.

$$\textit{Area of header bar in } L_2 \textit{ direction for fluid 1} = 2\times b_1\times L_1\times N_p \tag{3.40}$$

Plate and header bar's area of fluid 2 at fluid 1 inlet $= 2\times(b2+2\times\delta)\times(N_p+1)\times L_2$ (3.41)

Total surface area on primary side for fluid 1= Total area of plate- Primary surface area of plate covered by the fin base+ Area of header bar in L_2 direction for fluid 1+ Area of plates and header bars of fluid 2 at fluid 1 inlet

$$A_{p1}=2\times L_1\times L_2\times N_p-2\times\delta\times L_f\times L_2\times N_p+2\times b_1\times L_1\times N_p+2\times(b2+2\times\delta)\times(N_p+1)\times L_2 \quad (3.42)$$

Similarly, for secondary fin surface area, three components are given by

$$Area\ of\ fin\ height=2\times(b_1-\delta)\times L_f\times n_f \quad (3.43)$$

$$Area\ of\ fin\ edge\ height=2\times(b_1-\delta)\times\delta\times n_f \quad (3.44)$$

$$Area\ of\ fin\ edge\ width=2\times p_f\times\delta\times n_f \quad (3.45)$$

Total surface area on secondary side for fluid 1 = Area of fin height + Area of fin edge height + Area of fin edge width

$$A_{f1}=2\times(b_1-\delta)\times L_f\times n_f+2\times(b_1-\delta)\times\delta\times n_f+2\times p_f\times\delta\times n_f \quad (3.46)$$

So the total heat transfer area on fluid 1 side is

$$A_1=A_{p1}+A_{f1} \quad (3.47)$$

Free flow frontal area on the side of fluid 1 is calculated by subtracting area blocked by fins at the core entrance of fluid 1 side from free frontal area on that side.

$$A_{01}=b_1\times L_2\times N_p-[(b1-\delta)+p_f\times\delta\times n_f] \quad (3.48)$$

3.4.2 Circular Geometry

The geometrical configuration of cross flow circular microchannel heat exchanger can be visualized in Figure 3.8 and 3.9. As the geometrical characteristics for heat transfer analysis is straight forward given in Equation from (3.49) to (3.57).

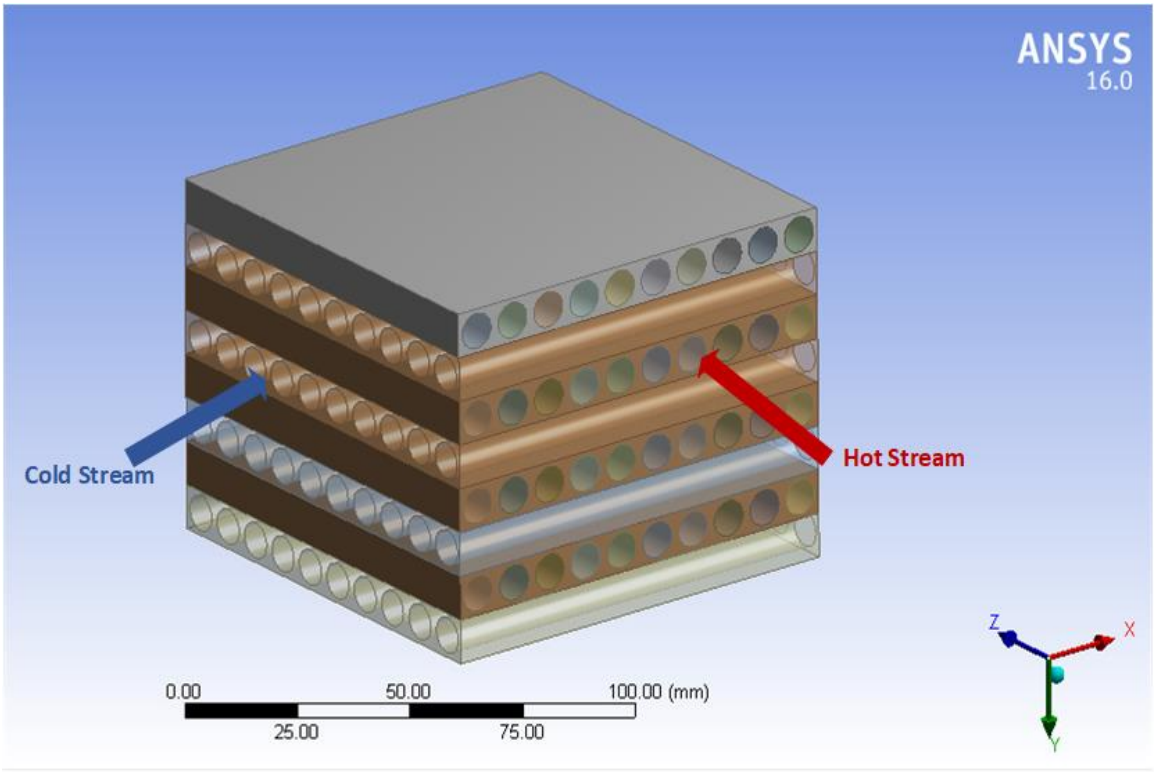

Figure 3.8: Diagram of cross flow plate and circular tube heat exchanger

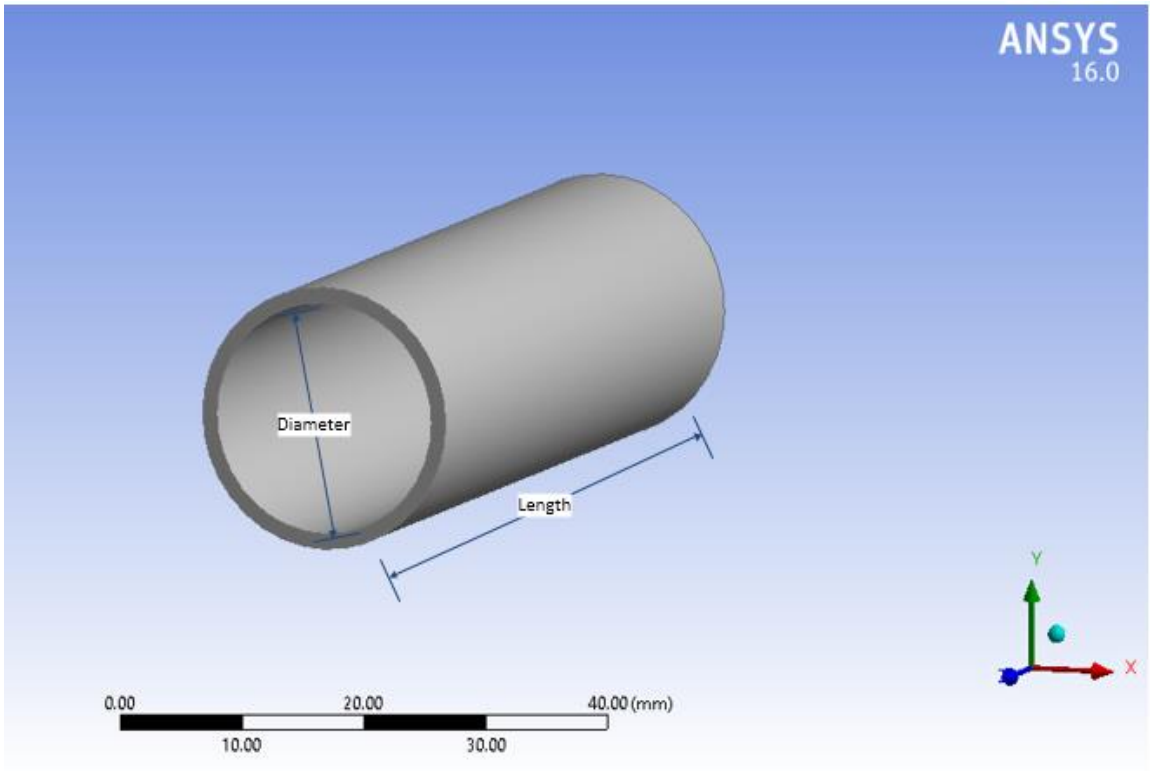

Figure 3.9: Representation of a singular circular tube

$$\text{Total area of heat transfer, } A=\pi\times L1\times D\times N_t \quad (3.49)$$

$$\text{Free flow frontal area, } A_f=(\pi/4)\times D^2\times N_t \quad (3.50)$$

$$\text{Core frontal area, } A_{fr}=L_2\times L_3 \quad (3.51)$$

$$\text{Total volume of microchannel heat exchanger, } V_t=L_1\times L_2\times L_3 \quad (3.52)$$

$$\text{Ratio of free flow to frontal area, } \sigma=(\pi/4)\times D^2\times N_t/(L_2\times L_3) \quad (3.53)$$

$$\text{Hydraulic diameter, } D_h=D \quad (3.54)$$

$$\text{Length of circular channel for heat transfer, } Lc=L_1 \quad (3.55)$$

$$\text{Length of circular channel for pressure drop, } P_d=L_1+2\times\delta_h \quad (3.56)$$

$$\text{Surface area density ratio, } \alpha=A/V_{total}=\pi\times D\times L_1\times N_t/L_1\times L_2\times L_3 \quad (3.57)$$

3.4.3 Triangular Geometry

The triangular channel geometry can be seen in Figure 3.10 to 3.12. Whereas Equations from (3.58) to (3.66) are used to design the triangular geometry.

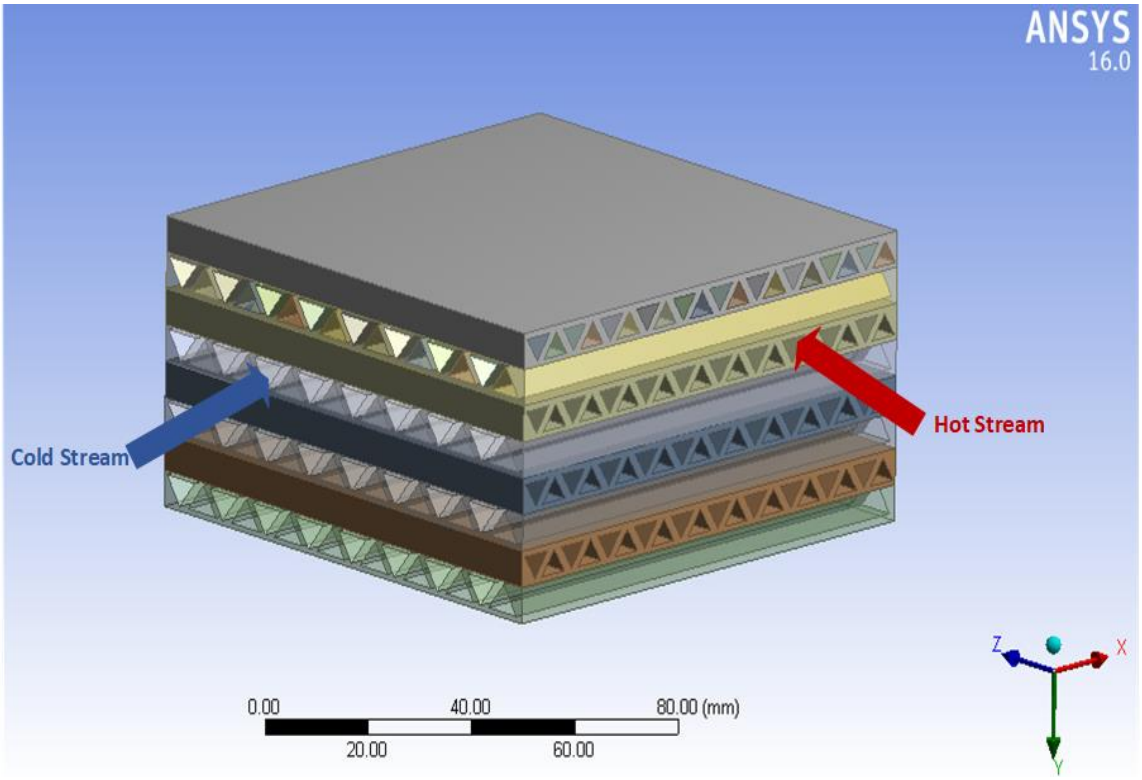

Figure 3.10: Schematic diagram of cross flow triangular microchannel heat exchanger

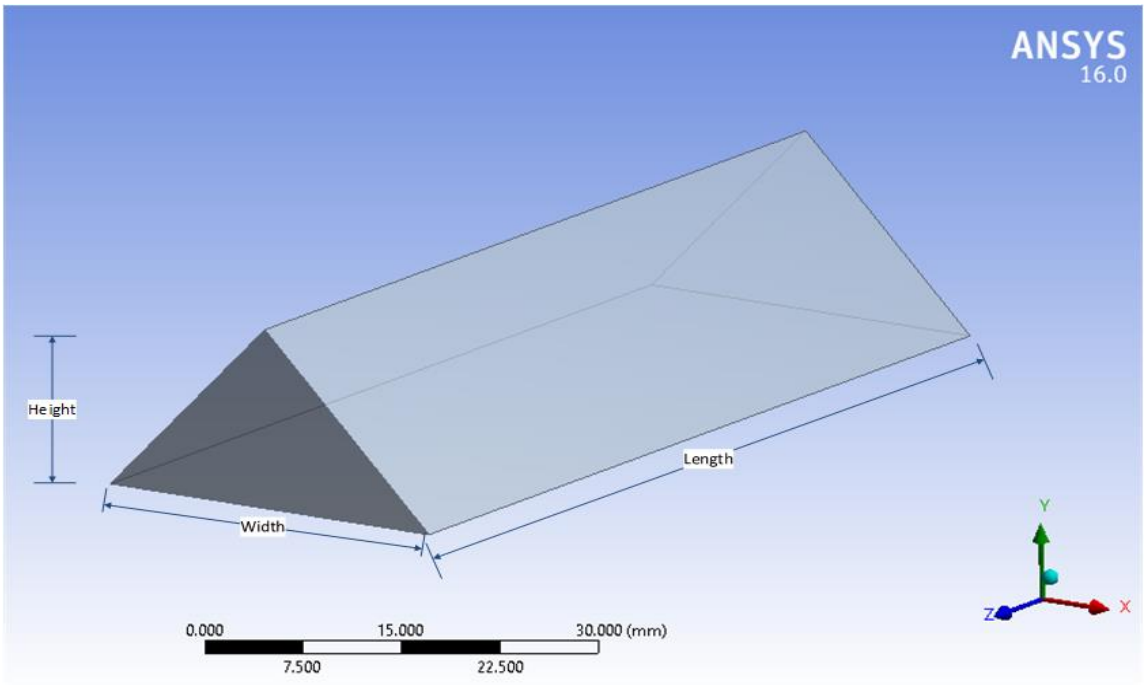

Figure 3.11: Diagram of a singular triangular fin

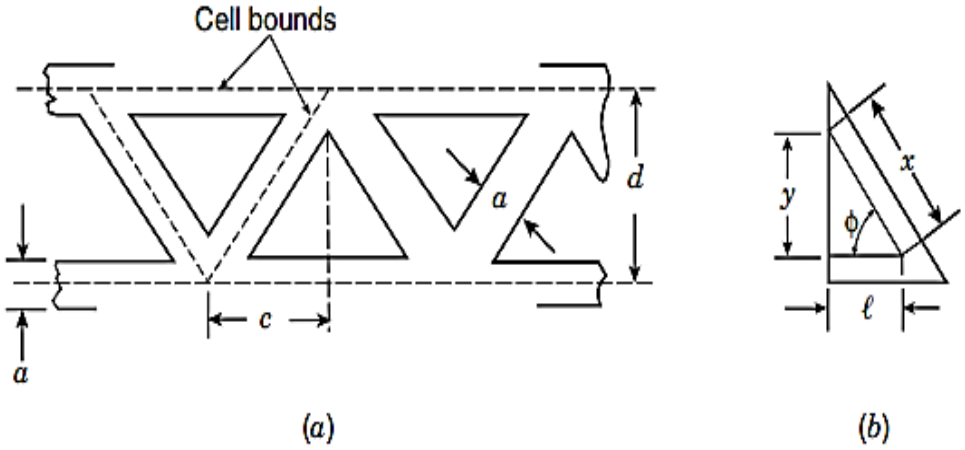

Figure 3.12: (a) Representation of triangular channel model; (b) half unit cell triangular model [2]

N_c= Number of unit cells per unit area, Area for single unit cell= face area per unit area

$$Face\ area\ for\ a\ single\ cell = face\ area/unit\ area = 1/N_c = dc \quad (3.58)$$

$$Heat\ transfer\ area\ of\ a\ single\ cell,\ A_{cell} = 2(l+x)L \quad (3.59)$$

$$Side\ length\ of\ triangle,\ x = l/\cos\emptyset \quad (3.60)$$

$$Whereas\ \cos\emptyset = c/(d^2+c^2)^{1/2} \quad (3.61)$$

$$By\ substituting\ \cos\emptyset\ in\ above\ equation\ of\ x\ value,\ we\ get\ X = l\times\ [(d/c)^2+1]^{1/2} \quad (3.62)$$

Now the area of unit cell is given as $A_{cell}=2Ll\times\{1+[(d/c)^2+1]^{1/2}\}$ (3.63)

Porosity for a unit cell is a ratio of free flow to frontal area, $\alpha=l_y\times N_c$ (3.64)

Surface area density, $\beta= A_{cell}/V_{cell}-2\times N_c(l+x)$ (3.65)

Hydraulic diameter, $D_h=4\times\alpha/\beta$ (3.66)

Summary

In this chapter, Methodology and modelling of different shaped of microchannel geometries is discussed. Basic heat transfer equations are utilized for analyzing the single phase heat transfer and pressure drop effect inside channels geometries of various shapes like rectangular, square, triangular and circular channels with use of refrigerant R-134a. Mathematical modelling is done based on EES (Engineering Equation Solver) program to determine the microchannel heat exchanger performance and to solved different complex parametric heat transfer equations by introducing different correlations of Nusselt number, Reynold number and pressure drop.

References

[1] S. Kakaç and H. Liu, “Heat exchangers selection, rating and thermal design,” CRC

Press Taylor and Francis Group, USA, 3rd Edition, 2002.

[2] S. Kakaç, A.E. Bergles, F. Mayinger, “Heat exchangers thermal hydraulic fundamentals and design,” Hemisphere Publishing Corporation, USA, pp. 455–459, 1981.

[3] Nouman Ali, “Designing of compact rectangular microchannel heat exchanger based on thermal resistance network for waste heat recovery systems,” IEEE. International Conference on Energy Conservation and Efficiency (ICECE), pp. 38–43, 22-23 November, 2017.

[4] F. OSWEILLER, “Tubesheet heat exchangers, analysis and comparison of TEMA, codap and ASME methods,” vol. CETIM, February 12, 2018.

[5] Michael A. Vanderputten, Tabeel A. Jacob, Nouman Ali, Maria Sattar, Brian M. Fronk, “Two-phase flow regimes of condensing R-134a at low mass flux in rectangular microchannels, ”International Journal of Refrigeration, vol. 84, pp. 92–103, 2017.

[6] P.S. Lee, S.V. Garimella, D. Liu, "Investigation of heat transfer in rectangular microchannels," International Journal of Heat and Mass Transfer, vol. 48, pp. 1688–1704, 2005.

[7] S. G. Kandlikar, “Heat transfer and fluid flow in minichannels and microchannels.” Journel of Science, Elsevier, 1st Edition, 2006..

[8] R. Chein, J. Chen, "Numerical study of the inlet/outlet arrangement effect on microchannel heat sink performance," International Journal of Thermal Sciences, vol. 48, pp. 1627–1638, 2009.

[9] X.F. Peng, G.P. Peterson, "The effect of thermofluid and geometrical parameters onconvection of liquids through rectangular microchannels," International Journal of Heat and Mass Transfer, vol. 38, pp. 755–758, 1995.

Chapter 4: Single Phase Flow in Microchannels

4.1 Comparison of Various Geometries

Initial data points including temperatures and mass flow rates of exhaust gases is taken from Kubota SQ-14 diesel engine [1], whereas unknown parameters are determined by doing energy balancing equations in EES (Engineering Equation Solver) program [2]. Although the Nusselt number and pressure drop correlations [3][4] proposed by different authors for different shapes of microchannel geometries like rectangular, circular, square and triangular are utilized for the measurement of thermal performance and pressure drop inside channels then finally comparison is done to find out which channel is best regarding heat transfer and effectiveness.

4.1.1 Heat Transfer

The data analyzed from EES code is shown in Table 4.1 and detail of each channel geometry is shown in Appendix-A.

Table 4.1: Output data obtained as a result of EES code

Variables	Symbols	Values	Units
Working Fluid Inlet & Outlet Temperature	T_{in,out_ref}	447, 399	K
Cooling Fluid Inlet & Outlet Temperature	T_{in,out_a}	304, 347	K
Channel Hydraulic Diameter of Air & R-134a	$D_{h\_air,ref}$	665, 668	μm
Length, Width, Height of HEX	L, W. H	110, 60, 115	mm
Mass Flow Rate of Cooling Fluid Air	$\dot{m}_a$	0.0129-0.0125	kg s^{-1}
Mass Flow Rate of Working Fluid R-134a	$\dot{m}_{ref}$	0.0162-0.048	kg s^{-1}
Thickness of Wall	δ_w	100	μm
Number of Channels for Air and R-134a Side	$N_{c\_a,ref}$	8, 8	-
Total Area Required	A_t	1.169	m^2
Overall Heat Transfer Coefficient	UA	13.41	W K^{-1}
Nusselt Number of Air & R-134a Side	$Nu_{\_a,ref}$	3.54, 3.71	-
Reynold Number of Air & R-134a Side	$Re_{\_a,ref}$	181, 1788	-
Average Heat Transfer	$\dot{Q}_{avg}$	1.4	kW
Average Pressure Drop	ΔP	250	kPa

4.1.1.1 Effect of Mass flow Rate on Average Heat Transfer

To analyze the average heat transfer behavior in different shapes of microchannel geometries like square, circular, triangular and rectangular as shown in Figure 4.1. Which is plotted in between mass flow rate of exhaust air against average heat transfer. As the mass flow rate of exhaust air increases, the average heat transfer from air to R-134a increases according to heat transfer principle that have directly proportionality relationship in between them. The maximum average heat transfer value of about 1.4 kW is observed in case of circular channel geometry at mass flow rate of 0.048 kg s^{-1}. Which is more than any other channel geometries and minimum average heat transfer is seen in case of triangular channel geometry. The reason is that circular channel geometry has maximum area contact in term of heat transfer in between air and R-134a as compare to other surfaces.

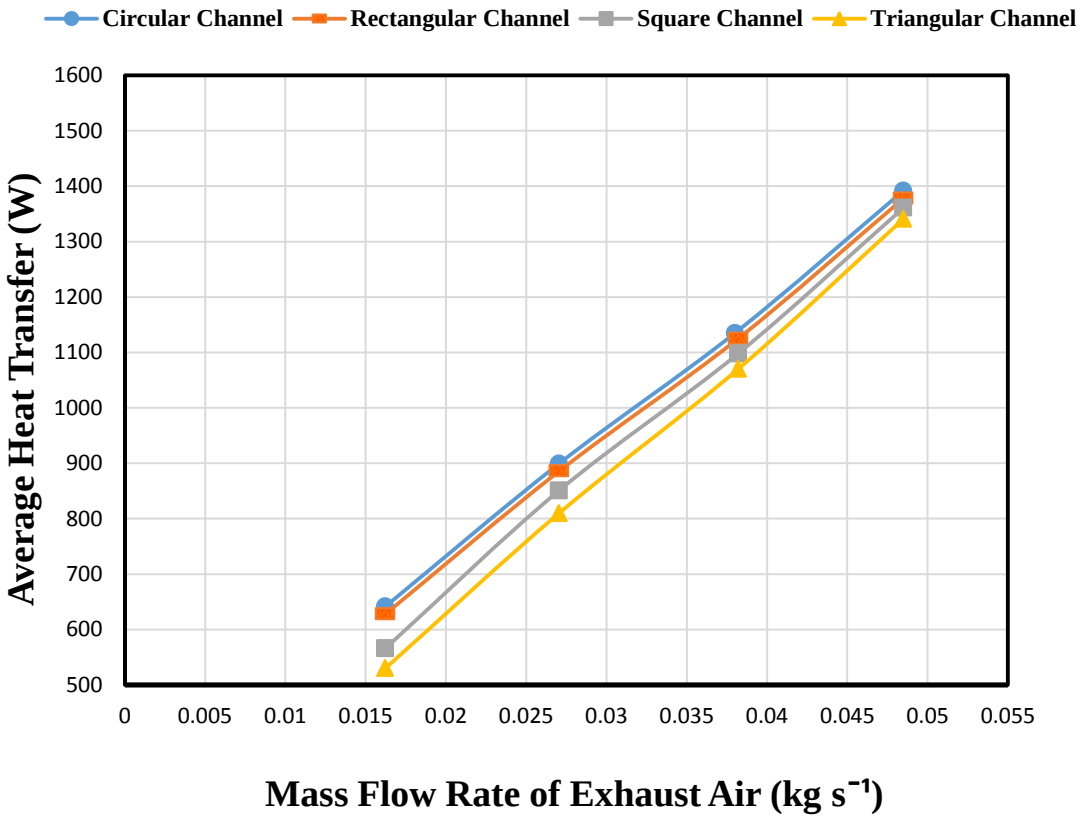

Figure 4.1: Effect of mass flow rate on heat transfer

4.1.1.2 Effect of Reynold Number on Heat Transfer Coefficient

The graph as shown in Figure 4.2 is plotted against Reynold number verses heat transfer coefficient. Which shows that increases of Reynold number causes to increase of turbulence in the fluid flow due to which 'h' heat transfer coefficient increases. Reynold number also has the highest effect on systems efficiency and performance with respect to pressure drop. Circular channel gives best performance regarding heat transfer coefficient but have lower pressure drop as compare to other channel shapes. Whereas rectangular channel gives better performance after the circular channel.

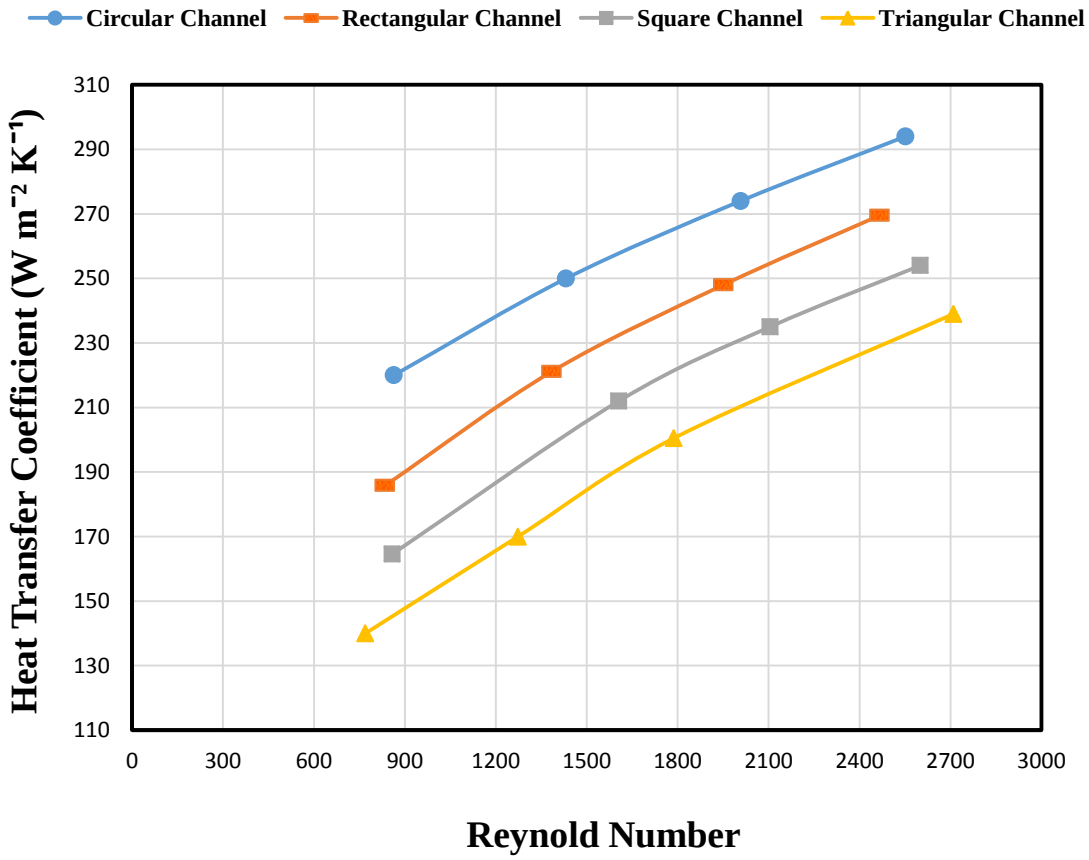

Figure 4.2: Effect of Reynold number on heat transfer coefficient

4.1.1.3 Effect of Mass Flow Rate of Air on Overall Heat Transfer Coefficient

Similar to individual heat transfer coefficient as described above, overall heat transfer coefficient graph in Figure 4.3 is plotted against mass flow rate of air. Which also depicts that circular channel have highest value of overall heat transfer coefficient. Whereas triangular channel have lowest due to less surface area contact for transferring heat energy in between respective fluids through wall and results in more thermal losses.

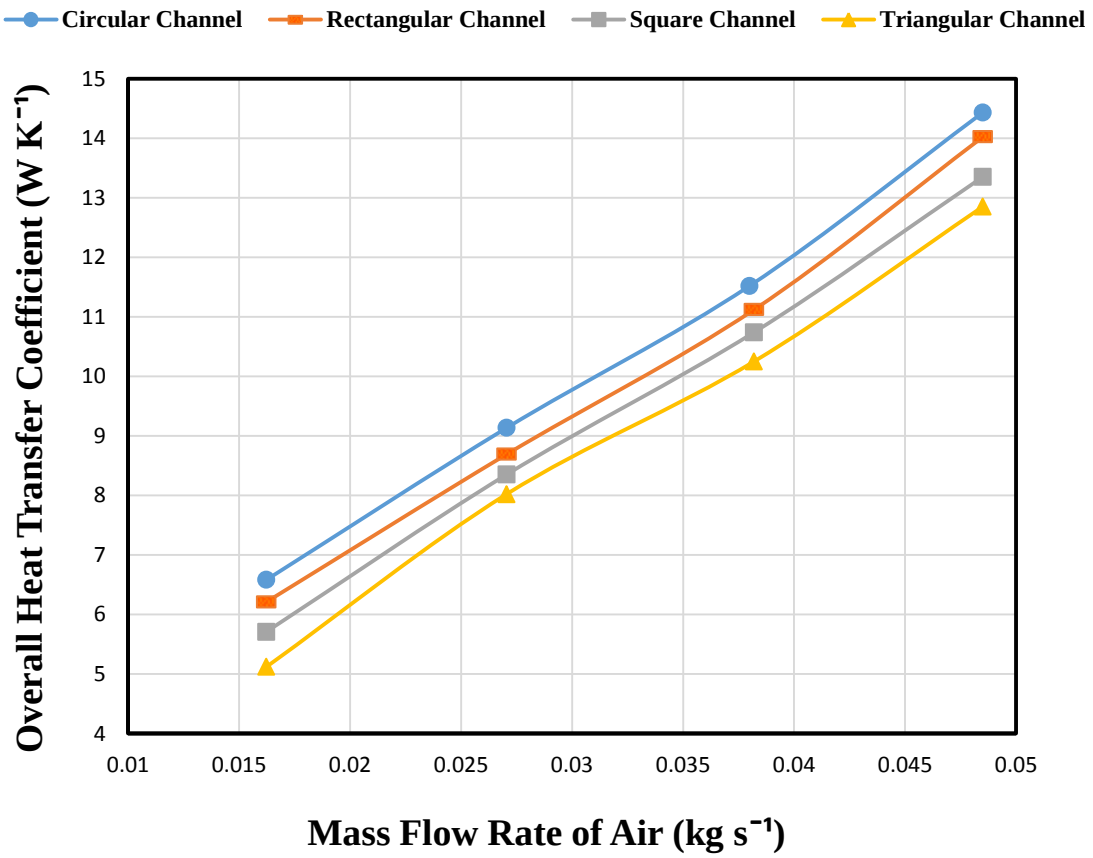

Figure 4.3: Effect of mass flow rate of exhaust air on overall heat transfer coefficient

4.1.1.4 Effect of Mass Flow Rate of R-134a on Maximum Heat Transfer

The graph plotted in between mass flow rate of R-134a and the maximum heat transfer rate as shown in Figure 4.4. The result shows the availability of maximum heat transfer increases with the increase of mass flow rate of R-134a at constant mass flux of exhaust air because at lower mass flux of air, heat transfer to R-134a is lower but as we increases the mass flow rate of R-134a in smaller diameter of channel geometry from 30 kg s^{-1} to 90 kg s^{-1}, heat transfer gradually increases. Circular channel topped again regarding maximum heat transfer and lower pressure drop in channel geometry.

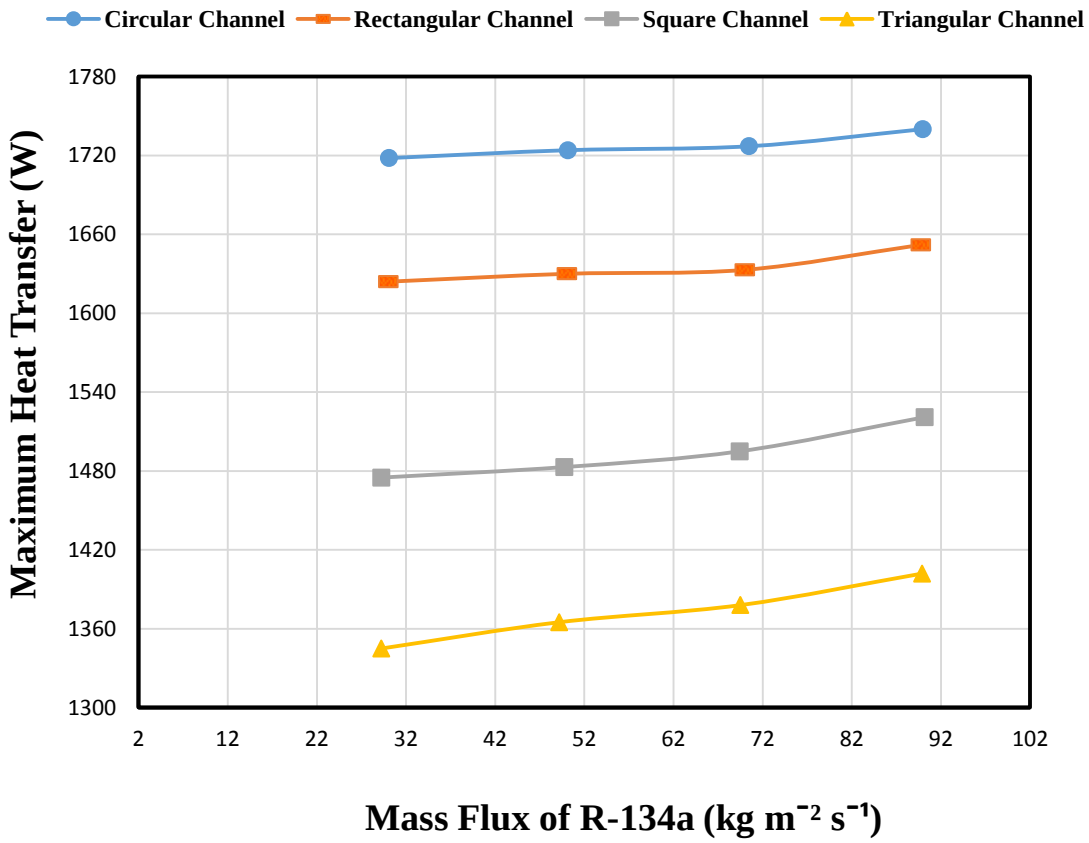

Figure 4.4: Effect of mass flow rate of R-134a on maximum heat transfer

4.1.2 Pressure Drop

4.1.2.1 Effect of Reynold Number on Pressure Drop

The graph is plotted in between pressure drop and Reynold number for various types of microchannels configuration as shown in Figure 4.5. Which depicts that the pressure drop increases linearly with the increase of Reynold number along the channel length. When Reynold number increases, average velocity of fluid rises that leads to transition from laminar flow to turbulent flow and due to that turbulence effect inside microchannels. The pressure drop increase along with increasing effect of heat transfer coefficient. The maximum pressure drop is occurred in case of triangular shaped channel due to lowest hydraulic diameter and minimum in case of square shaped channel due to larger hydraulic diameter.

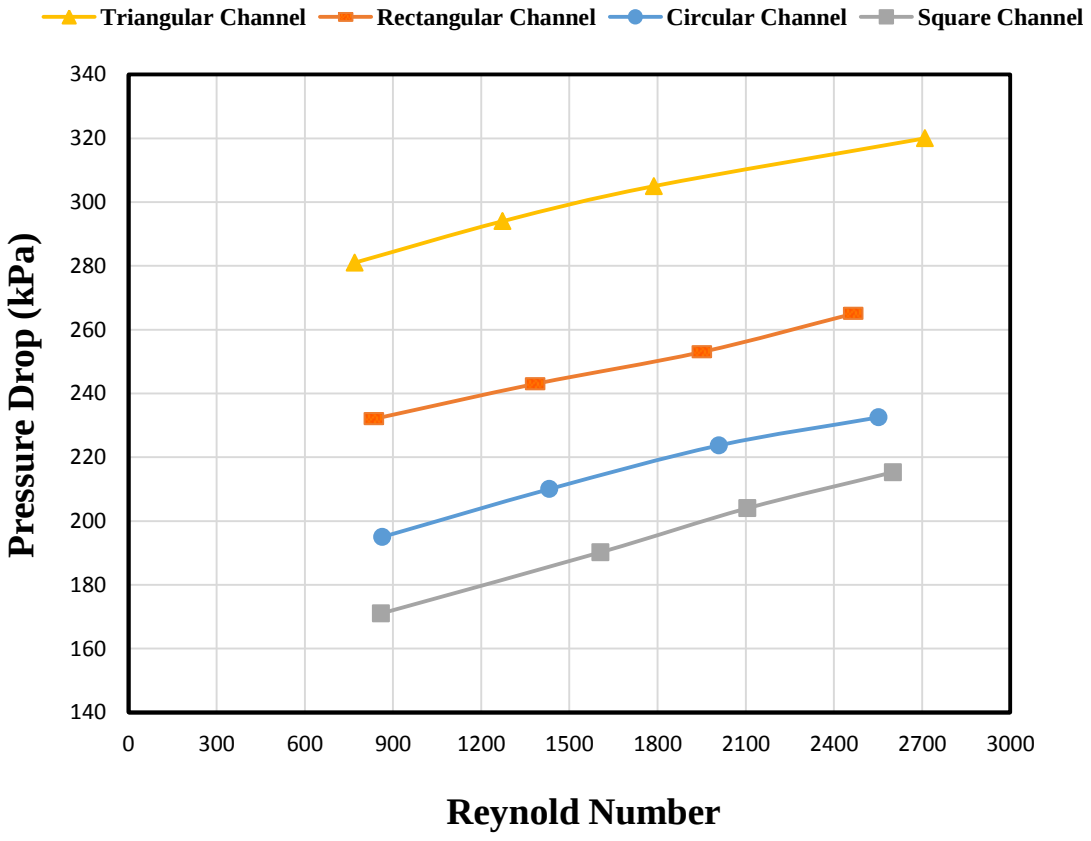

Figure 4.5: Variation of pressure drop against Reynold number

4.1.2.2 Effect of Microchannel Length on Pressure Drop

Variation of pressure drop along the length of microchannels of different shapes of microchannels is shown in Figure 4.6. Which shows that with the increment of channel length, pressure drop also increases respectively. Triangular channel has highest pressure drop of 327 kPa among other channels of various shapes due to its geometrical configuration and lower value of channel hydraulic diameter. Whereas square shaped microchannels has lowest pressure drop of 218 kPa because of having larger hydraulic channel diameter and larger cross sectional area. It is to be noted that the microchannels with various shapes have different volume or hydraulic diameter even though they occupied similar total volume for the overall microchannel heat exchanger system.

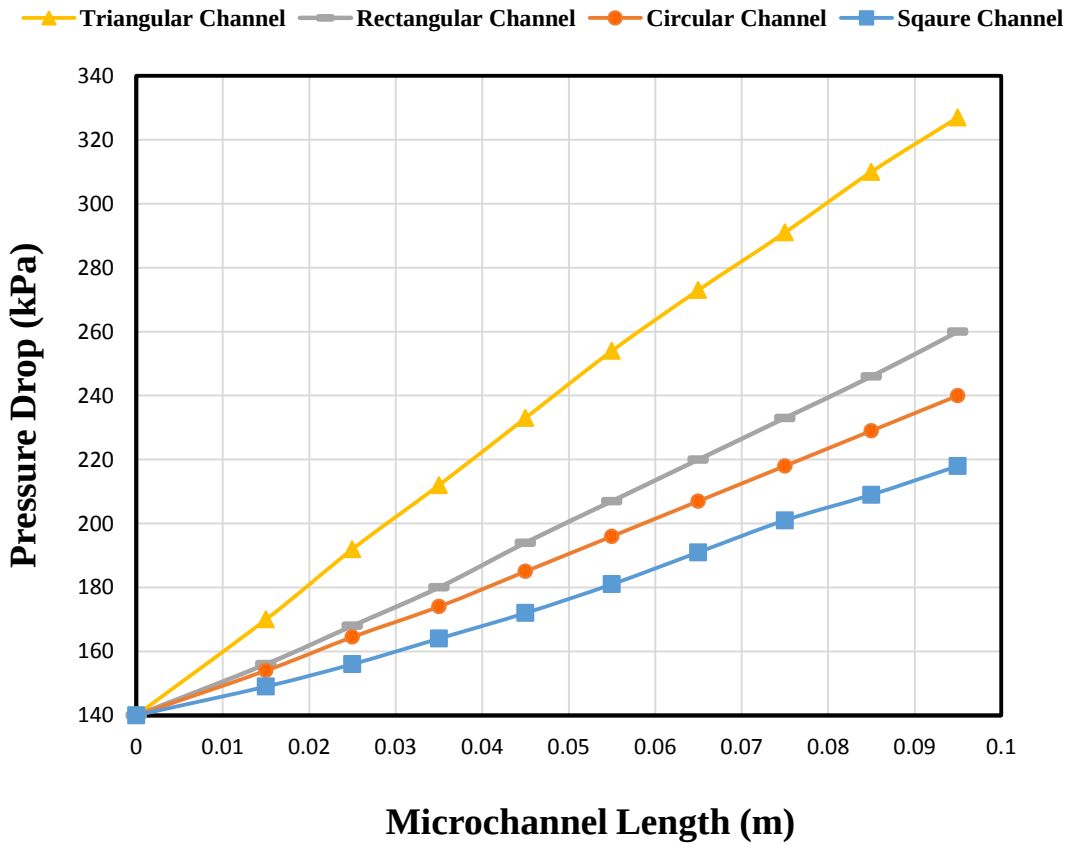

Figure 4.6: Distribution of pressure drop on channel length of different geometries

4.1.2.3 Effect of Pressure drop on Number of Channels

The variation of pressure drop over number of different shaped of microchannels has been shown in Figure from 4.7 to 4.10. Which shows variation of pressure drop is proportional to the number of channels over different Reynold number values. At higher value of Reynold number, pressure drop is higher due to transition from laminar flow towards turbulent flow and maximum pressure drop is seen in case of triangular shaped channels in comparison to other shaped channels. The channel hydraulic diameter also plays vital role in heat transfer and pressure drop results. Although reducing channel hydraulic diameter for different shapes of geometry is responsible for higher thermal performance that leads towards higher pressure drop too. However, decreasing or increasing size of microchannel in cross flow heat exchanger depends on the suitable application like space applications. Where pressure drop must be controlled and minimized across the system because the cost associated with the total mass of system (motors, pumps) is incredible higher. Therefore the size of channels is increases to avoid from higher pressure drop against increase heat transfer.

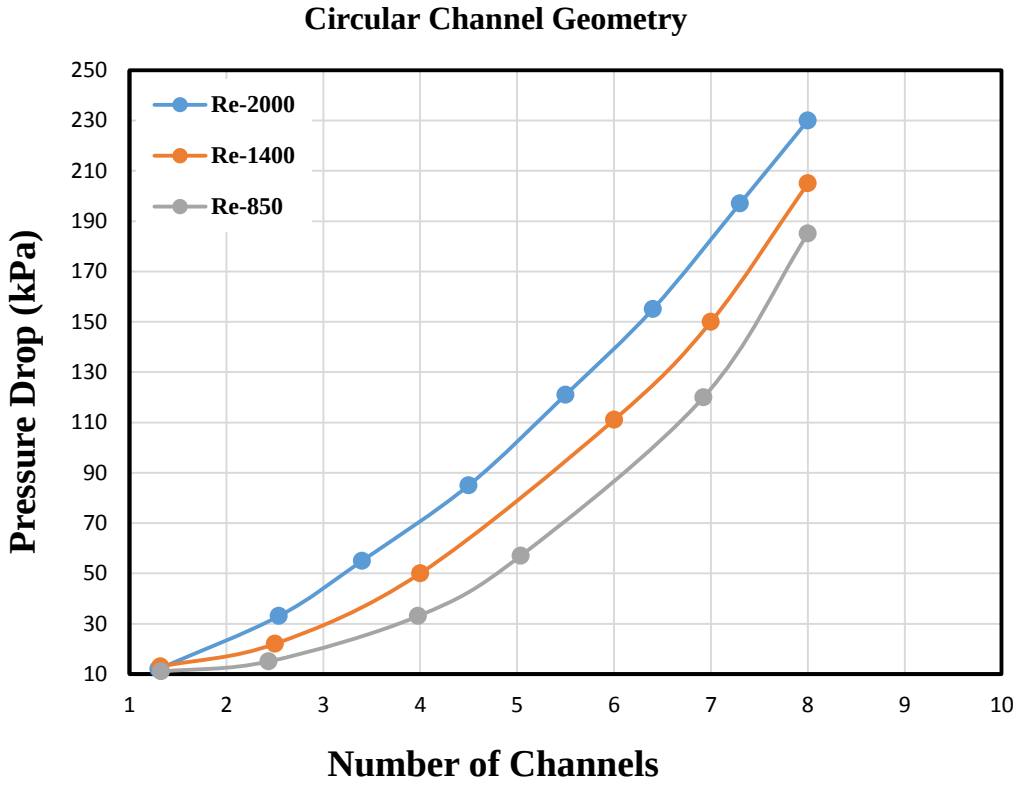

Figure 4.7: Distribution of pressure drop on channel length of different geometries

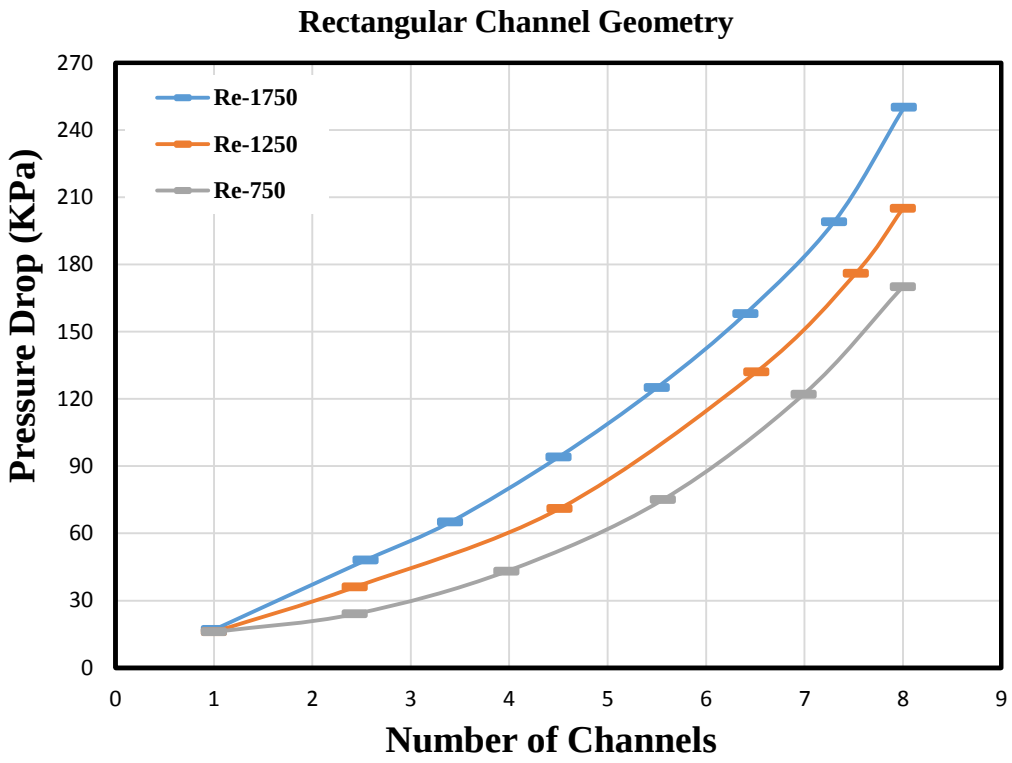

Figure 4.8: Distribution of pressure drop on channel length of different geometries

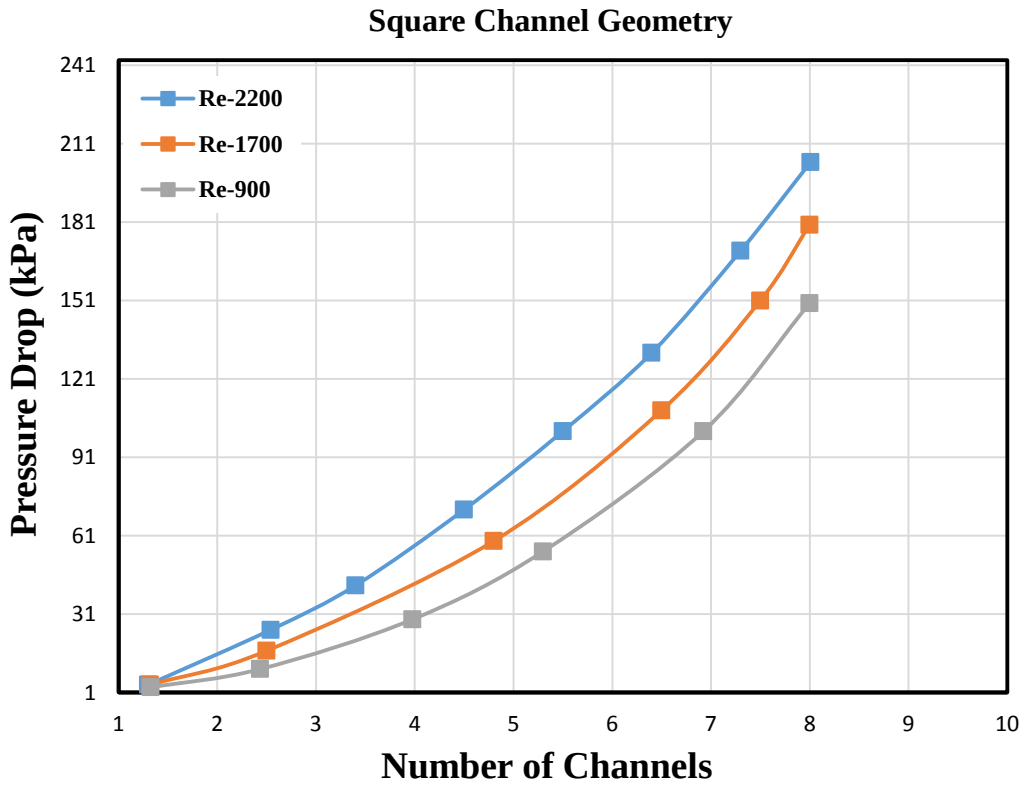

Figure 4.9: Variations of pressure drop against number of square channels

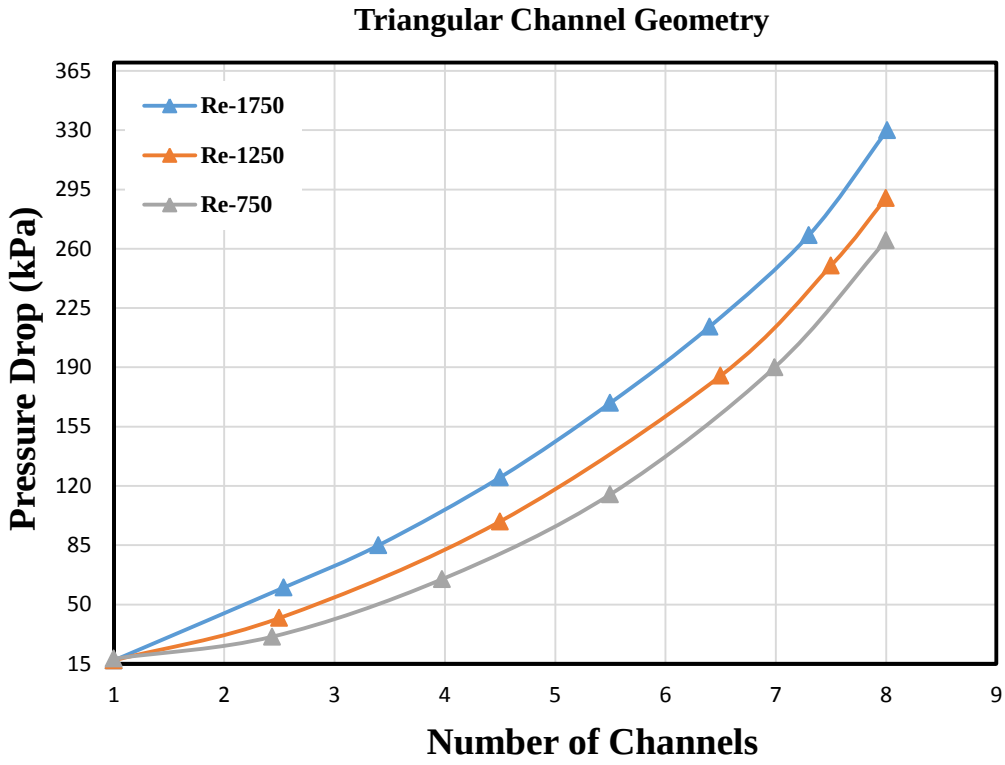

Figure 4.10: Variations of pressure drop against number of triangular channels

4.1.3 Effectiveness

4.1.3.1 Effect of Effectiveness over Number of Channels

As Figure 4.11 to 4.14 shows the effect of effectiveness against the number of different shaped of channels at different Reynold numbers. The effectiveness increases with the increases number of channels because of decreasing volume of channels and increasing heat transfer surface area for the fluids to be in contact. That's a reason, microchannel have higher heat transfer coefficient with respect to smaller volume and ability to overcome the larger pressure drop occurring in the system. With the increasing effect of Reynold number, the value of effectiveness decreases gradually due to increase of flow velocity of fluid and therefore residual time for fluid to contact with surface area of channel is decreases. It has been observed that at lower values of Reynold number, the effectiveness of heat exchanger increases with the increase number of channels and vice versa. To get better thermal performance, the system should be divided into number of smaller channels to increase heat transfer area and work under lower values of Reynold number. But there is disadvantage associated with smaller channels is the increase of pressure drop across microchannel heat exchanger.

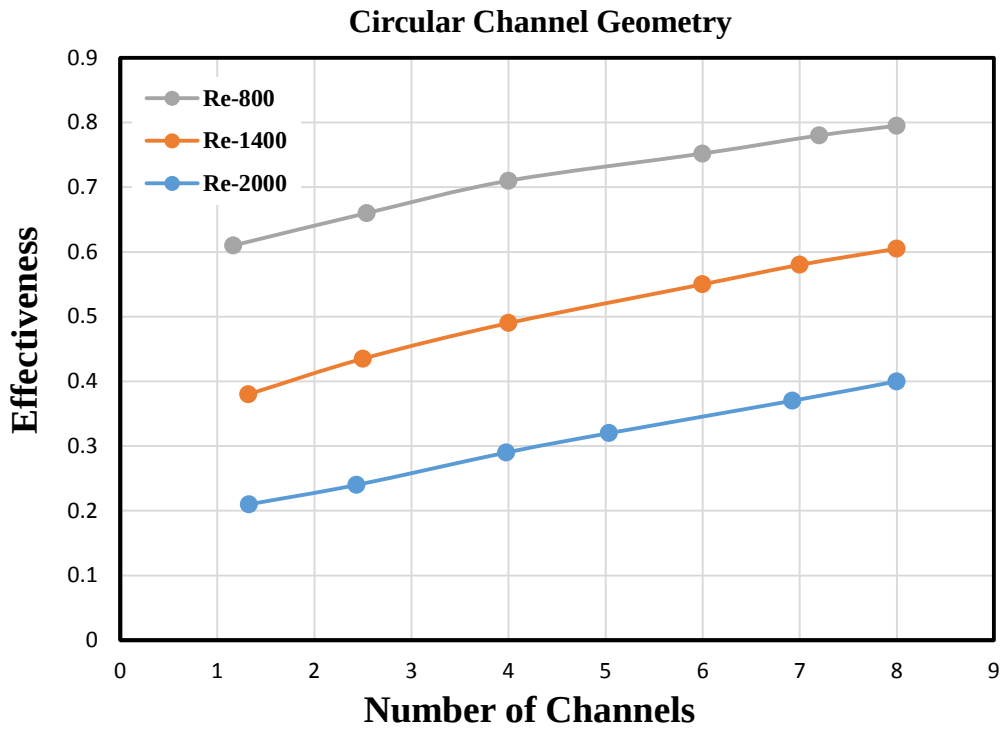

Figure 4.11: Variations of pressure drop against number of triangular channels

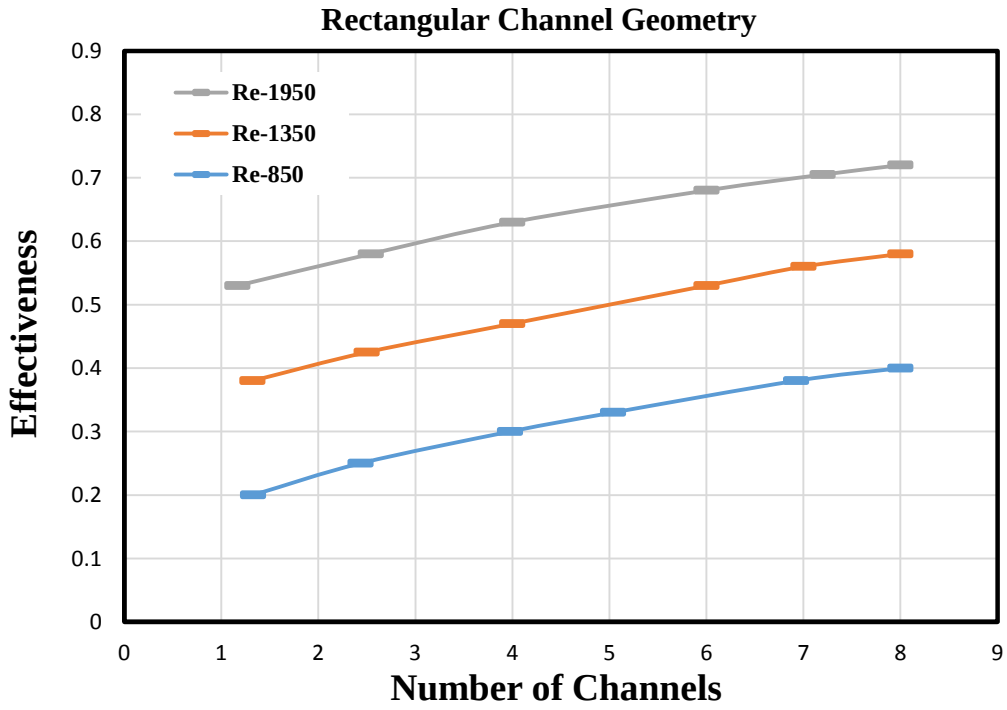

Figure 4.12: Variations of pressure drop against number of triangular channels

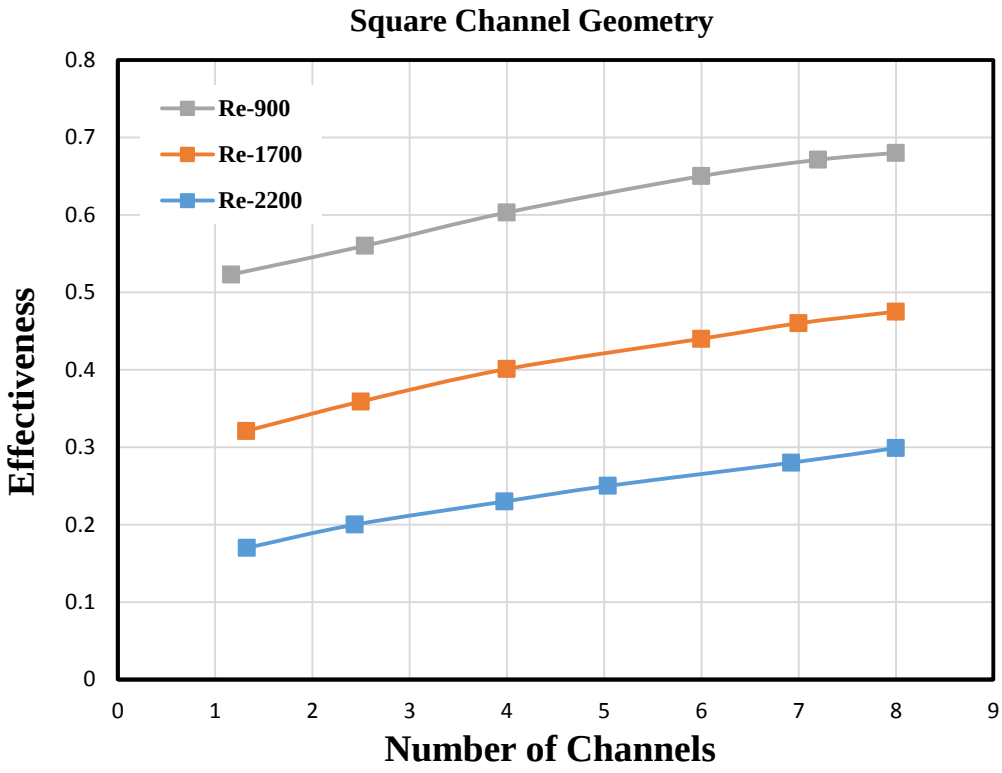

Figure 4.13: Variations of pressure drop against number of triangular channels

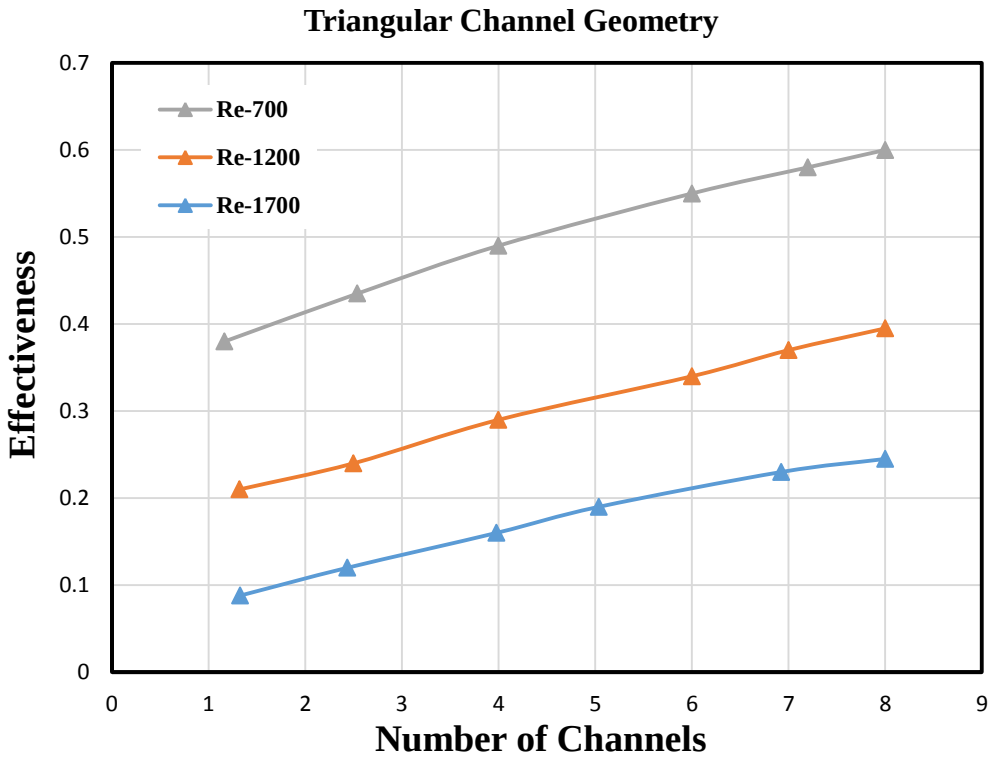

Figure 4.14: Variations of pressure drop against number of triangular channels

4.1.4 Heat Transfer Coefficient

4.1.4.1 Effect of Heat Transfer Coefficient over Number of Channels

The variation of heat transfer coefficient in each number of shaped channels at different hydraulic diameter is shown in Figure from 4.15 to 4.18. Which shows that the magnitude of heat transfer coefficient for various shaped of channels is decreases when hydraulic diameter of channels is increases. The reason is that pressure drop in larger hydraulic diameter is smaller and flow becomes fully developed laminar and there is no sign of vertices formation or turbulence inside channels. Also due to the difference of hydraulic diameter of channel which is caused by difference of area and perimeter of channels, the heat transfer coefficient in each channel is different. As the average heat transfer coefficient for all channels shaped is approximately symmetrical with respect to the center line of channel. However overall microchannels heat exchanger gives higher heat transformation for smaller hydraulic channel diameter. But circular channels at lower diameter has highest heat transfer coefficient value. Whereas rectangular comes after circular channel.

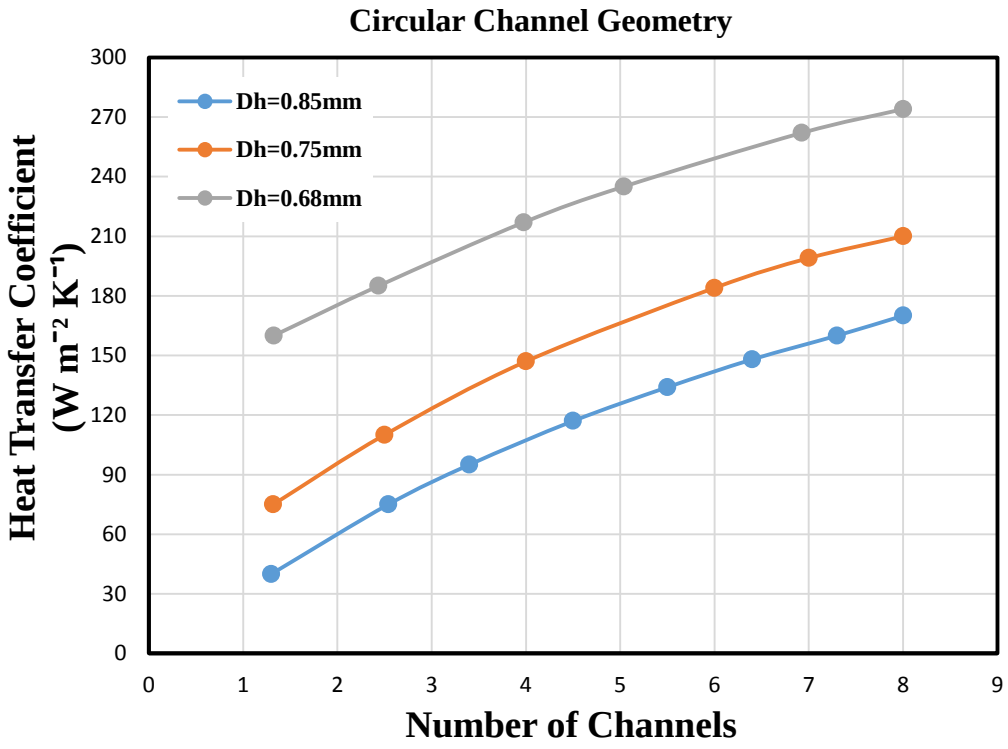

Figure 4.15: Effect of heat transfer coefficient against number of circular channels

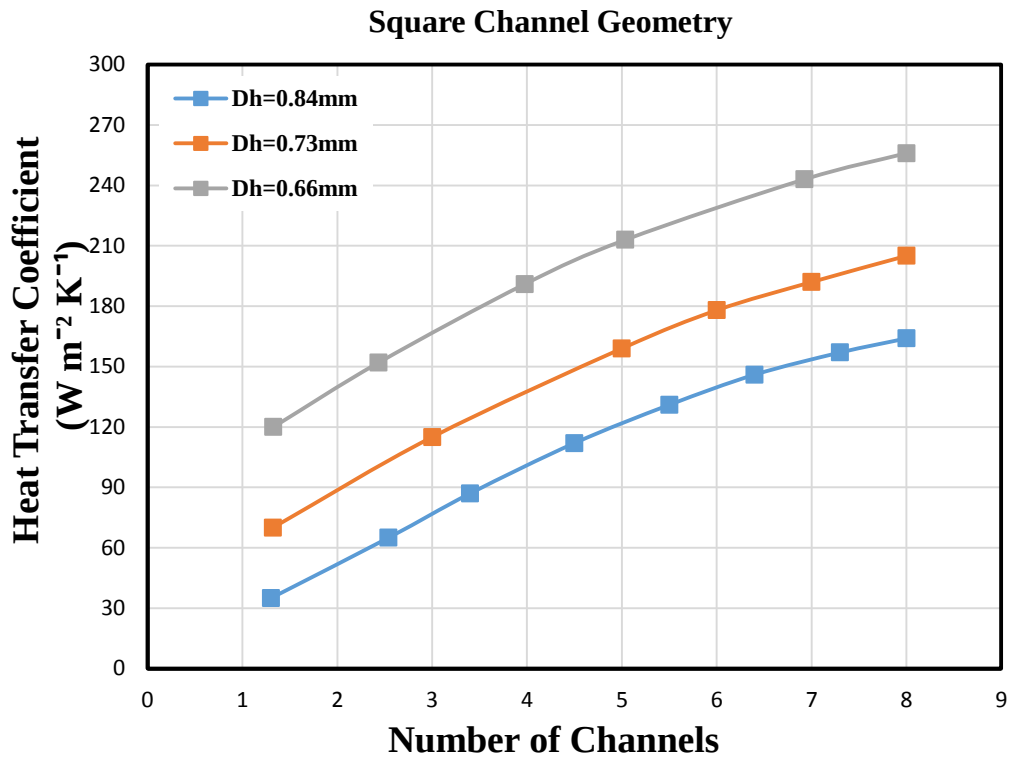

Figure 4.16: Effect of heat transfer coefficient against number of square channels

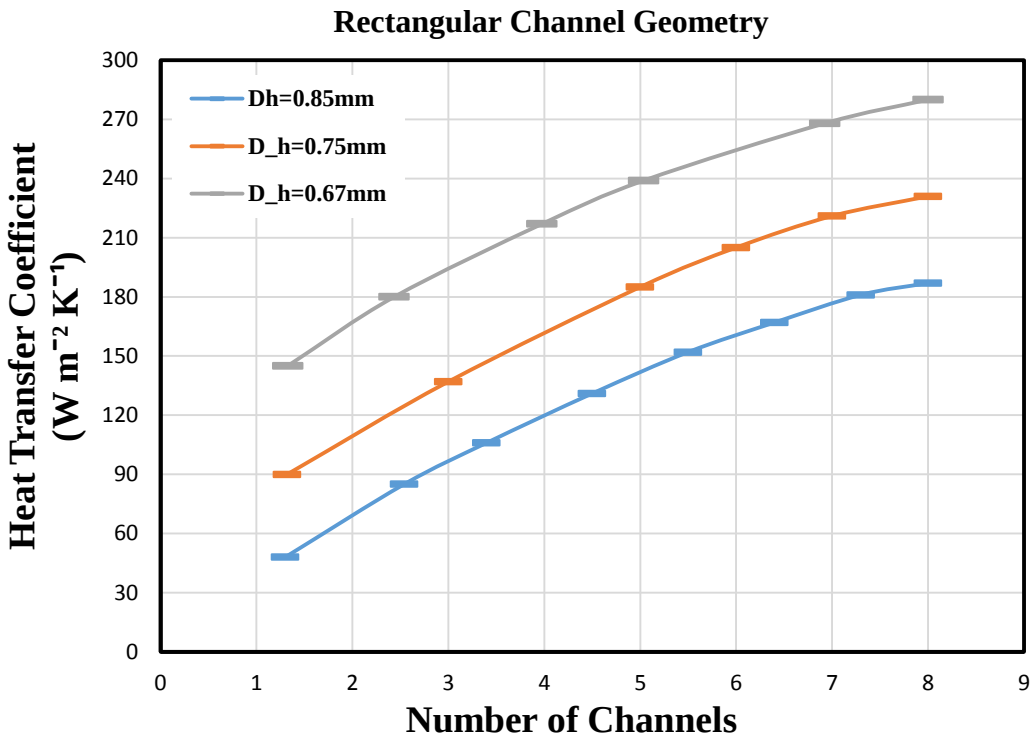

Figure 4.17: Effect of heat transfer coefficient against number of rectangular channels

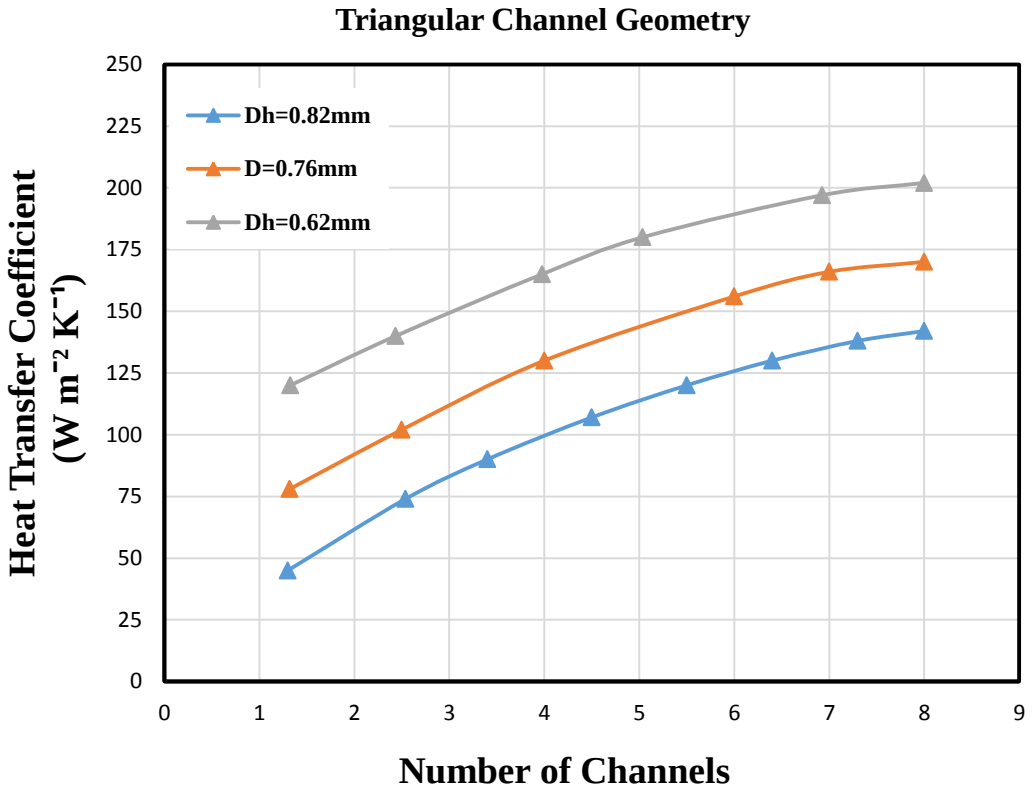

Figure 4.18: Effect of heat transfer coefficient against number of triangular channels

4.2 Theoretical and Experimental Validation

4.2.1 Comparison with Murat Model

To validate our theoretical model based on Engineering Equation Solver Program, a comparison was made possible with the experimental model of Murat Cetin et al. as shown in Figure 4.19 to 4.21. There is an excellent agreement seen of theoretical results with the data points of experimental model by using Kays and Crawford's correlation of Nusselt number for laminar fully developed flow inside rectangular plate fin microchannel as given in equation below.

$$Nu = \frac{h \times D_h}{K_f} = [8.235 \times (1 - 1.883\alpha_c + 3.767\alpha_c^2 - 5.814\alpha_c^3 + 5.361\alpha_c^4 - 2\alpha_c^5)] \times \left(\frac{\mu_b}{\mu_w}\right)^{-0.14} \quad (4.1)$$

As Table 4.2 represents the geometrical detail with input data and Table 4.3 shows output data obtained from EES code. Whereas complete EES code is given in Appendix-A.

Table 4.2: Input data obtained from Murat experimental model [5]

Input Variables	**Symbols**	**Values**	**Units**
Avg Temp. Inlet Cooling Fluid	T_{avg_a}	309	K
Working Fluid Inlet Temperature	T_{out_w}	337	K
Cooling Fluid Inlet Temperature	T_{a_in}	297	K
Cooling Fluid Outlet Temperature	T_{a_out}	318	K
Hydraulic Diameter of Water Channel	D_{h_w}	656	µm
Hydraulic Diameter of Air Channel	D_{h_a}	687	µm
Length, Width, Height of HEX	L, W, H	105, 56, 109	mm
Mass Flow of Cooling Fluid	$\dot{m}_a$	0.013-0.0053	kg s^{-1}
Mass Flow of Working Fluid	$\dot{m}_w$	0.09-0.024	kg s^{-1}
Thickness of Wall	δ_w	100	µm

Table 4.3: Output results of rectangular plate fin microchannel heat exchanger

Output Results	Symbols	Values	Units
Working Fluid Outlet Temperature	T_{out}	318	K
Average Heat Transfer	$\dot{Q}_{avg}$	0.496	kW
Maximum Heat Transfer	$\dot{Q}_{max}$	0.528	kW
Average Pressure Drop	ΔP	0.033	bar
Total Area Required	A_t	1.169	m^2
Heat Transfer Coefficient for Water Side	h_w	7147	$W\ m^{-2}\ K^{-1}$
Heat Transfer Coefficient for Air Side	h_a	302.2	$W\ m^{-2}\ K^{-1}$
Overall Heat Transfer Coefficient	UA	24.7	$W\ K^{-1}$
Total Volume of Heat Exchanger	V	0.00064	m^2
Total Thermal Resistance	R_t	0.0128	$K\ W^{-1}$
Nusselt Number of Air Side	Nu_a	7.71	-
Nusselt Number of Water Side	Nu_w	7.38	-
Number of Channels for Water Side	N_w	6	-
Number of Channels for Air Side	N_a	7	-
Prandtl Number for Water Side	Pr_w	3.353	-
Prandtl Number for Air Side	Pr_a	0.706	-
Reynold Number for Water Side	Re_w	21.5	-
Reynold Number for Air Side	Re_a	127	-
Overall Surface Efficiency for Water Side	η_w	0.76	-
Overall Surface Efficiency for Air Side	η_a	0.89	-
Effectiveness of Heat Exchanger	E	0.94	-
Stanton Number for Water Side	St_w	0.1025	-
Stanton Number for Air Side	St_a	0.0861	-

4.2.2 Effect of Outlet Temperature with Mass Flow Rate of Water

A comparison on the basis of theoretical results is done with the experimental model of Murat Cetin as shown in Figure 4.19. Which is plotted in between outlet temperature and mass flow rate of water to observe the heat transfer behavior. The result shows that increases in mass flow rate of water results in increases of outlet temperature of water, while decreasing mass flow rate of air. Because it's very complex for water to exchanger more thermal energy with air due to its higher mass flow rate and less time of contact with surface area of geometry. That's result in higher outlet temperature of water.

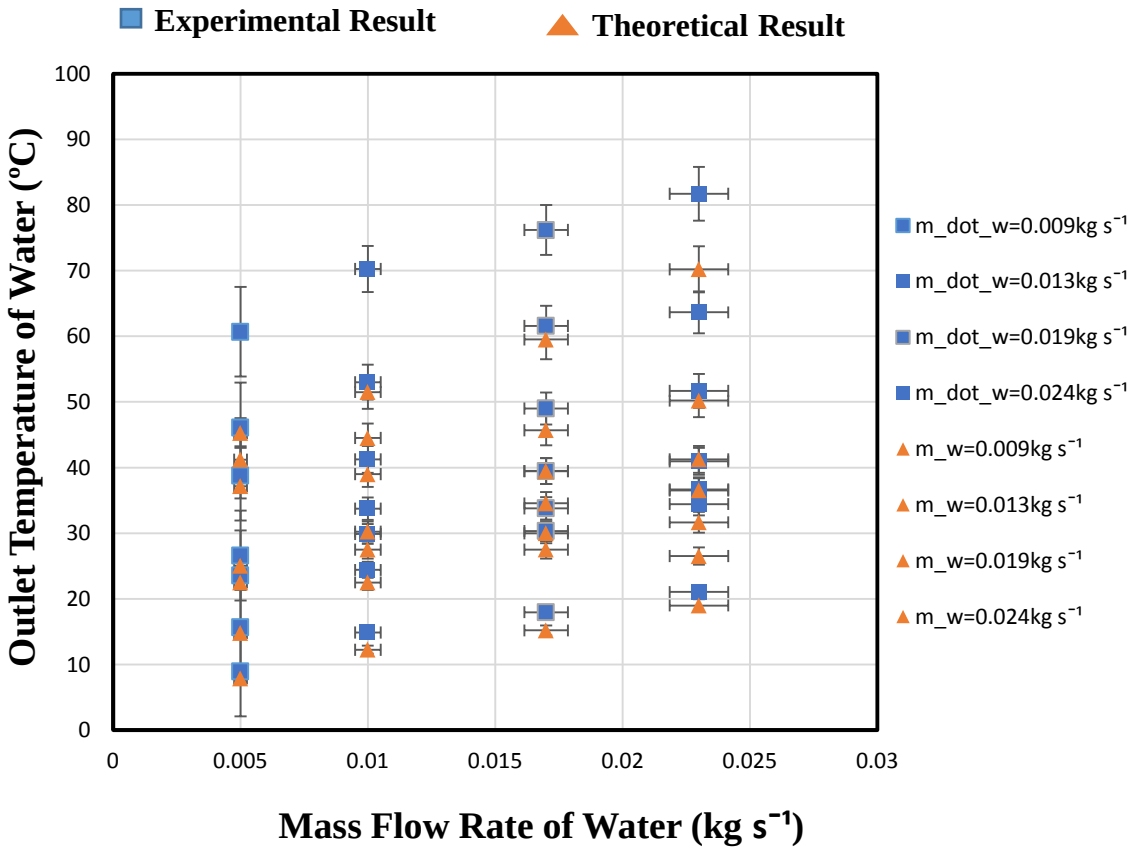

Figure 4.19: Validation of results at outlet temperature verses mass flow rate of water

4.2.3 Effect of Pressure Drop with Mass Flow Rate of Water

Comparison with the experimental model as in Figure 4.20, which shows that experimental results are closer to the theoretical data points with a very minor difference due to some thermal losses occurring during experimentation. Which might be neglected. The graph actually explain the increasing behavior of pressure drop in microchannels during increases of mass flow rate of water. Which can be seen that at lower mass flow rate, pressure difference is lower. However with the increase of mass flow rate of water, the drop of pressure is gradually increases due to transition from laminar to turbulent flow that causes the increasing effect of pressure difference. As overall pressure drop in experimental model is little bit higher as compare to theoretical data point.

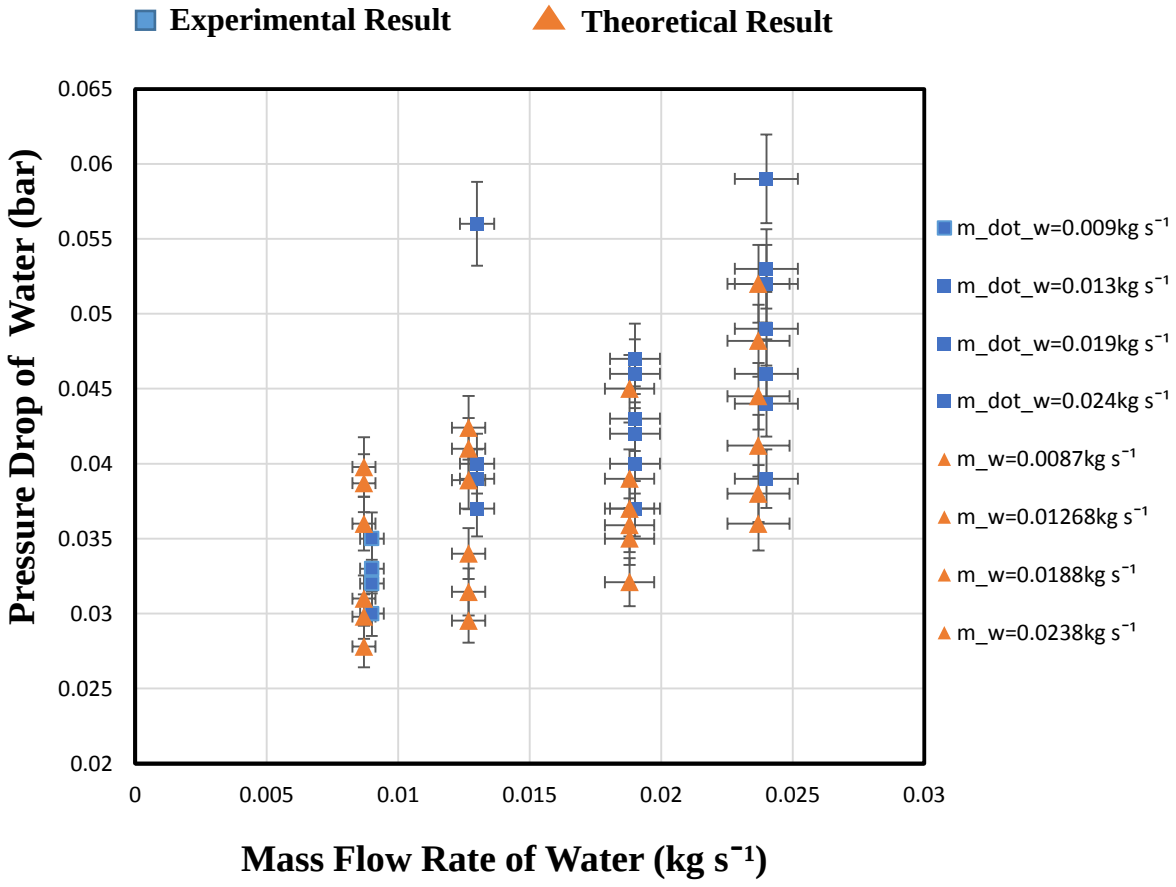

Figure 4.20: Validation of results at pressure drop verses mass flow rate of water

4.2.4 Effect of Effectiveness with Mass Rate of Water

From Figure 4.21, it can visualized that at lower mass flow rate of water, the effectiveness increases about 9-10% with the decreases of mass flow rate of air. While up to 6-7% increase in effectiveness value is obtained at mass flow rate of 0.013 kg s^{-1}. However, the trend observed for the higher mass flow rate is different. The effectiveness of heat exchanger is gradually decreases with decrease mass flow rate of air and increase mass flow rate of water. Because the residual time for water to transfer heat energy to air is reduces and results in decreases of effectiveness of heat exchanger. Although, the theoretical results are approaching towards the experimental one with good agreement.

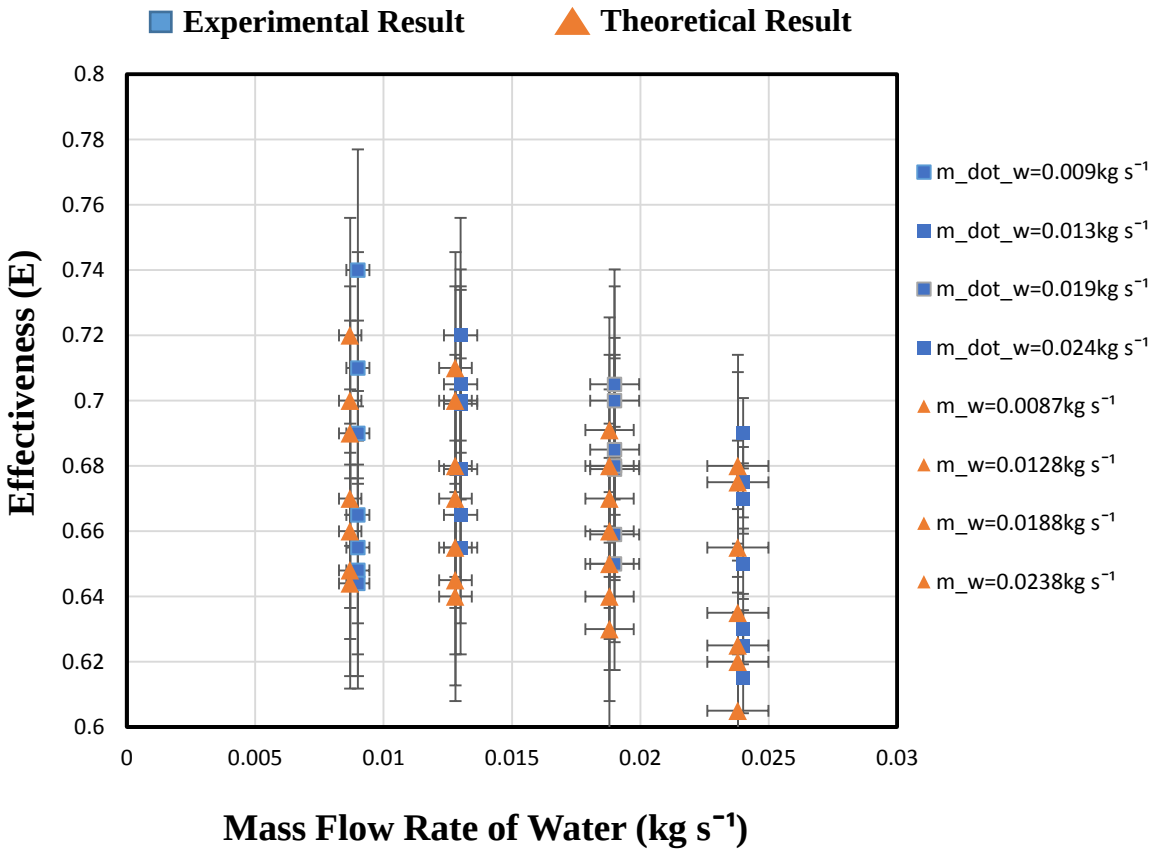

Figure 4.21: Validation of results at pressure drop verses mass flow rate of water

4.2.5 Uncertainty Calculations

For any research work, uncertainty analysis tells us about the reliability of the data that how much our data points are deviating from the mean values. This technique is particularly used for measuring the uncertainty related to different quantitative parameters. In experimental work, we used different instruments to measure physical quantities. Each instrument has an uncertainty associated with its results and is normally provided in equipment's data in the form of a percentage of measured value. Such uncertainty is called as design uncertainty. In above graphical representation, theoretical data points were plotted on flow map of Murat et al. and some little bit uncertainty has been observed in theoretical data points with respect to experimental results as given in Table 4.4 that is calculated for pressure drop, outlet temperature and mass flow rate by using standard deviation formula as shown in Equation 4.2.

Table 4.4: Uncertainty in theoretical results

Parameter	**Uncertainty**
Pressure Drop	± 0.0083kPa
Outlet Temperature	± 4.58^{o}C
Flow Rate	± 0.0017kg s^{-1}

$$S.D = \sqrt{\frac{\sum_{i-1}^{n}(x_i - \bar{x})^2}{n-1}} \tag{4.2}$$

n = Number of data points

$\bar{x}$ = Mean of x_i

x_i= Each value of the data

Summary

In this chapter, comparison of theoretical results with the experimental model of Murat Cetin is validated for the application of waste heat recovery systems and then data points taken from Kubota SQ-14 diesel engine is analyzed on EES program to determine the heat transfer coefficient, effectiveness of heat exchanger, thermal performance and pressure difference relationships for the various shapes of channel geometries like circular, triangular, rectangular and square. It is concluded from results that maximum availability of heat transfer is observed in the case of circular shaped channels due to smaller channel diameter and maximum contact of refrigerant with area of channels and lower heat transfer in case of triangular channel is due to less contact with area of channels geometry and higher pressure drop due to transition from laminar flow towards turbulent flow. The detail in the form of graphical representation between different parameters as given above in chapter 4.

References

[1] Kubota Engine America - SQ Series (CSA Certified), United States.

[2] Klein, S. A., Engineering Equation Solver (EES), F-Chart Software, Madison, WI, 2011.

[3] Yu, S. and Ameel, T. A., "Slip-flow heat transfer in rectangular microchannels," International Journal of Heat and Mass Transfer, vol. 44(22), pp. 4225–4234, 2001.

[4] Rohsenow,W. M., Hartnett, J. P., and Cho,Y. I., "Handbook of heat transfer," vol. 3rd edition., McGraw-Hill, USA, 1998.

[5] A. G. Çetin, Murat, "Design and experimental investigation of a microchannel heat exchanger," Mechanical Engineering, Middle East Technical University, 2010.

Chapter 5: Conclusions and Recommendations

Utilization of waste heat before vented into atmosphere is very important for producing power, cooling and heating the systems by using of microchannels technology. In this research work, different shaped of microchannels are used to recover the waste heat from exhaust of Kubota SQ-14 diesel engine for cooling and heating system through Organic Rankine Cycle (ORC). The data was taken from literature to do comparison with the experimental work of Murat Cetin. Engineering Equation Solver program is used to model the heat transfer equations and determined the heat transfer coefficient, pressure drop, effectiveness of microchannel heat exchanger. From results, following conclusions were drawn and highlighted below.

- Increasing mass flow rate of exhaust air also increases the heat transfer due to transition from laminar to turbulent flow. Circular channel have higher thermal performance and effectiveness due to maximum availability of surface area for fluids to be in contact. Whereas rectangular channel gives better performance followed by the circular channel.
- Reynold number also has the highest effect on systems thermal performance with respect to pressure drop. Circular channels gives best performance regarding overall heat transfer coefficient due to increases of Reynold number. Whereas triangular channel have larger pressure drop due to lowest channel hydraulic diameter.
- Decreasing volume of channel is only feasible option to increase the heat transfer by dividing total volume of system into number of smaller channels. However the pressure drop as well as pumping power also increases too. Therefore the decision in increases or decreases the channels number depends upon the various applications.

Future Work to be recommended

- Comparison with Computational Fluid Dynamics results
- Comparison with two phase flow model

Chapter 6: Two Phase Flow in Microchannels

6.1 Abstract

The study of two phase condensation of R-134a inside rectangular microchannels shows the observation of fluid flow regimes at lower mass fluxes from 75-150 kg m^{-2} s^{-1} at saturation temperatures of 40°C and 55°C and quality from 0.1 to 0.7. The superheated vapors of R-134a is introduced inside multiple rectangular microchannels to partially condensed by applying water in coolant section in a counter wise flow direction to observe the behavior of flow regimes by using Phantom V-310 high speed resolution camera. Engineering Equation Solver program is used to model the governing heat transfer equations and also to determine the vapor quality of R-134a at exist of test section. As the wavy-annular or wavy-stratified flow regimes were observed at given conditions. Data obtained was after that compared with the mini/microchannel flow maps. Which were over predict the occurrence of intermittent flow regimes.

6.2 Introduction

Energy is necessary for the development of any society and also impact on the economic growth of the country. Energy consumption is the main concern that become a serve problem now a days. Natural resources like oil, gas, fossil fuels, biomass and coal are depleting with the passage of time and causes of increase in demand by domestic and industries for heating, cooling and refrigeration systems. The thermal performance of thermal systems depends upon the refrigerant as well as carbon foot prints. Thermal energy generated as a result of heating and cooling can be saved by approximately 50% of the total energy. So, energy can be saved by adopting of efficient energy systems.[1]. According to the US Environmental Protection Agency report of 2014 [2], about 51% of the United State total greenhouse gases being produced by industries and power plants running on major sources of coal, fossil fuels, nuclear, crude oil and natural gases. These sources of energy becoming a causes of global warming and increases amount of carbon footprints in atmosphere that is dangerous not for only animals but also for marine life and human beings. With the increases of population on earth and change of ecosystem, the fossil fuels are depleted day by day and the world is going to shift into renewable technologies to eliminate these carbon foot prints produced by fossil fuels. The

development of renewable technologies are becoming more viable for the designing and working of thermal systems because these are efficient, cost effective, and compact in size and clean energy by its nature.

6.2.1 Refrigerant Selection

As air-water were the initial natural refrigerants used in heat ventilation and air conditioning systems. With the passage of time, different refrigerants came in market upon their usage and they were neglected due to their negative impact on environment. Here R-134a have beneficial effect over others, R-134a replaces the HCFC, ammonia and other gases because of its low value of global warming potential and zero value of ozone depletion potential [3].

6.2.2 Study of Two Phase Flow

The study of two phase flow plays a vital role in transferring of heat energy from one fluid to other fluid. With the usage of microchannels and new refrigerants, there is more research going on visualization of different flow regimes at different operating conditions to observe the behavior of gravitational and surface tensional forces that dominate over each other during two phase flow transitions in thermal systems that have crucial effect on heat and mass transfer mechanism [4].

6.2.3 Mini and Microchannels

The thermal capability and performance of any system can be increases by introducing mini/microchannel technology as shown in Figure 6.1. Microchannels are widely used over the conventional macrochannels in large varieties of industrial applications to yield compact geometries for efficient heat transfer. The reason of high heat transfer coefficient through microchannels/minichannels condensers is compactness and increases of area to volume ratio. Heat transfer in microchannel is mainly depends upon hydraulic diameter of the channel, which is effective enough to produce the partially or fully condensation inside microchannel. Mini/Microchannels are highly recommended in industries for capturing of high heat flux from electronic equipments for cooling and heating purposes [5].

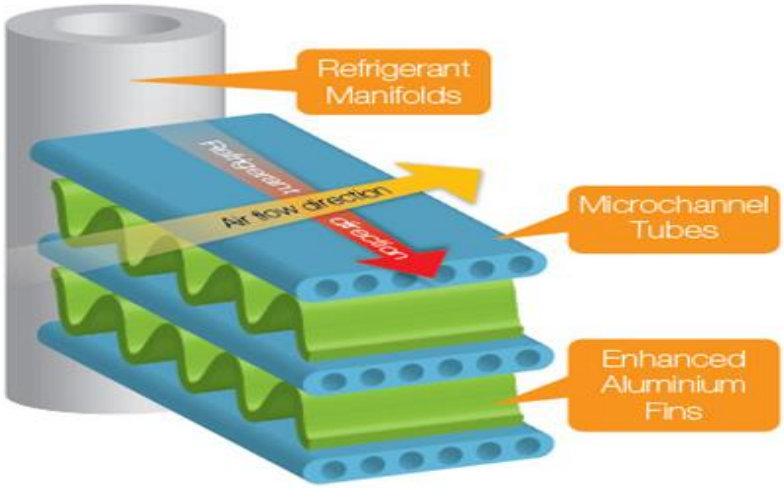

Figure 6.1: Schematic of a microchannel tubes with flow of refrigerants [5]

6.2.4 Objectives

Thus objective of two phase flow study is to visualize the flow regimes of R-134a inside rectangular based microchannels of hydraulic diameter (D_h = 840 μm) by using high speed camera at lower values of flux ranges from 75 to 150 kg m^{-2} s^{-1}. Superheated vapors of R-134a entered into multiple parallel rectangular channels and partially condensed by supplying the deionized water in opposite direction to the flow of R-134a to get desired quality of vapor at the exit of channel section that ranges from 0.1 to 0.7. Whereas R-134a is fully condensed into liquid inside the double copper tube heat exchanger before entering into the gear pump. The experimental data points obtained from LabVIEW program was used to compare with the flow maps of literature.

6.3 Literature Review

Comprehension of two phase flow of various fluid inside the microchannel can be analyzed and studied by the flow regime maps. That depends on nature and thermodynamic qualities of fluid flow, channel shape and their diameter. Many authors searched and proposed models for two phase flow transition of fluids during condensation inside microchannels. In result of condensation of refrigerant inside microchannels, superheated vapors partially condensed by using water as a coolant flowing in counter flow wise direction to the refrigerant flow and converted into the saturated liquid due to the magnitude of gravitational and surface tensional forces that changes with the flow and overcome on each other during the two phase flow transition.

Due to which different types of flow regimes observed like bubbly, plug, slug, wavy, annular, stratified, dispersed and churn flow [5]. Bubbly flow is observed in circular form of vapors at high velocity of fluid flow, intermittent flow is categorized by discontinuity of elongated bullet shape of vapors in the channel by keeping the liquid phase outside periphery of channel. Which is called as slug flow. Dispersed flow is observed and differentiated by presence of dispersed bubble in the liquid phase [6]. Annular flow is distinguished by moving of vapors through core of channel by displacing the uniform liquid films on the upper and lower wall of channel. Where as in wavy flow, vapors sticks to the top of channel by keeping the liquid at the bottom of channel.

Garimella and Coleman [7] conducted various studies on air-water mixture flow in small diameter tubes to analyze flow transitions inside rectangular, circular and triangular channels and visualized different flows including slug, slug-annular, bubbly, wavy and annular-wavy, stratified and annular flow. Wambsgabss et al. [8] conducted experiments on determination of flow regimes in a rectangular microchannel of 5.45 mm diameter and observed transition from bubbly to slug flow by means of rms (root means square) pressure change method. Yang and Shieh [9] observed the behavior of flow transition of R-134a from slug to annular flow inside diameter of microchannel between 1 mm and 3 mm at lowest gas velocities and at larger value of liquid velocities, They noted transition behavior from intermittent flow towards bubbly flow.

Wu and Cheng [10] conducted experiments on trapezoidal silicon microchannels by condensing steam to observe the behavior of different flow arrangements by using inlet pressure along with different mass flux conditions and found annular, slug, droplet and injection flow that are generated as a result of steam condensation in microchannels. Cavallini et al. [11] did experiments in a circular shaped minichannel to determine the heat transfer mechanism. He designed a test facility to analyze the heat flux from temperature distribution of refrigerant in minichannel by supplying cooling water. So, the cooling water flow could increase the heat transfer surface area and minimizes the heat resistant in a better way.

Suo & Griffith [12] studied flow regime of fluids inside the small sized channel geometry under adiabatic condition. He proposed that transition is proceeded into two steps during condensation flow in small hydraulic diameter channel. Initially transition

turned from slug to bubbly flow. Whereas in second stage, transition seen from bubbly to annular flow at higher velocity. He concluded that inertial as well as surface tensional forces are the influential forces in transition of fluid flow.

Taitel and Dukler [13] proposed flow regime transition model based upon five dimensionless parameters. Which are named as stratified-wavy, annular-intermittent, dispersed-intermittent, annular-wavy and intermittent-stratified flow regime as given in Figure 6.2. They found intermittent flow regime in smaller channel of diameter of 0.5 mm at lower value of mass fluxes but at higher flow rates annular flow regime observed due to instability in flow. They also generalized the graph between proposed Martinelli parameter and modified Froude number [14].

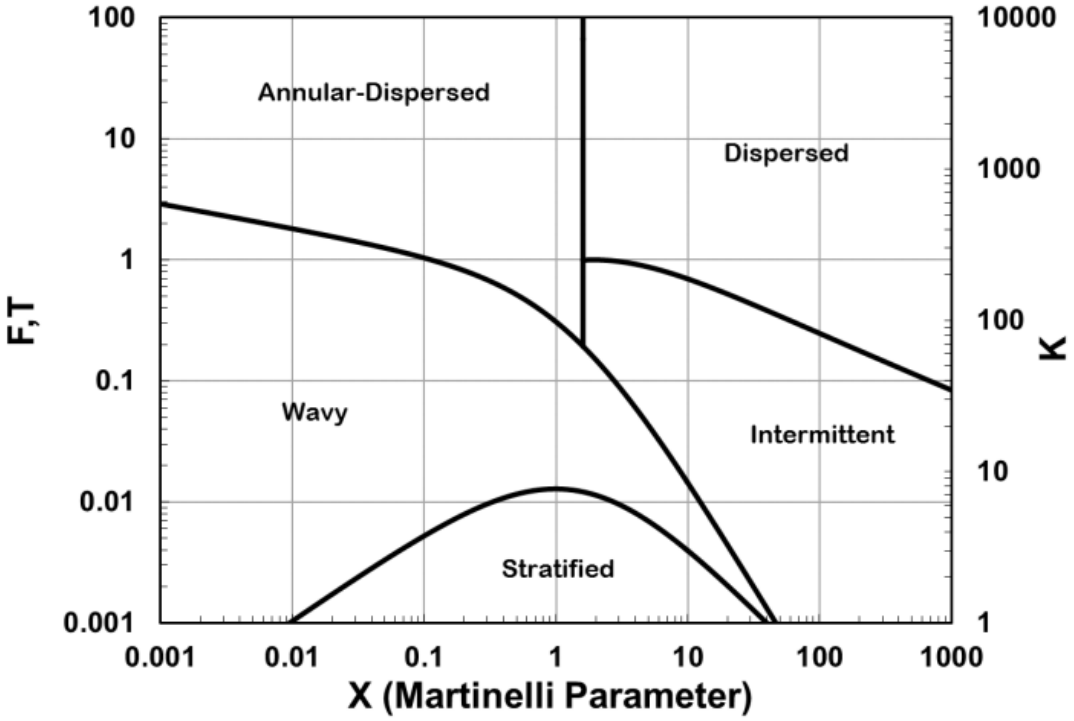

Figure 6.2: Initially flow map predicted by Taital and Dukler

Breber et al. [15] proposed his flow model of condensation that agreed with Taital and Dukler's theoretical model for condensation of two phase flow. They used various refrigerants through circular channels of diameter 4.8 mm-22 mm and observed annular, wavy, and stratified, slug, plug and bubble flow regimes up to maximum pressure of 1248 kPa. They used following dimensionless parameters T, F (Froude number), K, J_g (Superficial vapor velocity) and X (Martinelli parameter) to described adiabatic two

phase flow and suggest gravitational dominated stratified and wavy flow regimes and shear dominated annular flow regimes.

Barnea et al. [16] did early attempts in understanding the influence of decreasing diameters and surface tension forces dominance on adiabatic flow regime transitions. They investigated the behavior of different flow regime by using the air-water mixture in smaller size circular diameter channels ranging from 4 mm-12 mm in both orientation of vertical and horizontal. They modified flow map of Taitel and Dukler and apart from stratified-to-slug flow transition, they found flow regimes of stratified smooth, wavy, intermittent and annular by considering surface tension and gravitational effect. As study of liquid to vapor superficial velocities were under the focus in two phase flow inside microchannels recently [17].

Martinelli [18] and Chisholm [19] studied behavior of different refrigerants in conventional microchannels and proposed correlations related to heat transfer under specific geometric conditions with different flow rates. As there correlations contradict with data of smaller size channels. So, their correlations become basis for the others. Chen et al. [20] modified the model of pressure drop by using the Weber number as well as Bond number in his model to account for the mass flux and surface tensional forces.

6.4 Experimental Test Facility of R-134a

The condensation two phase experimental test facility consisted of refrigerant R-134a, which was conducted over mass flux range ($75 < G < 150$ kg m^{-2} s^{-1}) at saturation temperature ($40 < T_{sat} < 55°C$) and at saturation pressure of ($217 < P_{sat} < 147$ psi) in a rectangular stainless steel microchannel condenser as shown in Figure 6.3 and 6.4 representing schematic layout and photograph of R-134a experimental test facility. Which consisted of three cycles/loops: refrigerant, water and chiller loop. Although, system's loop comprised of four main components of the system: gear micro pump, pre-heater, rectangular microchannel test section, and post-condenser.

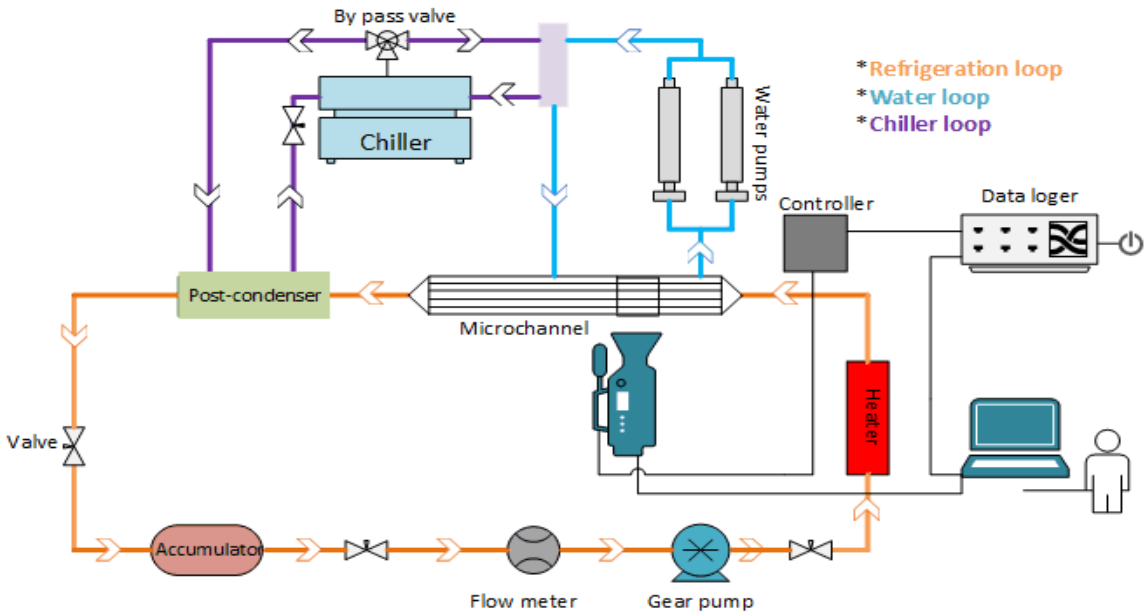

Figure 6.3: Schematic layout of experimental test facility

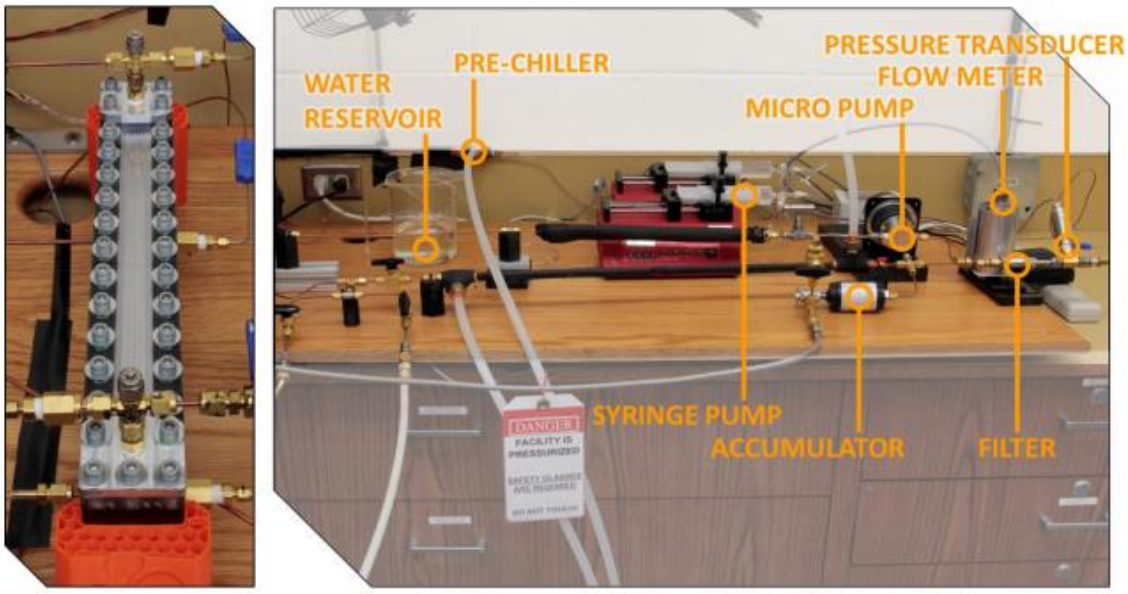

Figure 6.4: Photograph of experimental test facility [27]

Thus experimental facility composed of three loops differentiated by orange, blue and purple colors as shown in Figure 6.3. Before filling of R-134a in the refrigerant section, Vacuum pump was required to create the vacuum inside the system. Which cleaned it thoroughly to create ultimate level of vacuum by running the heavy duty motor. Which had a features of rotary vanes for efficient working. After creating vacuum, refrigerant loop was filled with R-134a through refrigerant R-134a cylinder. Then refrigerant loop

was pressurized by nitrogen gas via accumulator. Hydraulic accumulator consisted of piston cylinder arrangement to compress and raise the pressure of R-134a inside the system by using nitrogen gas. Accumulator had a temperature range from -29ºC to 74ºC with a capacity of 0.02 Liters.

6.4.1 Micro Gear Pump Section

Micro gear pump in Figure 6.5 was manufactured by Micropump to pump the working refrigerant R-134a through the refrigerant loop. The pump was selected on this basis that no lubricating oil or grease will contact with the working refrigerant of the system. Low mass flow rates of refrigerant R-134a in the system can be obtained by available and replaceable variety of small meshing gears. Actually it consisted of meshing gears used to increase the pressure of working fluid and these are mostly used in refrigeration industry to pump the fluid that's having high viscosity. Motor is used to drive the gears through motor shaft and driven magnets. When these small spur gears mesh with each other then they created vacuum at the inlet of the gear pump. Due to pressure difference inside gear and outside atmosphere, the refrigerant sucked inside and move towards outer periphery of meshing gear and result in compressing of refrigerant at the exist of gear pump. Whereas gear pump was controlled by pump controller (KORAD, M/N: KD3005D) [21]. To obtain mass flux in the range between 75-150 kg m^{-2} s^{-1} throughout the five rectangular microchannels, the required volumetric flow rate at pump section was vary in range between 10-25 mL min^{-1}. Micro spur gears provides smooth, precise and pulseless flow and having very negligible slip ratio, maintain long life time due to their small size, chemically resistant, easy to service installation, and proven reliability [21].

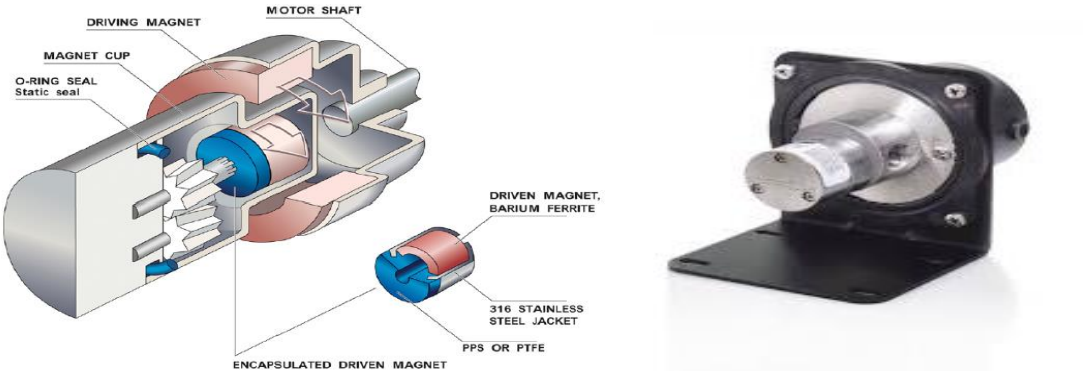

a) (b)

Figure 6.5: (a) Internal over view of micro gear pump (b) External gear pump visualization [21]

6.4.2 Pre-Heater Section

Before entering of refrigerant into the preheater section, the working refrigerant enter into the expansion valve system whose purpose is to control any fluctuations rising from flow of refrigerant inside system. R-134a enter through lead wire into the cartridge pre-heating section as shown in Figure 6.6, where Nichrome material based coil heated by external supply of variac transformer heater (M/N: SC-3M) to heat the refrigerant inside the shell until the superheated vapors formed inside the cartridge heater. To increase the life time of cartridge heater and to reduce the thermal losses to surrounding, outer sheath is covered with insulation rubber foam and aluminum covering. Watlow PID (Partial integration differential) control unit was used to control flow temperature of the cartridge heater. Which depends upon closing and opening of relay to set the system temperature. It was seen through system visualization and inspection, there were unsteadiness in the flow of refrigerant as the cartridge heater was on and off. The heater was operated by using of variac variable voltage controller.

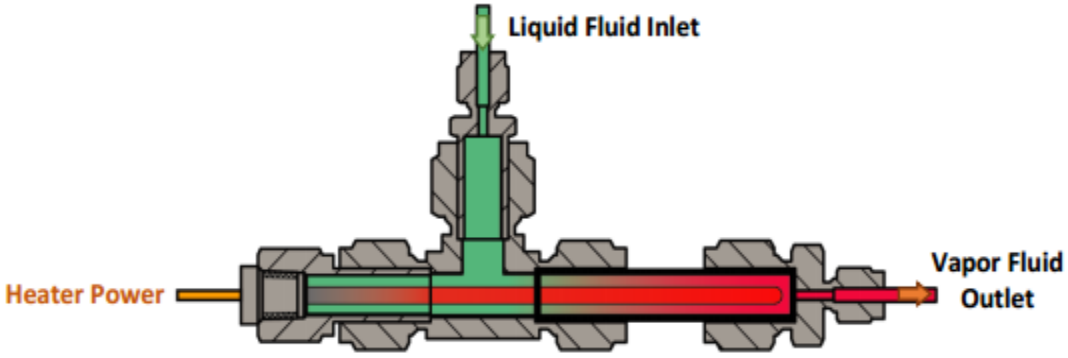

Figure 6.6: Diagram of heating section for vaporizing R-134a [27]

6.4.3 Microchannel Test Section

Next to the Pre-heater section, there was a rectangular based microchannel condenser as shown in Figure 6.7 to 6.9. The material selected for rectangular microchannels was stainless steel due to its flexibility. Whereas channel length was about 290 mm, width 0.794 mm, depth 0.794 mm and hydraulic diameter 0.84 mm. The insulation of condenser was done with wool and thick sheet of aluminum to minimize the heat losses to external environment. When superheated vapors of R-134a enter into rectangular microchannels then they were condensed by cooling water flowing in opposite direction to the

refrigerant flow to partially and fully condense the refrigerant and visualize their different flow regimes by using high speed resolution camera. As detailed specification of rectangular microchannel condenser is given in Table 6.1.

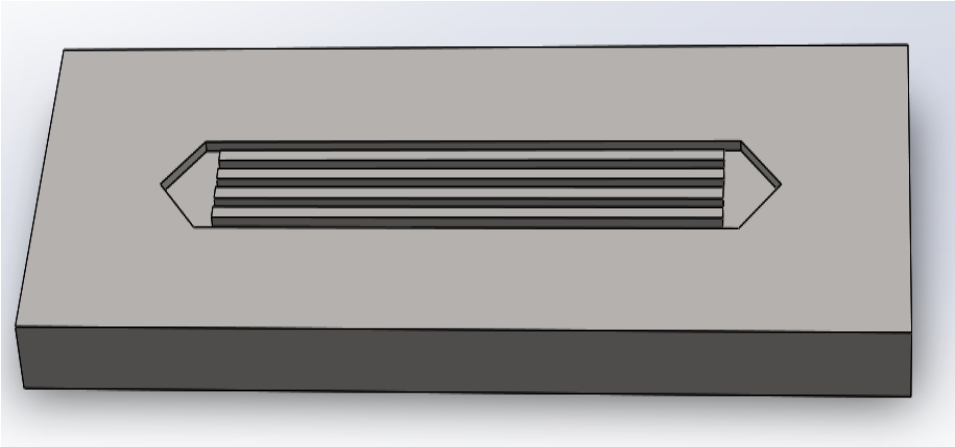

Figure 6.7: Representation of microchannels geometry

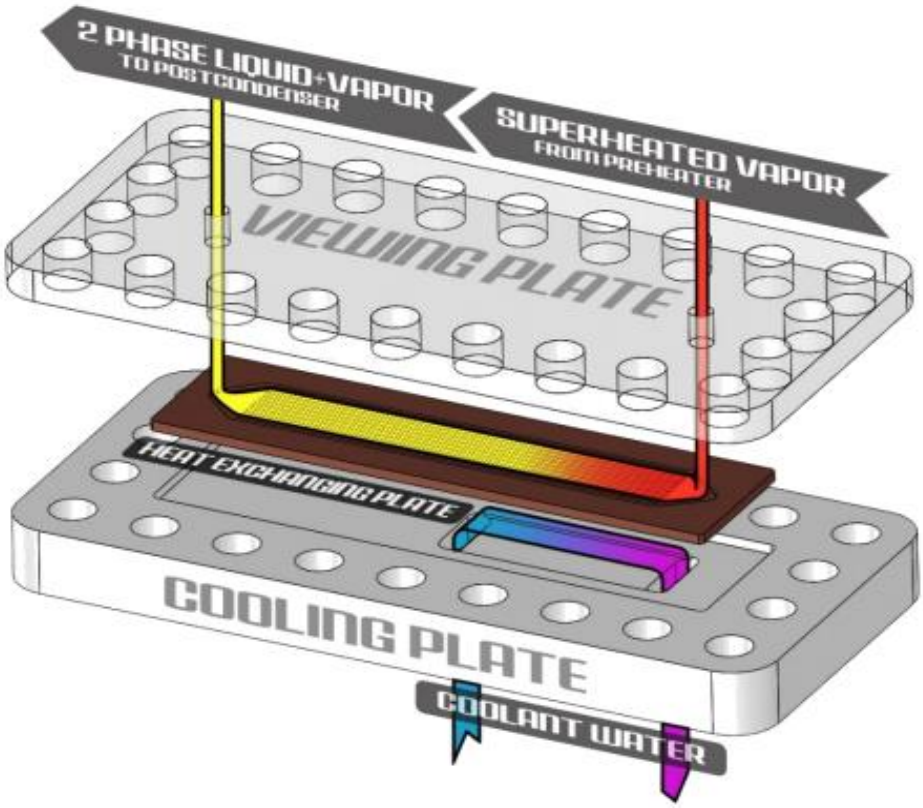

Figure 6.8: Visualization of two phase flow of R-134a inside rectangular microchannel [27]

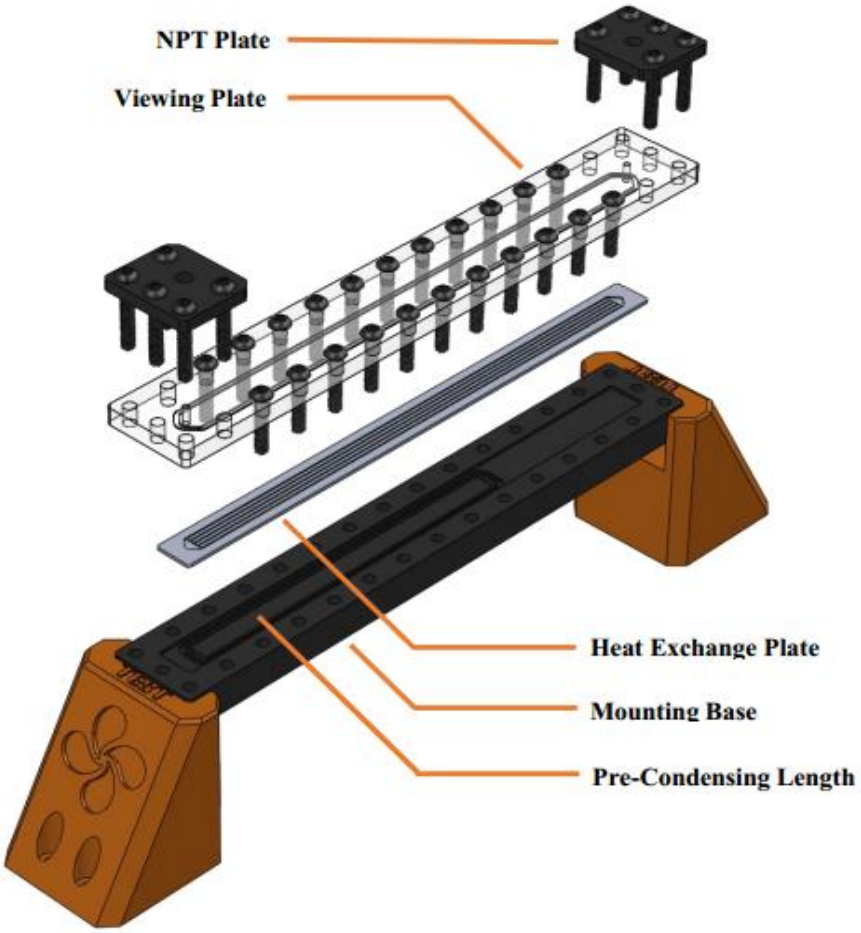

Figure 6.9: Detail of experimental test section model [27]

Microchannel Dimension	Symbol	Value
Material	S_t	Stainless steel 306/316
Hydraulic Diameter	D_H	0.84 mm
Pre-Condensing Length	L_c	200 mm
Viewing Length	L_v	90 mm
Channel Width	W_c	0.794 mm
Channel Depth	D_c	0.794 mm
Heat Exchanger Thickness	δ_t	1 mm

Table 6.1: Specification of rectangular microchannel condenser [27]

6.4.4 Post Condenser Section

After partially condensing of refrigerant inside microchannels, refrigerant R-134a exist in two phase vapors and liquid form and enter into the concentric double copper tube post-condenser heat exchanger as shown in Figure 6.10. Where it was fully condensed and converted into single liquid phase by using chiller solution of equal concentration of ethylene glycol and water mixture and it again moves towards the pump and repeat the cycle in similar manner. After fully condensed of condensate inside tube in tube heat exchanger, the liquid refrigerant passed through 15 micro size swagelok inline filter in order to filtrate particulates present in the flow arrangement. So that these particles cannot accumulate inside flow meter and pump. As large pressure drop occurred inside the inline filter of 15 micron due to more experimentations. So, due to improper functioning of inline filter, it was replaced by new inline filter of 230 micron size. Who gave very less pressure drop and worked quite well.

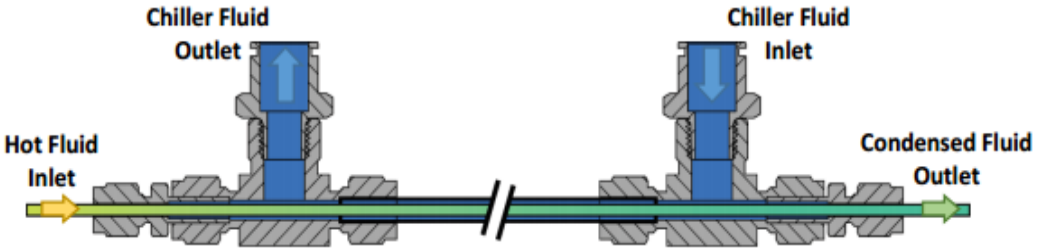

Figure 6.10: Double copper tube heat exchanger for condensing R-134a [27]

6.4.5 Coolant Loop

The second loop was the water loop which consisted of deionized water. Deionized water circulating in opposite direction around the condenser for partially condensing of R-134a. Two 50 mL syringe water pumps as shown in Figure 6.11 connected to deionized water reservoir worked alternatively in sucking and delivering of deionized water to and from microchannels test section by a set of single way valve.

Figure 6.11: Micro syringe water pump

6.4.6 Chiller Loop

The chiller loop consisted of an equal ratio of ethylene-glycol and water mixture used to fully condense R-134a inside the copper double heat exchanger. Its function was to lower the temperature of deionized water up to 5ºC prior entrance to test section by adjusting the temperature of chiller solution. NESLAB Thermo Scientific M-75 Merlin chiller as shown in Figure 6.12 used for this purpose, which was compact in size, reliable, easily movable from place to place, easily adjustable up to desired value of temperature and had better cooling impact.

Figure 6.12: Schematic of NASLAB Merlin M-75 Chiller [22]

6.5 Flow Visualization

An optical images of refrigerant flow through microchannel test section were taken by using Phantom V-310 high speed resolution camera by striking light onto the viewing channels of test section as shown in Figure 6.13. As two lights of 120 W, 55 V ALDER (M/N: AP-MB-T-CVR-120W55V-C-IP67) were used to enlighten the channels of test section visibility by adjust lighting system at proper angle. A Nikon micro lens of 60 mm was used to taken the images of viewing section of channel. So with this lens, 2400 fps (frames per second) were captured to visualize the flow regimes at different conditions.

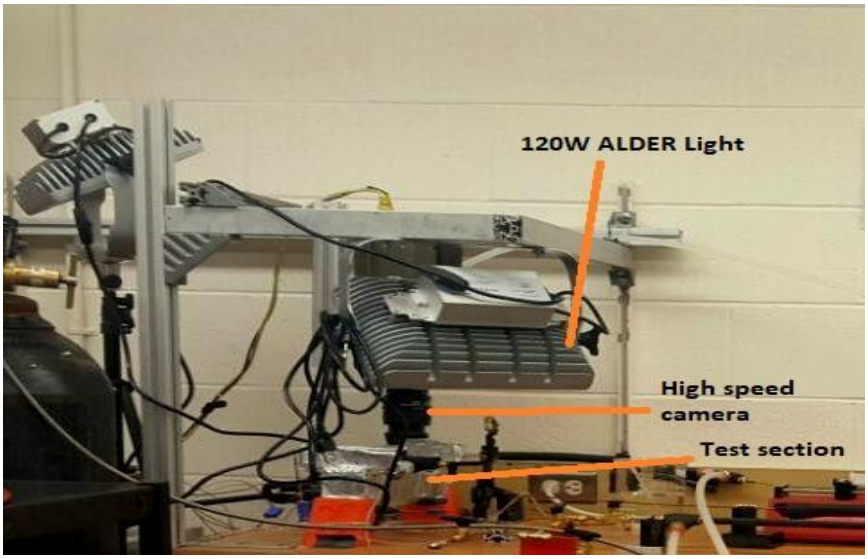

Figure 6.13: Setup for data capturing and flow visualization [27]

6.5.1 Measuring Instruments and Data Acquisition

The experimental test facility was provided with various measuring instruments that were capable to measure thermodynamic properties such as saturation pressure, temperature, flow rate and heat input values. These equipments used to minimizes the uncertainties occurring within the system through temperature and pressure devices. The location of these instruments is as shown in Table 6.2.

Table 6.2: Detail specification of measuring instruments of experimental facility

Measuring Instruments	Model Number	Supplier	Location	Range	Uncertainty
Thermocouple (T-type)	TMQSS-062U-6	OMEGA	Test section inlet/outlet	-270 to 350°C	0.4% or ±0.5 °C
Pressure Transducer	PX209-300AI	OMEGA	Test section inlet/outlet	300PSI	0.25% BFSL
Mass Flow Meter	FMTD4, SN 4658	DEA ENGG.	Refrigeration loop	3000psi,80ºC, 0-250CCPM	±0.1%
DAQ Analogue Module	NI cDAQ-9174,NI92,VN9211	National Instrument	R-134a System	-20 to 55ºC	-

In experimental test facility, the temperature of R-134a determined at the entrance and terminal section of rectangular microchannel by thermocouples of T-type (OMEGA, M/N: TMQSS-062U-6) with uncertainty of 0.4% or ± 0.5°C. The pressure was measured via two pressure transducers (OMEGA, M/N: PX209-300AI, S/N: 107920), Coriolis flow meter (DEA ENGG. M/N: FMTD4, S/N: 4658) was used before the gear pump to find out the flow rate of R-134a in refrigerant loop within uncertainty of ± 0.1%.

LabVIEW software on personal computer used to collect the real time experimental data observed at different conditions of saturation temperature. All experimental data acquired through temperature and pressure transducers by using National Instruments DAQ (Data Acquisition) system (M/N: NI-cDAQ-9174). More detail is shown in Table 6.3.

Modules	Model Number	Slots/Spaces
DAQ Chassis	NI-cDAQ-9174	4 Modules
Analog Module	NI cRIO-9211	16-Channels
Thermocouple Module	NI-9211	16-Channels

Table 6.3: Parts of DAQ system

6.6 Modelling Heat Transfer and Pressure Drop

6.6.1 Heat Transfer Modelling

Datasets obtained from visualization of R-134a through microchannel was modelled by doing energy balance equations on refrigerant and water side as shown in Equation (6.1) and (6.2). The total amount of heat energy leaving from the refrigerant is equal to the cumulative sum of energy received by the coolant water as well as the energy lost to the surrounding atmosphere from both the coolant and refrigerant flow. Q_{hl} in Equation (6.3) represents heat loss to surrounding. As the energy gain by coolant water is a combination of mass flow rate, specific heat and the change in temperature.

$$\dot{Q}_w = \dot{m}_w \times C_p \times (T_{out} - T_{in}) \tag{6.1}$$

$$\dot{Q}_{ref} = \dot{m}_{ref} \times (h_{out} - h_{in}) \tag{6.2}$$

$$\dot{m}_{ref} \times (h_{out} - h_{in}) = \dot{m}_w \times C_p \times (T_{out} - T_{in}) - Q_{hl,ref,out} - Q_{hl,w,out} \tag{6.3}$$

Logarithm mean temperature difference ΔT_{LM} at inlet and exit temperature of test section for counter flow heat exchanger describe in Equation (6.4) to (6.6).

$$\Delta T_{in} = T_{in} - T_{amb} \tag{6.4}$$

$$\Delta T_{out} = T_{out} - T_{amb} \tag{6.5}$$

$$\Delta T_{LM} = \frac{\Delta T_{in} - \Delta T_{out}}{ln\left(\frac{\Delta T_{in}}{\Delta T_{out}}\right)} \tag{6.6}$$

The conductive and convective thermal resistances are used to determine the overall thermal coefficient 'U' as shown in Equation (6.7). The Equation (6.8) represents inter-relationship among heat exchanger areas, number of channels and heat transfer flow rate through system. Although, the number of channels can be found by Equation (6.9) and thermal resistance network is shown in Figure 6.14.

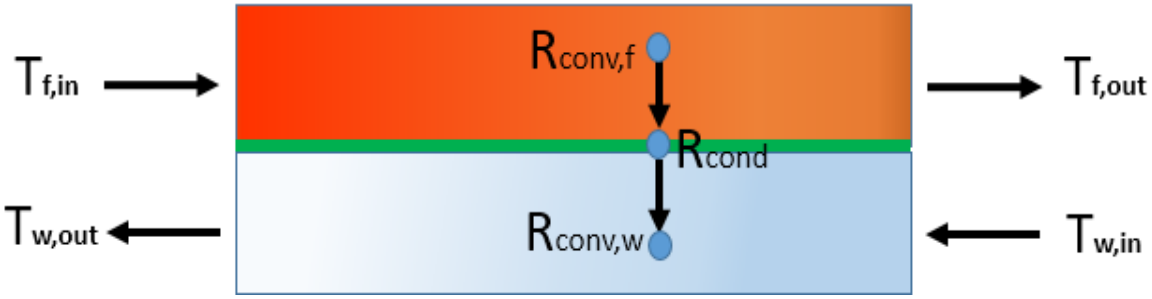

Figure 6.14: Heat transfer thermal resistance network model

$$\frac{1}{U} = \frac{1}{h_f} + \frac{t}{K_{wall}} + \frac{1}{h_w} \tag{6.7}$$

$$A_{req} = \frac{\dot{Q}}{U \times N \times LMTD} \tag{6.8}$$

$$\dot{V} = \frac{G(N \times W \times H)}{\rho_l} \tag{6.9}$$

The thermodynamic vapor quality at outlet of microchannel test section is obtained from Equation (6.10) which is a function of enthalpies at inlet and exit of microchannel test section. But quality at post-condenser part will be calculated by heat loss from refrigerant to coolant during flow inside channel geometry.

$$x_{out} = \frac{h_{out} - h_l}{h_v - h_l} \tag{6.10}$$

$$h_{in,test} = h_{in,pre} - \left|\frac{\dot{Q}_w}{\dot{m}_{ref}}\right| \tag{6.11}$$

6.6.2 Pressure Drop Modelling

Pressure drop is obtained by using Blasius's correlation for the Fanning friction factor as given in Equation (6.12) and (6.13).

$$\Delta P_f = f \times \frac{Re^2 \times \mu_l^2 \times 4l}{2 \times \rho_l \times D_h^2} \tag{6.12}$$

$$f_t = 0.079 \times Re^{-0.25} \tag{6.13}$$

6.7 Experimental Results

It was predicted based on previous research work that the regimes observed would either be intermittent/annular flow or might be transition occurs from annular to intermittent at given mass fluxes and vapor qualities. But actually wavy-annular or wavy-stratified flow regimes observed at given conditions based on the comparison.

6.7.1 Comparison of Visualization Results by varying Saturation Temperatures

The comparisons is done by varying the saturation temperature at 40ºC and 55ºC with keeping the same refrigerant's mass flux 150 kg m^{-2} s^{-1} and quality 0.36 as shown in Figure 6.15. The results shows that the density of liquid and viscosity of the vapor relatively remain same during two phase flow inside microchannels. When saturation temperature increases from 40ºC to 55ºC then vapors overcome the liquid layer due to which annular/wavy flow regimes observed at these conditions and they are identified by presence of so many vapors inside the core of channel surrounded by liquid layer.

T_{sat}=40ºC

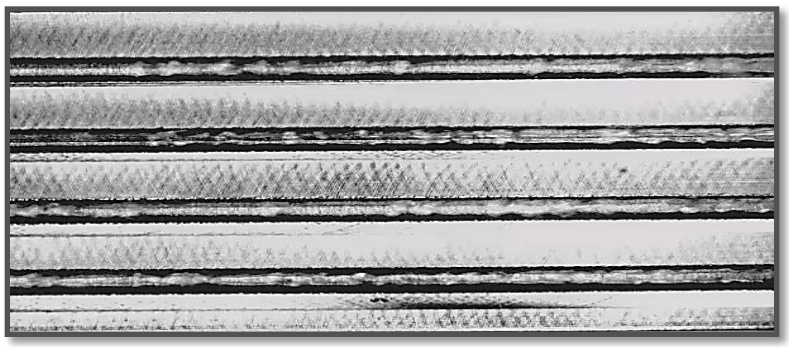

T_{sat}=55ºC

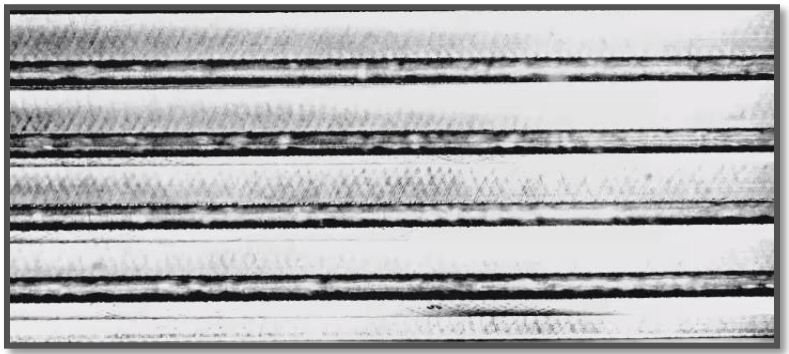

Figure 6.15: Comparison of visualization results at varying saturation temperature

6.7.2 Comparison of Visualization Results by Varying Qualities

Figure 6.16 shows the comparisons at varying qualities by keeping the same flux (G = 100 kg m^{-2} s^{-1}) and saturation temperature (T_{sat} = 55ºC). Although decreases of qualities from 0.5 to 0.1 shows that the number of vapors present in the liquid layer are going to decreases differentiated by wave trough of vapors surrounded by the smooth liquid layer. This ratio of wavy liquid to vapor formation does not remain same during flow because volume of liquid is increases due to the decreases in vapor quality as observed from below images.

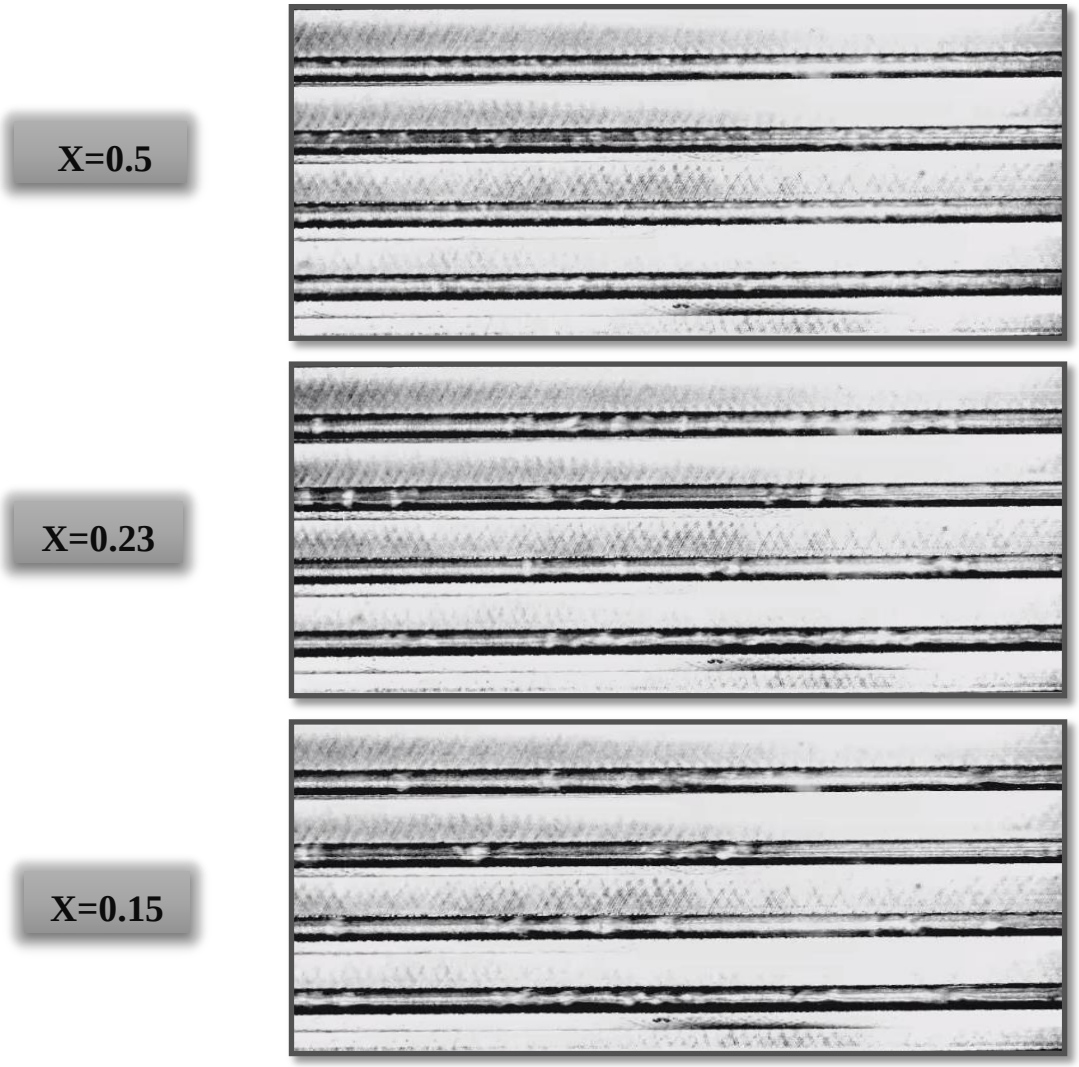

Figure 6.16: Comparison of visualization results at varying flow quality

6.7.3 Comparison of Visualization by varying Mass Fluxes

Figure 6.17 shows that varying of mass fluxes 75-150 kg m^{-2} s^{-1} by keeping same quality (x = 0.3) and saturation temperature (T_{sat} = 40ºC). Result shows visibility of annular flow regime in term of wavy vapor liquid interface from images of high speed camera. The wave turbulence gradually increases with mass flux due to the formation of small stable vapors surrounded by liquid layer that shows wavy annular flow irrespective of intermittent flow regime. So, it can be stated that the flow regime as visualized by high speed camera is simply wavy-annular or wavy-stratified flow inside the channels.

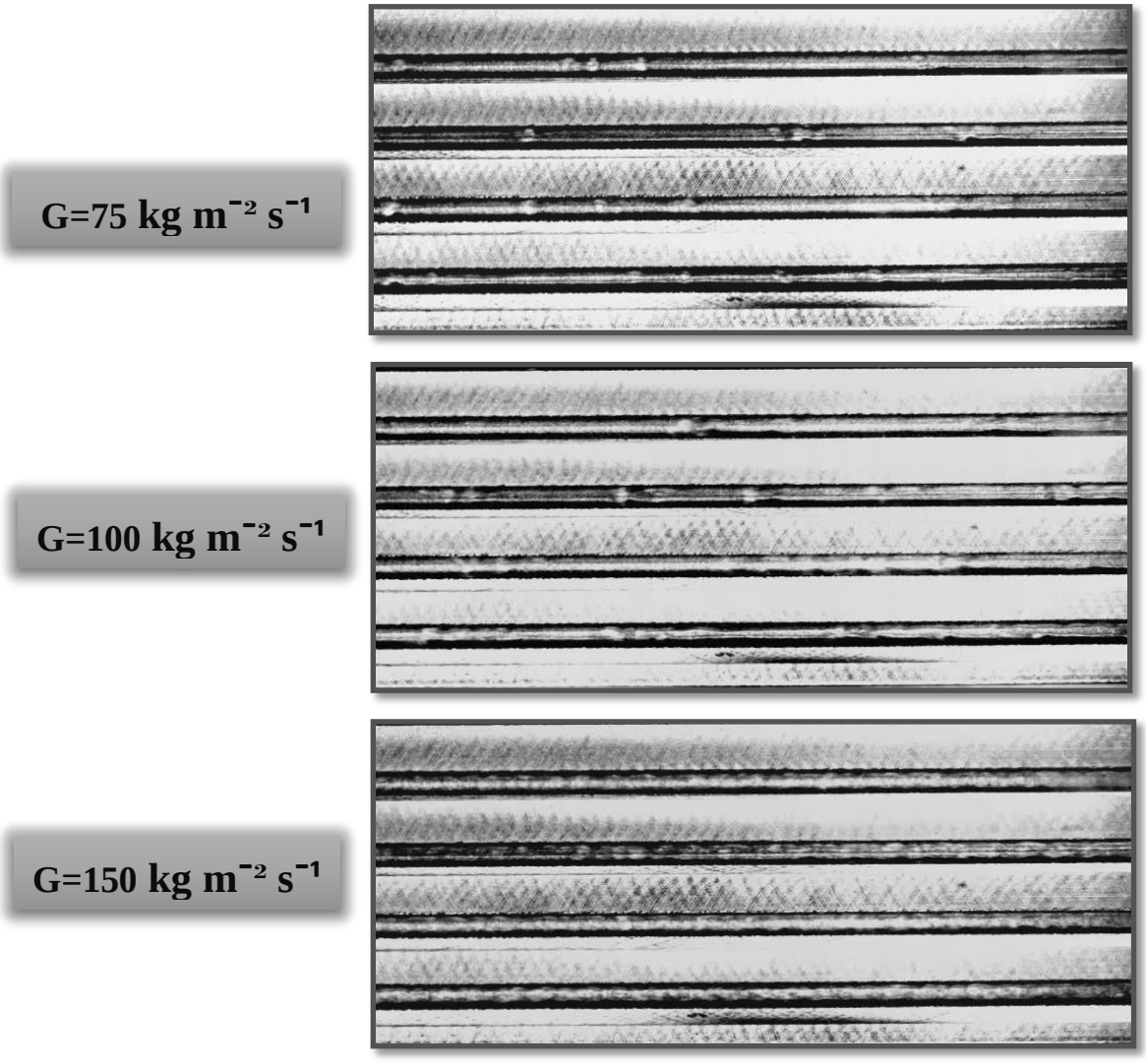

Figure 6.17: Comparison of visualization results at varying mass flux

6.7.4 Heat Transfer

Heat transfer mechanism is significant in transferring of thermal energy in between two or more fluids. Vapor quality, mass flow rate and saturation temperature are the main parameters which influences on the thermal energy transfer phenomenon. The term quasi local value are used to find out the heat transfer coefficient that how much heat is distributed between two fluid mediums. It's actually represent a small change in quality of vapor phase from initial to the final stage of the microchannel condenser section.

The graph plotted in between heat transfer coefficient verses mass flow rate of refrigerant R-134a without using of coolant water shows directly behavior as shown in Figure 6.18.

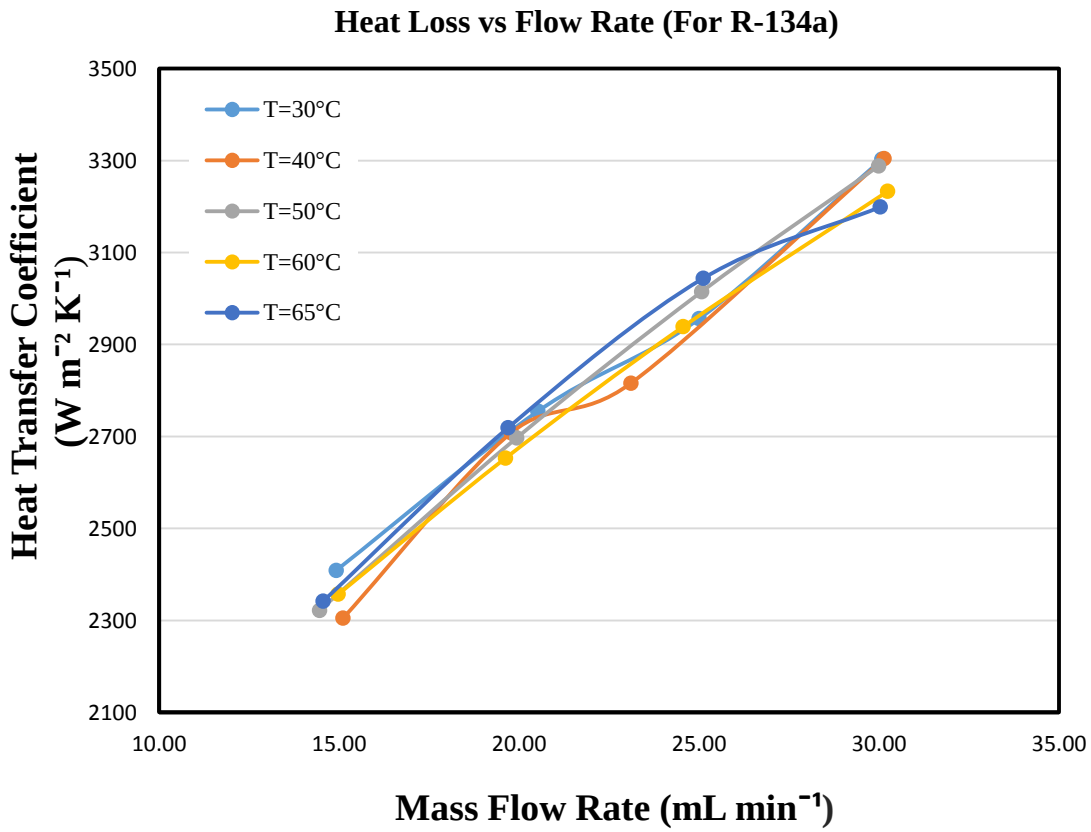

Figure 6.18: Experimental heat transfer coefficients plotted against mass flow rate of refrigerant without using of coolant

An increase in mass flow rate of refrigerant from 14-30 mL min^{-1}, there is a great stability seen in case of increase value of heat transfer coefficient from 2300 up to 3300 W m^{-2} K^{-1} at temperature range from 30-65ºC. At lower mass flow rate of refrigerant, the vapor quality become lower result in thick layer formation at the bottom of channel that

acts as a resistance in the passage of heat transfer. So thick liquid film condensation dominate over the heat transfer results in lower heat transfer coefficient. Similarly, at higher flow rate of refrigerant, there is increase in vapor velocity and thin layer film is deposited channel's bottom results in lower thermal resistance and higher heat transfer. So convective forced condensation dominate over the thermal resistance in transfer of higher heat energy.

Figure 6.19 shows the graph plotted against overall heat transfer coefficient and the mass flow rate of the refrigerant in the present of coolant water. Which shows that at lower value of flow rate results in higher heat transfer from refrigerant to coolant as well as to the surrounding environment. Which forms overall heat transfer coefficient. So by increasing of flow rate, overall heat transfer coefficient decreases because thin liquid layer formation at the bottom behave as a thermal resistance to the incoming condensate to be condense.

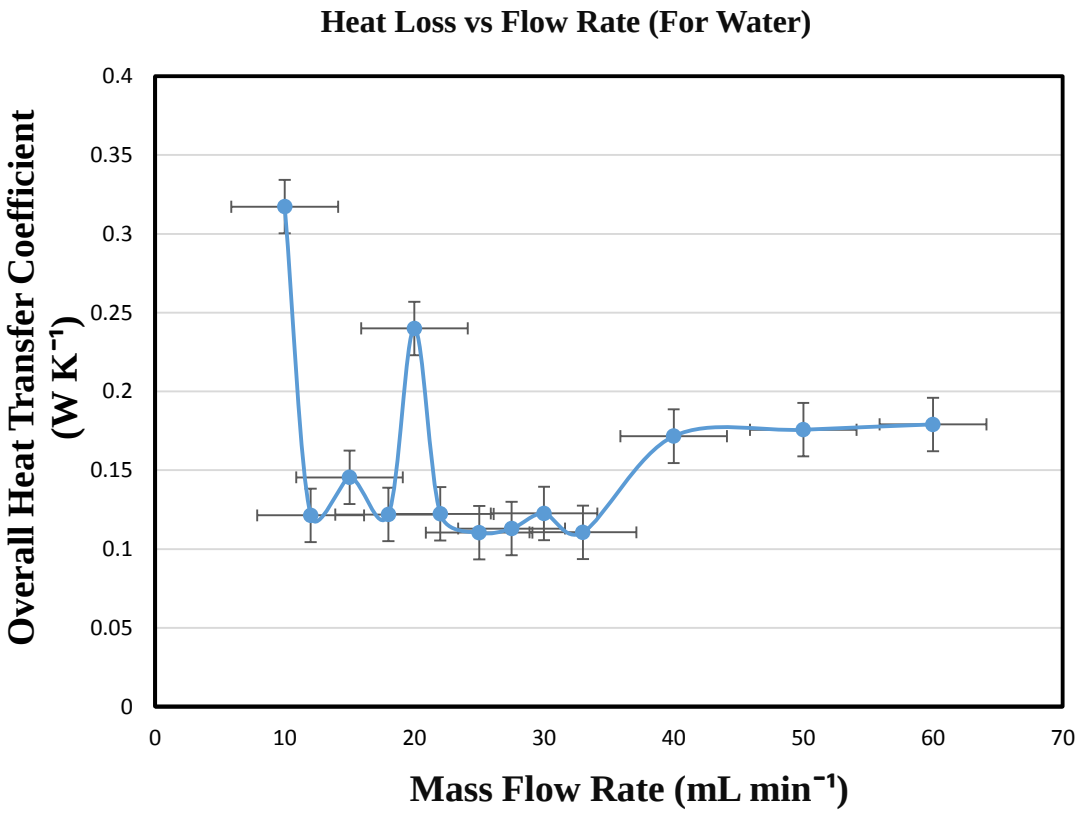

Figure 6.19: Representation of heat transfer coefficient verses mass flow rate of refrigerant in the present of coolant

Figure 6.20 shows that maximum heat transfer coefficient achieved is 900 W/m²-s at vapor quality of 0.7 and flux of 150 kg m^{-2} s^{-1} at saturation temperature of 40ºC. By increasing quality along with mass flux, heat transfer coefficient is also rises because of thin layer formation at the bottom of channel due to which chances of wavy annular flow formation is increases. Similarly shifting from saturation temperature 40ºC to 55ºC as in Figure 6.21, heat transfer coefficient is reduces with the increment of saturation temperature at same flux. Also the density of vapors increases as a result of higher quality due to which vapor shear force increases. Which tends to reduce the fraction of liquid.

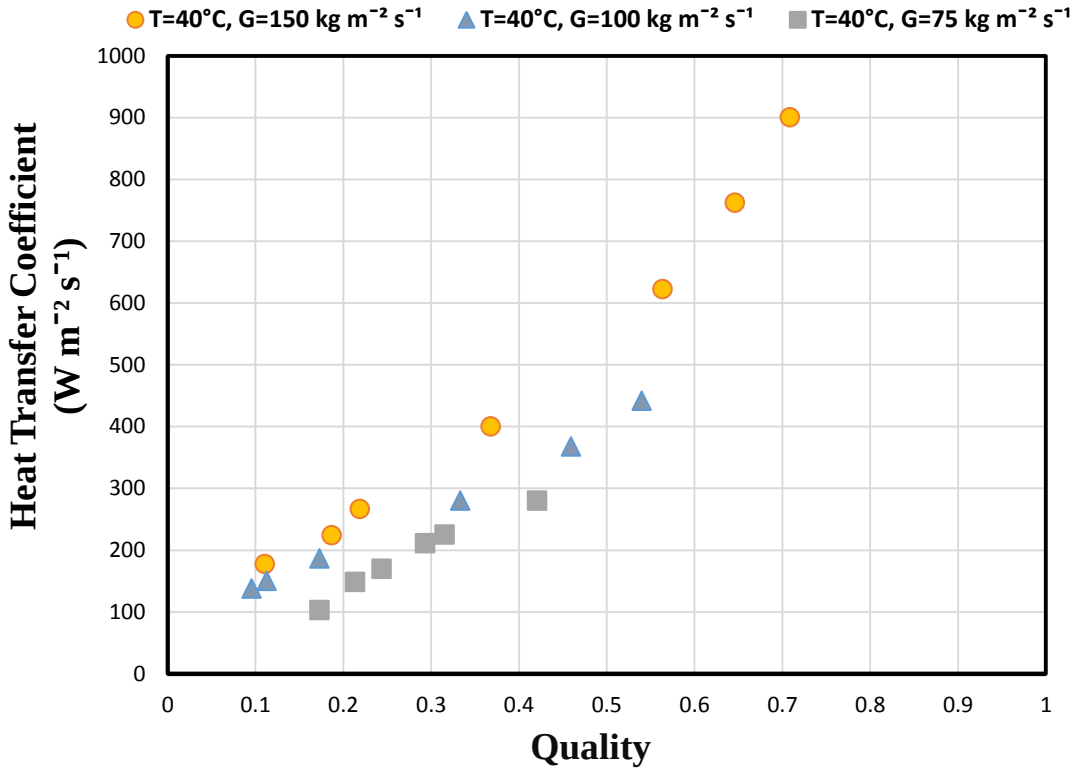

Figure 6.20: Experimental heat transfer coefficient plotted against quality at 40ºC

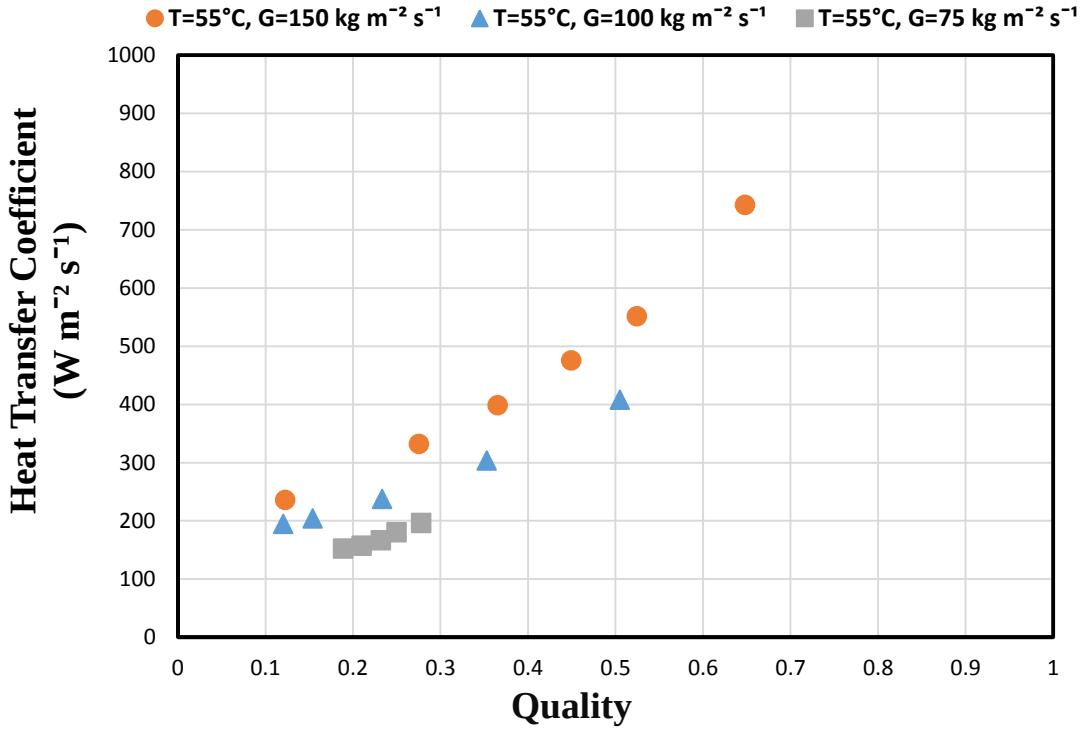

Figure 6.21: Experimental heat transfer coefficient plotted against quality at 55ºC

6.7.5 Pressure Drop

Pressure drop experiments are performed over the mass flux 75-150 kg m^{-2} s^{-1} and temperature of 40ºC and 55ºC with quality range from 0 to 1. Figure 6.22 and 6.23 shows that increases of pressure drop depends on vapor quality and mass flux. By increasing the vapor quality, vapor average velocity increases and interfacial shear stresses increases with the decrease of liquid fraction inside microchannels. But at higher quality, the pressure drop going to be minimum. When saturation temperature increases from 40ºC to 55ºC then pressure drop behavior is decreases.

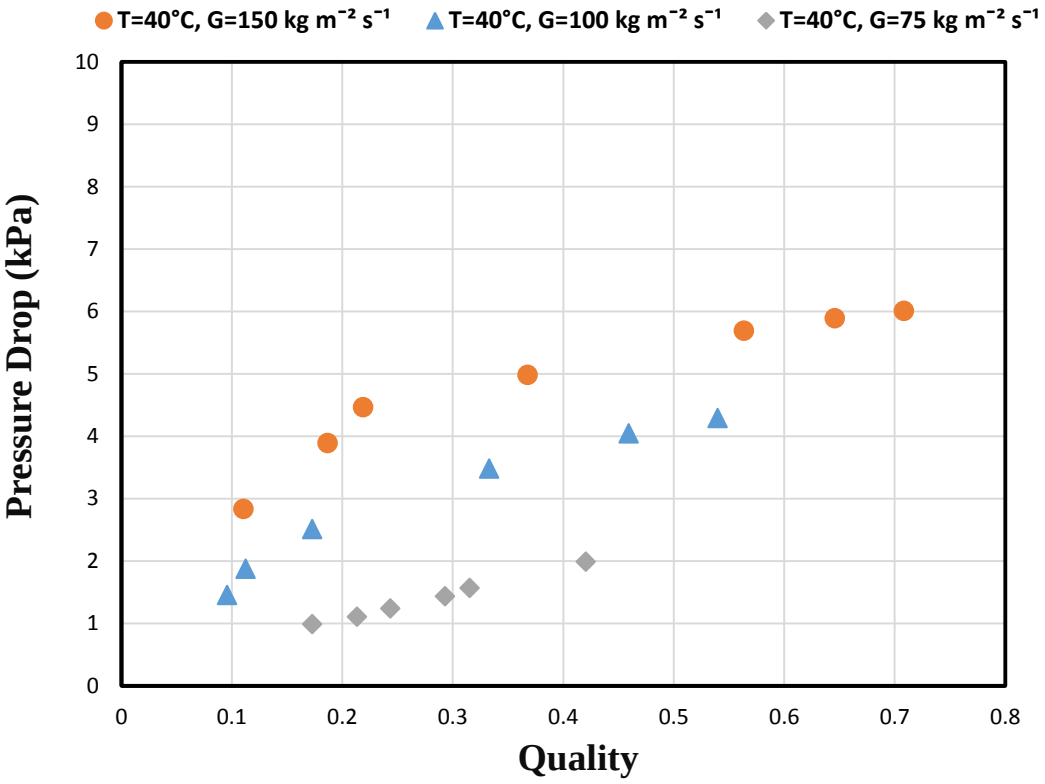

Figure 6.22: Experimental pressure drop plotted against quality at 40ºC

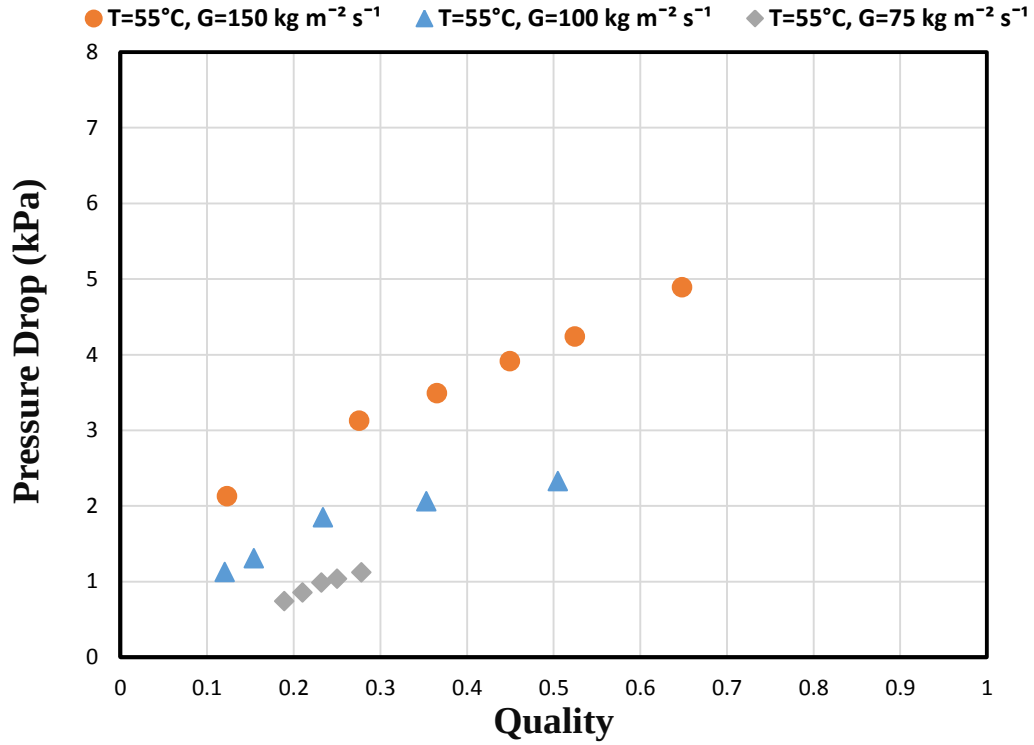

Figure 6.23: Experimental pressure drop plotted against quality at 55ºC

6.8 Comparison of Literature with the Flow Maps

6.8.1 Barnea Model

The early attempts in understanding the influence of decreasing diameters and surface tension forces dominance on adiabatic flow regime transitions proposed by Barnea et al. They investigated the behavior of different flow regime by using the air water mixture in both horizontal and vertical smaller size circular diameter channels ranging from 4 mm-12 mm. Barnea et al. developed flow map by compared their data points with the transition criteria of Taitel and Dukler to see the effect on mass flow rates and surface tensional forces of refrigerant. They proposed a modification to the model of Taitel and Dukler and apart from stratified-to-slug flow transition, they found flow regimes of stratified smooth, stratified wavy, intermittent, dispersed bubble and annular by considering transition criteria based on surface tension and gravitational effect. They consider the influence of both surface tension and gravitational effect in terms of the vapor-phase height in the channel as shown in Equation from (6.14) through (6.16).

$$h_G \leq \frac{\pi}{4}\sqrt{\frac{\sigma}{\rho g(1-\frac{\pi}{4})}} \tag{6.14}$$

$$\sigma = \rho g(y^2 - \frac{\pi}{4}y^2) \tag{6.15}$$

$$y = \frac{4}{\pi}h_G \tag{6.16}$$

The adiabatic flow is treated as two dimensional and bubble is assumed to be in circular with radius y and hg is equilibrium gas layer thickness that is obtained through momentum balance of liquid vapor two phase flow.

6.8.1.1 Comparison with Flow Map of Barnea at T_{sat} of 40ºC and 55ºC

The comparison of experimental data points at saturation temperature of 40ºC and 55ºC is done with the flow map of Barnea et al. as shown in Figure 6.24 and 6.25 shows that the data points observed at given conditions are either annular or wavy-stratified type but the predictions placed the data points in the transition region between intermittent and the annular region. The data points that have vapor quality of 0.64 and 0.70 are predicted in annular flow region agreed with the flow map of the Barnea et al. but the remaining data do not show any agreement with the flow model. So, it may be possible that the flow map

predict the behavior of trend accurately by doing some modification at small level in the transitional parameters.

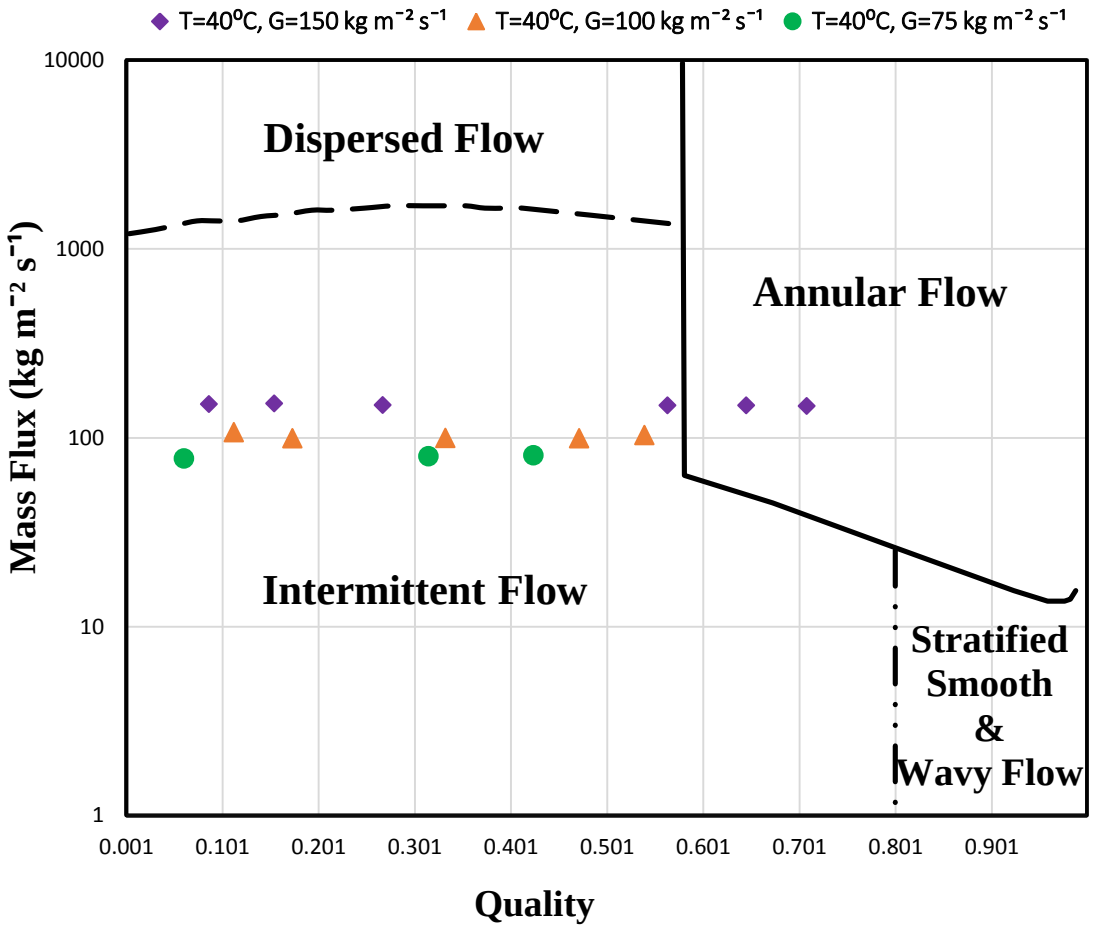

Figure 6.24: Data plotted against Barnea proposed map at temperature 40˚C

So by increasing the saturation temperature from 40ºC to 55ºC, prediction flow map shows more data points in the intermittent region and very less predicted in the annular region. But the observed data visualized from high speed camera shows only wavy-annular or wavy-stratified flow regimes were observed at given conditions.

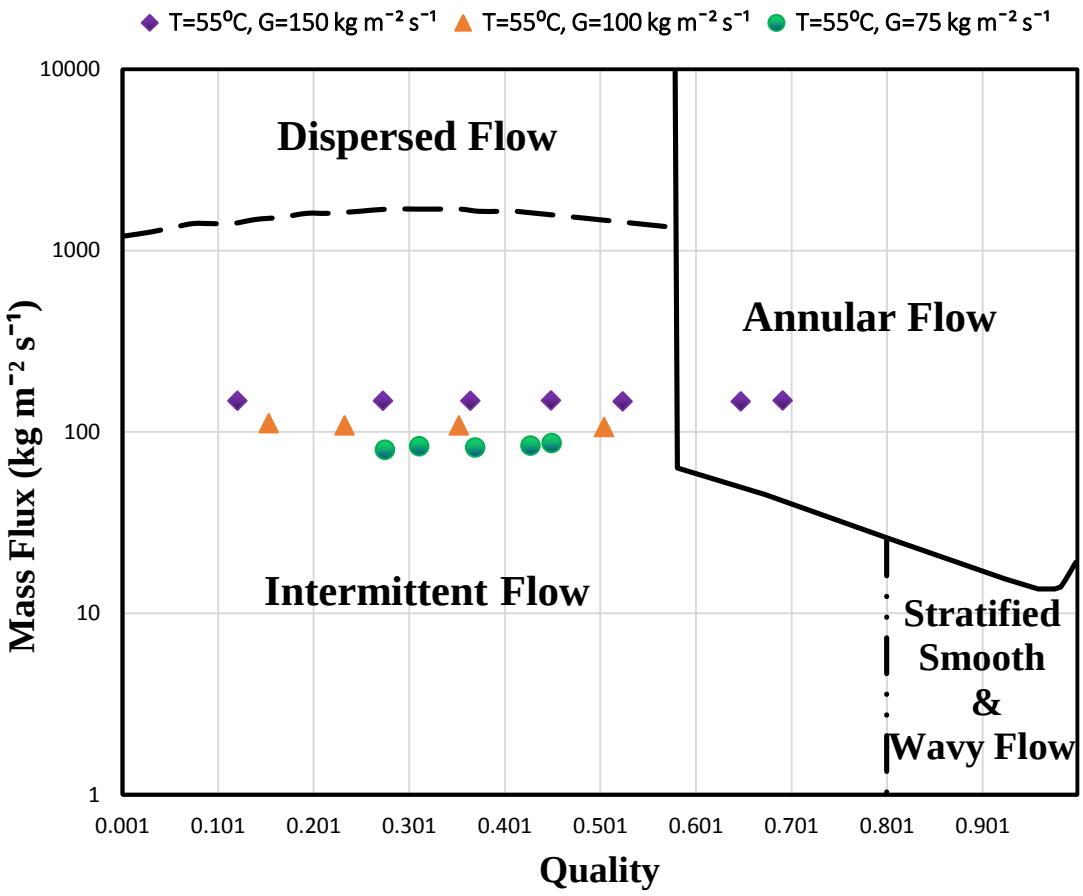

Figure 6.25: Data plotted against Barnea proposed map at temperature 55˚C

6.8.2 Breber Model

Breber et al. proposed his flow model of condensation that agreed with Taital and Dukler's theoretical model for condensation of two phase flow. They used these refrigerants R-11, R-12, R-113, steam and n-pentane through circular channels of diameter 4.8-22 mm and observed annular, mist annular, wavy, and stratified, slug, plug and bubble flow regimes up to maximum pressure of 1.2 MPa. They used following dimensionless parameters T, F (the modified Froude number), K, J_g (superficial vapor velocity) and X (Martinelli parameter) to described adiabatic two phase flow and suggest gravitational flow regimes. Which includes stratified, wavy and shear dominated annular flow regime [15]. They also proposed accurate heat transfer and pressure drop models. The transition criteria are presented by the following given Equations from (6.17) through (6.22) listed below.

$$X = \left(\frac{\rho_v}{\rho_l}\right)^{0.5} \left(\frac{\mu_v}{\mu_l}\right)^{0.1} \left(\frac{1-x}{x}\right)^{0.9} \quad (6.17)$$

$$J_g = \frac{Gx}{\sqrt{Dg\rho_v(\rho_l-\rho_v)}} \quad (6.18)$$

$$F_a = \frac{dP_s}{dL} = \frac{4f_g G_v^2}{D_i 2\rho_v} \quad (6.19)$$

$$F_r = \frac{dP_g}{dD_i} = g(\rho_l - \rho_v) \quad (6.20)$$

$$T = \frac{(\frac{dP}{dL})_l}{g(\rho_l-\rho_v)} \quad (6.21)$$

$$K_p = \left(\frac{\rho_v}{\rho_l}\right)^{0.5} \left(\frac{\mu_v}{\mu_l}\right)^{0.1} \quad (6.22)$$

The given model shows particular values of dimensionless parameters that can be compare to the defined flow transition lines. The parameters T, K, J_g and F plotted against the X (Martinelli parameter) to visualize and determine the flow regimes. As the summary of adiabatic flow regimes observed and transition criteria of flow map presented by Breber et al. in literature is given in Table 6.4 and 6.5.

Description	**Range**	**Flow Regimes Observed**
Refrigerant	R-11, R-12, R-113	Annular, Mist, Annular, Wavy, Stratified, Slug, Plug and Bubble Flow
Geometry	Circular	
Diameter	4.8 mm to 22 mm	
Pressure and Mass Flux	108.2 < P < 1248.6 kPa 17.63 < G < 990 kg m^{-2} s^{-1}	

Table 6.4: Summary of adiabatic flow regime from Breber literature [15]

Table 6.5: Flow transition criteria for Breber flow model [15]

Flow Regimes	**Transition Criteria**
Annular Flow	$J_g > 1.5$, X < 1. 0
Wavy or Stratified flow	$J_g < 0.5$, X < 1.0
Slug (Intermittent Flow)	$J_g < 1.5$, X > 1.5

Bubble Flow	$J_g > 1.5, X > 1.5$

6.8.2.1 Comparison with Flow Map of Breber at T_{sat} of 40ºC and 55ºC

As the comparison was made possible with the flow map of Breber et al. at saturation temperature of 40ºC and 55ºC as shown in Figure 6.26 and 6.27. The data is presented against X (Martinelli Parameter) and J_g (Dimensionless vapor velocity). The result shows that the experimental data points are not well predicted by Breber flow map and placed all the data points are in intermittent region except some points that are in transition region. But the flow regime visualized from high resolution camera was wavy annular regime that contradicted completely with the flow map of Berber at saturation temperature of 40ºC and 55ºC.

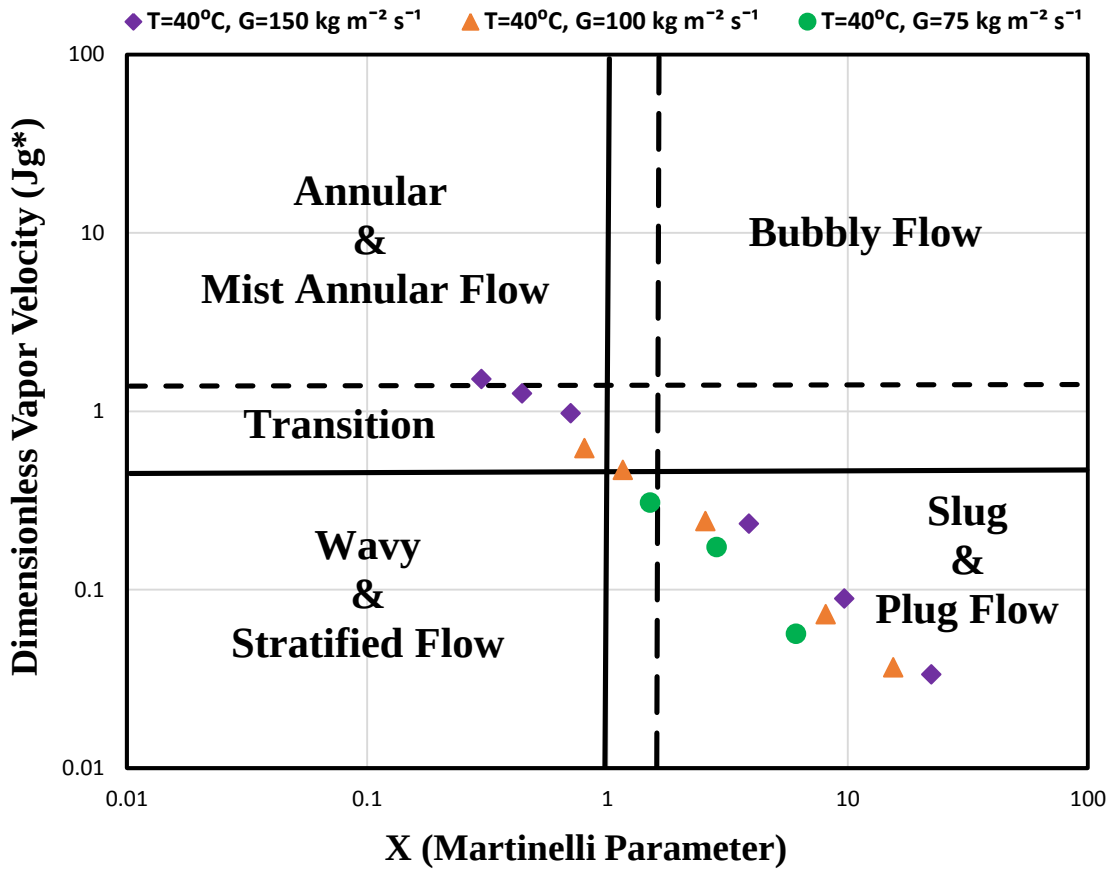

Figure 6.26: Data plotted against Breber proposed map at temperature 40˚C

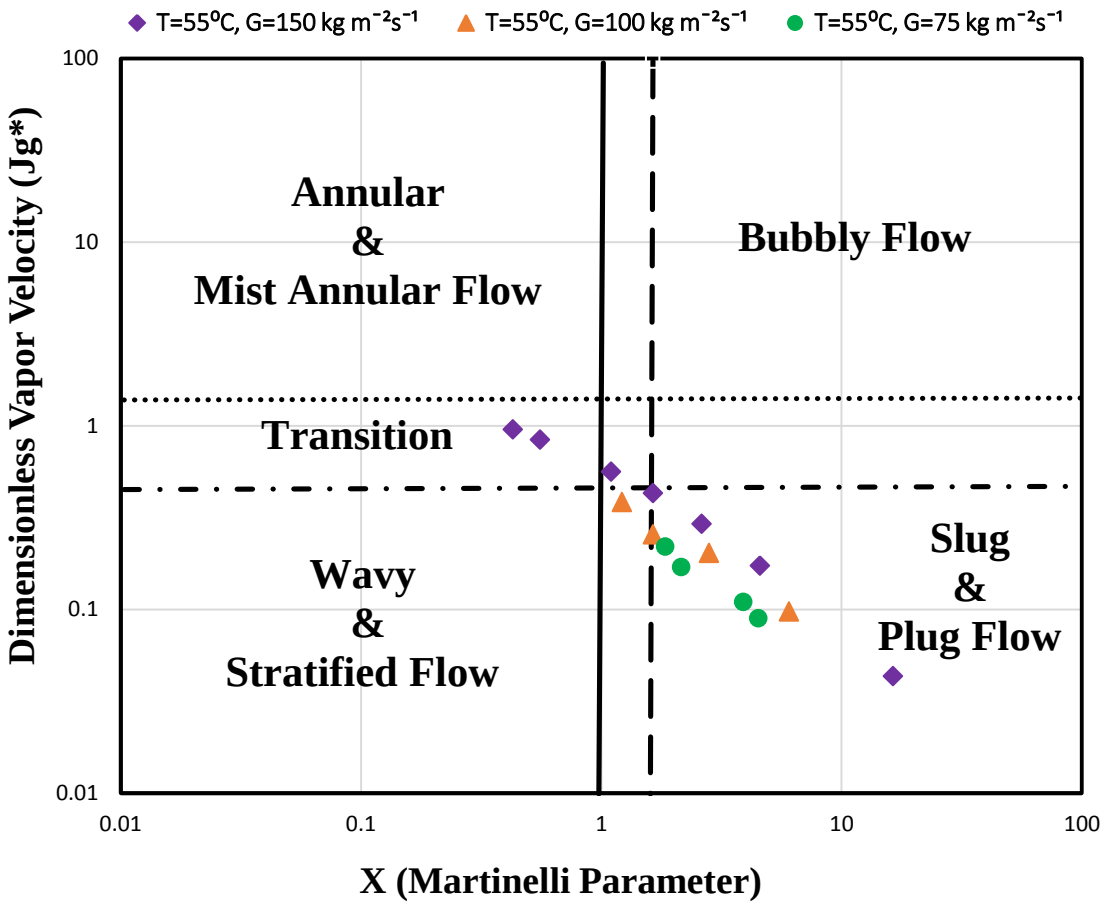

Figure 6.27: Data plotted against Breber proposed map at temperature 55˚C

6.8.3 Thome Model

Thome et al. studied two phase heat transfer to developed flow map and heat transfer based model for condensation of different refrigerants inside horizontal channels to visualize different regimes. They identified regimes either fully forced convective annular or regimes having multiple variations of gravity driven. They did some modification to the flow pattern map of Kattan et al. and introduced his model for flow boiling phenomenon inside the horizontal channels. The flow regimes observed by the Thome et al. was annular, intermittent, stratified, wavy-stratified and mist flow regimes at different saturation temperature and mass fluxes. They also calculated void fraction based on logarithmic mean void fraction that used in transition criteria of flow pattern map by using homogeneous model of Rouhani-Axelsson [11]. The transitional parameters in the form of Equations used in this model from (6.23) through (6.30) are defined below.

$$G_w = \left(\frac{\pi}{4}\right) F_r \sqrt{g} \rho_l D_H^{1.5} \tag{6.23}$$

$$x_{IA} = \left\{ \left[0.2914 \left(\frac{\rho_V}{\rho_L}\right)^{\frac{-1}{1.75}} \left(\frac{\mu_L}{\mu_V}\right)^{\frac{-1}{7}} \right] + 1 \right\}^{-1} \tag{6.24}$$

$$G_{bubbly} = \left\{ \frac{256 A_{vd} A_{ld}^2 d^{1.25} \rho_L (\rho_l - \rho_v) g}{0.3164 (1-x)^{1.75} \pi^2 P_{id} \mu_L^{0.25}} \right\}^{\frac{1}{1.75}} \tag{6.25}$$

$$G_{wavy} = \left\{ \frac{16 A_{Vd}^3 g d \rho_L \rho_V}{x^2 \pi^2 (1-(2h_{Ld}-1)^2)^{0.5}} \left[\frac{\pi^2}{25 h_{Ld}^2} \times \left(\frac{W_e}{F_r}\right)_L^{-1.023} + 1 \right] + 50 - 75 e^{-(x^2-0.97)^2 / x(1-x)} \right\} \tag{6.26}$$

$$G_{strat} = \left\{ \frac{226.3^2 A_{Ld} A_{Vd}^2 \rho_v (\rho_L - \rho_v) \mu_L g}{x^2 (1-x) \pi^3} \right\}^{\frac{1}{3}} + 20x \tag{6.27}$$

$$G_{mist} = \left\{ \frac{7680 A_{Vd}^2 g \rho_L \rho_V}{x^2 \pi^2 \varepsilon} \left(\frac{Fr}{We}\right)_L \right\}^{0.5} \tag{6.28}$$

$$\left(\frac{We}{Fr}\right)_L = \frac{g d^2 \rho_L}{\sigma} \tag{6.29}$$

$$\epsilon = \left[1.138 + 2log \left(\frac{\pi}{1.5 A_{Ld}} \right) \right]^{-2} \tag{6.30}$$

As the summary of adiabatic flow regimes observed and transition criteria of flow map presented by Thome et al. in literature is given in Table 6.6 and 6.7.

Table 6.6: Summary of adiabatic flow regime from Thome literature [11]

Description	**Range**	**Flow Regimes Observed**
Refrigerant	R-22, R-134a, R-236ea, R-125, R-32, R-410A	Fully Stratified, Stratified-Wavy, Intermittent, Annular, Mist and Bubbly Flow
Geometry	Circular horizontal	
Diameter	3.14 mm to 21.4 mm	
Prandtl Number and Mass Flux	$16 < G < 1532$ kg m^{-2} s^{-1} $0.02 < Pr < 0.8$	

Table 6.7: Flow transition criteria for the Thome flow model [11]

Flow Regimes	**Transition Criteria**
Annular Flow	$G > G_{wavy}$, $G < G_{mist}$, $x > x_{IA}$
Intermittent Flow	$G > G_{wavy}$, $G < G_{mist}$ or $G < G_{bubbly}$ and $x < x_{IA}$

Stratified-Wavy Flow	$G_{strat} < G < G_{wavy}$
Fully Stratified Flow	$G < G_{strat}$
Mist Flow	$G > G_{mist}$

6.8.3.1 Comparison with Flow Map of Thome at T_{sat} of 40ºC and 55ºC

Thome et al. flow model well predicts all the available data points in the stratified wavy flow regime. The visualization of flow regimes by high speed camera shows that only wavy-annular or wavy-stratified flow regimes appeared. But it's not cleared to differentiate either it was completely wavy-annular or wavy-stratified flow that occurred inside rectangular microchannels. So overall, there is a good agreement seen at saturation temperature of 40ºC and 55ºC with the flow map of Thome et al. as shown in Figure 6.28 and 6.29.

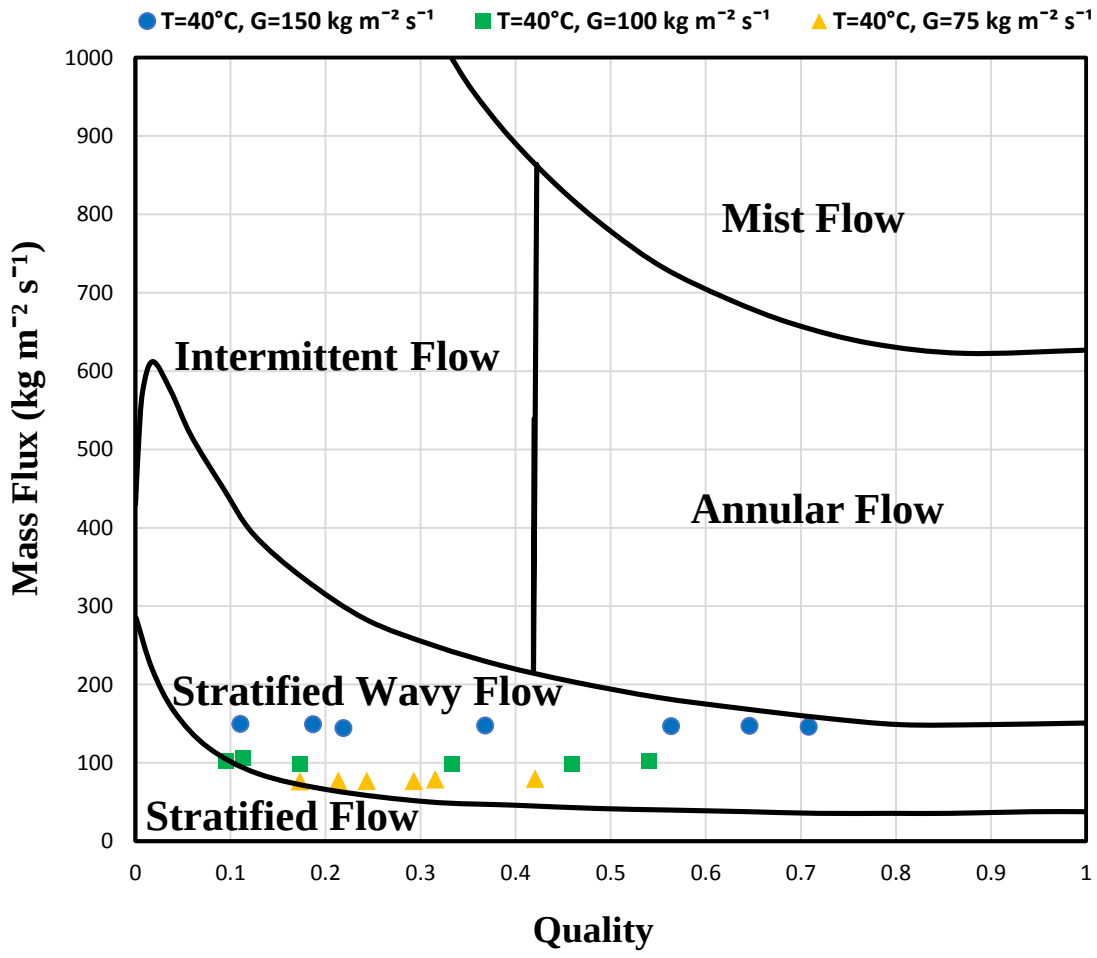

Figure 6.28: Data plotted against Thome proposed map at temperature 40˚C

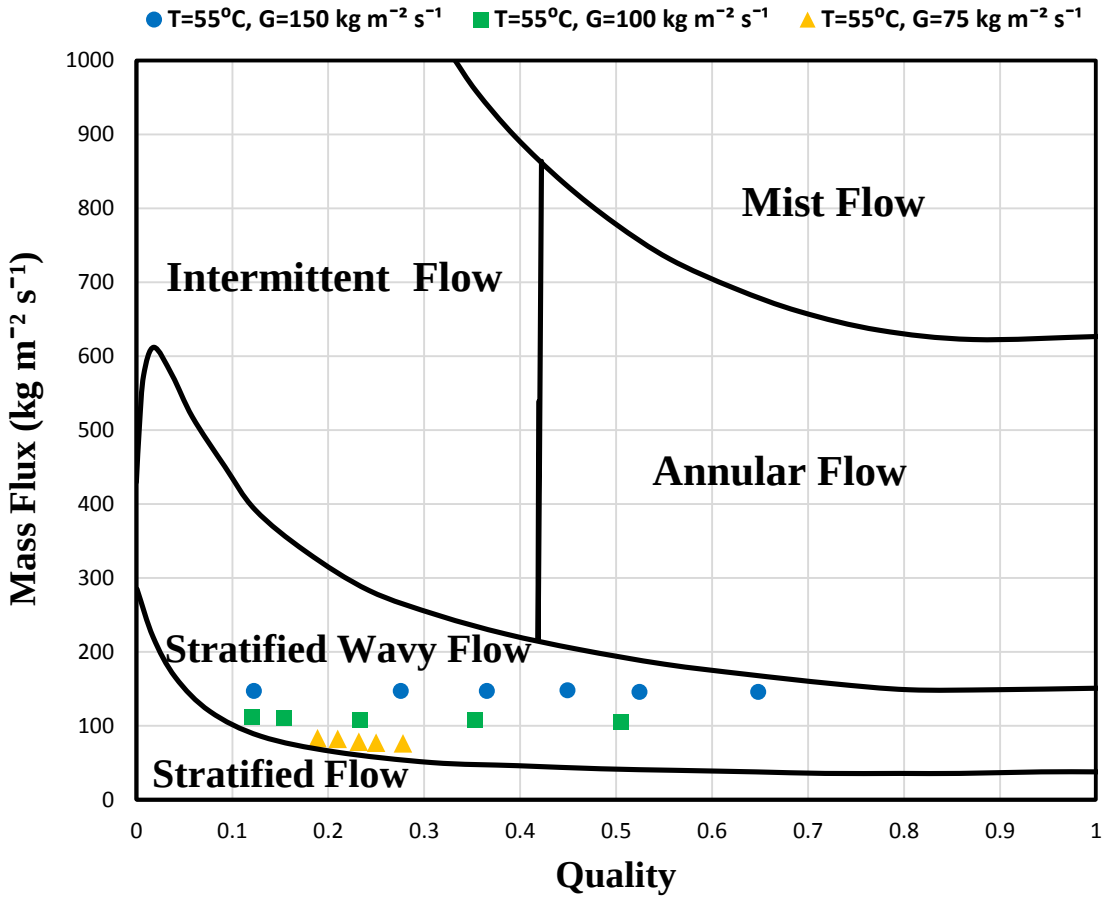

Figure 6.29: Data plotted against Thome proposed map at temperature 55˚C

6.8.4 Damianides & Westwater Model

Damianides and Westwater proposed their individuals flow regime maps by conducting air water mixture through channels diameter of range 1 mm < D_h < 5 mm to see the hydraulic diameter effect on flow map transitions. They observed dispersed-bubbly, bubbly, plug, slug, pseudo-slug and stratified wavy flow regime at various velocities of vapors. They also stated the effect of surface tension on smaller and larger hydraulic diameter of channels. They observed flow transition from intermittent to disperse at larger flow rate of liquid inside larger hydraulic diameter of channel and transition from intermittent to annular due to larger flow rate of vapors inside smaller hydraulic diameter of channel and stated that stratified flow regime not appeared in the channel that have hydraulic diameter 1 mm [23]. They have agreement for channel hydraulic diameter of 5

mm with Taitel and Dukler (1976). But have poor agreement for 1 mm hydraulic diameter of channel.

The transitional parameters in the form of Equations used in this model from (6.31) through (6.33) are defined as below

$$U_g = \frac{V_{g,s}}{\alpha} \tag{6.31}$$

$$U_l = \frac{V_{l,s}}{(1-\alpha)} \tag{6.32}$$

$$X = \left(\frac{\rho_v}{\rho_l}\right)^{0.5} \times \left(\frac{\mu_v}{\mu_l}\right)^{0.1} \times \left(\frac{1-x}{x}\right)^{0.9} \tag{6.33}$$

As the summary of two phase adiabatic flow regime observed at various conditions by Damianides and Westwater are shown in Table 6.8.

Table 6.8: Summary of flow regime from Damianides and Westwater literature [23]

Description	Range	Flow Regimes Observed
Refrigerant	Air-Water	Dispersed-Bubbly, Bubbly, Plug, Slug, Pseudo-Slug Flow
Geometry	Circular Horizontal	
Diameter	1 mm to 5 mm	
Prandtl Number and Mass Flux	P=5 atm T=15-20ºC	

6.8.4.1 Comparison with Damianides & Westwater's map at T_{sat} of 40ºC and 55ºC

In comparison of our dataset with the flow map of Damianides and Westwater as in Figure 6.30 and 6.31 shows that predicted flow map have placed majority of the experimental data points in the intermittent flow region as compare to the annular flow region that is visualized by high speed camera. So, the vapor quality above 0.5 at mass flux of 150 kg m^{-2} s^{-1} shows that only two to three data points are in good agreement with the given flow map in term of annular flow regime at both saturation temperature of 40ºC and 55ºC. But the mass flux lower than 150 kg m^{-2} s^{-1} contradict with the flow map of Damianides and Westwater.

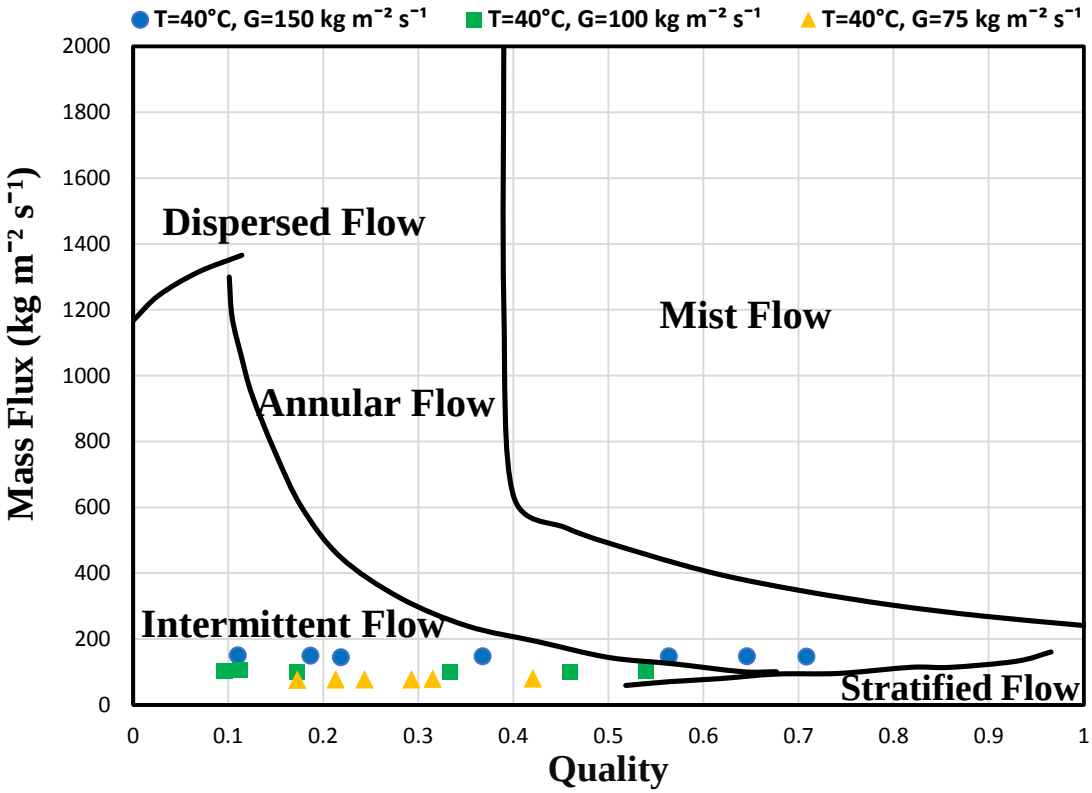

Figure 6.30: Data plotted against Damianides and Westwater proposed map at 40˚C

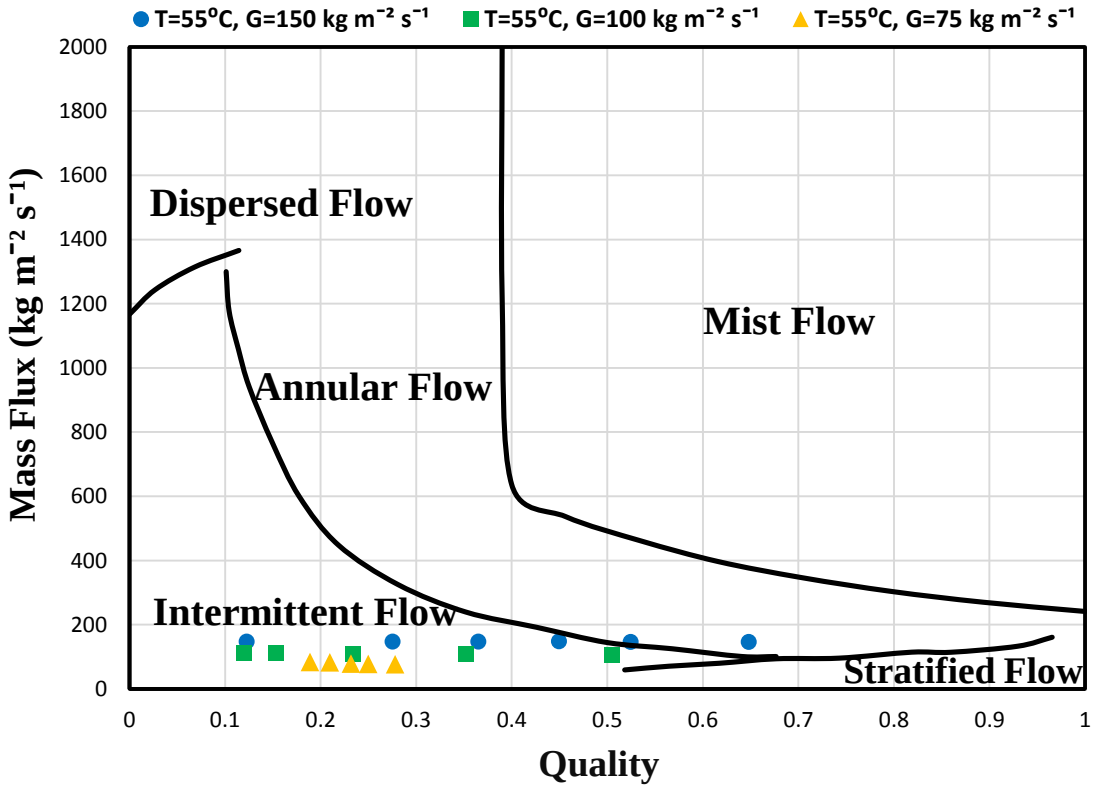

Figure 6.31: Data plotted against Damianides and Westwater proposed map at 55˚C

6.9 Comparison of Theoretical Data Points with Experimental Models

It was going to be considered that the prediction by flow map will be annular, intermittent, stratified, and stratified-wavy or mist flow. But percentage of flow regimes predicted by proposed model for most of the data points were in intermittent region and there were less data points in the region of annular, wavy, stratified flow regime as shown in Table 6.9. From the visualization of high speed camera, it was clear intermittent flow regime was not observed at all. Only wavy-annular/wavy-stratified flow regime observed at low mass fluxes. So comparison of our data points with the proposed model shows that no model have good agreement with the experimental collected data points except Thome et al. flow map.

Experimental data predicted by flow map of proposed model in term of percentage						
Proposed Model	**Stratified**	**Wavy**	**Annular**	**Intermittent**	**Dispersed**	**Mist**
Barnea (1983)	0%	0%	10%	91%	0%	0%
Breber (1980)	0%	10%	24%	66%	0%	0%
Thome (2003)	6%	94%	0%	0%	0%	0%
Damianides & Westwater (1988)	0%	0%	14%	86%	0%	0%

Table 6.9: Description of flow regime prediction by proposed model

6.10 Conclusions

In this present study, R-134a was partially condensed inside rectangular microchannel at low mass fluxes ($75 < G < 150$ kg m^{-2} s^{-1}) and at two saturation temperatures of 40°C and 55°C to determine the flow regimes by visualization of high speed camera. Which was applied under adiabatic condition to determine the heat transfer and pressure drop inside the channel geometry. As there was a very little agreement of our data point with the flow map of Thome et al. but remaining flow maps contradict to experimental data points and the prediction for occurring of intermittent and wavy flow in microchannels was wrong. So, other data points are also required to find out the transition flow in between annular, intermittent flow and stratified flow. From the results, it is cleared that

given proposed model did not show any agreement with experimental data sets except flow model of Thome et al. Who well predicted 94% of data points in wavy flow regime.

Summary

The study of two phase condensation of R-134a inside rectangular microchannels has been observed at lower mass fluxes from 75-150 kg m^{-2} s^{-1} and saturation temperatures of 40°C and 55°C and quality from 0.1 to 0.7. The superheated vapors of R-134a is introduced inside multiple rectangular microchannels geometry to partially condensed by applying deionized water in coolant section in a counter wise flow direction to observe the behavior of flow regimes by using Phantom V-310 high speed camera. Engineering Equation Solver program is used to model the governing heat transfer equations and also to determine the vapor quality of R-134a at exist of channel section. The wavy-annular or wavy-stratified flow regimes were observed from high speed camera. Data obtained was after that compared with the flow maps proposed by different authors. Which were over predict the occurrence of intermittent flow regimes at given conditions.

References

[1] World Economic Forum, “Energy for economic growth: Energy vision update 2012,” pp. 46, 2012.

[2] USEPA, “Advancing sustainable materials management: 2014 fact sheet,” United States Environ. Prot. Agency, Off. L. Emerg. Manag. Washington, DC 20460, no. November, pp. 22, 2016.

[3] J. M. Calm, “The next generation of refrigerants - Historical review, considerations, and outlook,” International Journal of Refrigeration, vol. 31, no. 7, pp. 1123–1133, 2008.

[4] A. Agarwal, “Heat transfer and pressure drop during condensation of refrigerants in microchannels,” Mechanical Engineering, Georgia Institute of Technology, 2006.

[5] J. W. Coleman and S. Garimella, “Two-phase flow regimes in round, square and rectangular tubes during condensation of refrigerant R134a,” International Journal of Refrigeration, vol. 26, no. 1, pp. 117–128, 2003.

[6] G. Nema, S. Garimella, and B. M. Fronk, “Flow regime transitions during condensation in microchannels,” International Journal of Refrigeration, vol. 40, pp. 227–240, 2014.

[7] J. A. Milkie, S. Garimella, and M. P. Macdonald, “Flow regimes and void fractions during condensation of hydrocarbons in horizontal smooth tubes,” International Journal of Heat and Mass Transfer, vol. 92, pp. 252–267, 2016.

[8] D. M. F. Wambsganss, "Two-phase flow patterns and transitions in a small horizontal rectangular channel," International Journal of Multiphase Flow, vol. 17(3), pp. 327-342, 1991.

[9] An Extension of the Flow Boiling Correlation to Transition, Laminar, and Deep Laminar Flows and Microchannels," Heat Transfer Engineering, vol. 25(3), pp. 86-93, April 2004.

[10] Wu, H. Y. and P. Cheng, "Condensation flow patterns in silicon microchannels," International Journal of Heat and Mass Transfer, vol. 48(11), pp. 2186-2197, 2005.

[11] J. El Hajal, J. R. Thome, and A. Cavallini, “Condensation in horizontal tubes, part 1: Two-phase flow pattern map,” International Journal of Heat and Mass Transfer, vol. 46, no. 18, pp. 3349–3363, 2003.

[12] Griffith, P, and K Lee, “The stability of an annulus of liquid in a tube.” Journal of Basic Engineering, vol. 86, pp. 666, 1964.

[13] Taitel, Y., and A. E. Dukler, “A model for predicting flow regime transitions in horizontal and near horizontal gas- liquid flow.” AIChE Journal, vol. 22 (1), pp. 47–55, 1976..

[14] Y. and P. C. Chen, “Chen, Y. and P. Cheng, "condensation of steam in silicon microchannels," International Communications in Heat and Mass Transfer, vol. 32(1-2), pp. 175-183, 2005.

[15] G. Breber, J. W. Palen, and J. Taborek, “Prediction of horizontal tubeside condensation of pure components using flow regime criteria,” Journal of Heat Transfer, vol. 102, no. 3, pp. 471, 1980.

[16] D. Barnea, Y. Luninski, and Y. Taitel, “Flow pattern in horizontal and vertical two phase flow in small diameter pipes,” Canadian Journal of Chemical Engineering, vol. 61, no. 5, pp. 617–620, Oct. 1983.

[17] Thome, J.R., J. El Hajal, and A. Cavallini, “Condensation in horizontal tubes, part 2: new heat transfer model based on flow regimes.” International Journal of Heat and Mass Transfer, vol. 46 (18), pp. 3365–87, 2003.

[18] Lockhart, R. W. and R. C. Martinelli, "Proposed correlation of data for isothermal two-phase, two-component flow in pipes," Chemical Engineering Progress, vol. 45(1), pp. 39-45, 1949.

[19] Chisholm, D. "Pressure gradients due to friction during the flow of evaporating two-phase mixtures in smooth tubes and channels," International Journal of Heat and Mass Transfer. vol. 16(2), pp. 347-358, 1973.

[20] Chen, I. Y., K.-S. Yang, Y.-J. Chang and C.-C. Wang, ‘Two-phase pressure drop of air-water and r-410a in small horizontal tubes,’ International Journal of Multiphase Flow. vol. 27(7), pp. 1293-1299, 2001.

[21] Micropump Magnetic Drive Gear Pump GA Series.

[22] R. Chiller, “Thermo Scientific NESLAB Merlin Installation Operation Basic Service,” no. 800.

[23] Coleman, John W., and Srinivas Garimella, “Characterization of two-phase flow patterns in small diameter round and rectangular tubes.” International Journal of Heat and Mass Transfer, vol. 42 (15), 1999.

ACKNOWLEDGEMENT

First and foremost, I would like to thank Allah Almighty, Who is the creator of this world and without His blessings, I would not have been able to finish my MS Thesis.

I would like to acknowledge my supervisor Dr. Majid Ali for his unprecedented support and guidance in completing this research work and his continuous suggestion brings a lot of changes in me during my research work at NUST and Oregon State University, USA.

I am immensely obliged to Dr. Brian Fronk for his support throughout my stay at Thermal Energy and System Transport Laboratory, Oregon State University. I would also acknowledged research scholar Tabeel Jacob of OSU who has been a constant source of motivation and encouragement for me. I have learned a lot from his experience.

I would like to thank my GEC members Dr. Muhammad Bilal Sajid, Dr. Naseem Iqbal, Dr. Adeel Waqas of U.S.-PCASE NUST for their valuable complements and suggestions to my research work.

I would like to express my sincere gratitude to all humanitarian and TEST Lab Fellows of MIME Dept. OSU. Who were with me during my stay at OSU and also thank full to Thermal Energy Engineering lab fellows of U.S.-PCASE NUST.

I am also thankful to U.S.-PCASE NUST and specially USAID for providing me scholarship and golden chance to study at Oregon State University, USA. I am highly thankful to my family members who supported me and has been a constant source of motivation and inspiration for me during my study.

APPENDIX-A

SAMPLE CALCULATIONS

EES MODELLING

"%_DESIGNING OF SQUARE MICROCHANNEL HEAT EXCHANGER__%"

"%%%%%----------Geometrical Parameters----------%%%%%%"

F_thick=0.2*convert(mm,m) "Fin thickness for both R-134a and Air side"

F_hei_ref=8*convert(mm,m) "Fin height for R-134a side"

F_hei_air=4.4*convert(mm,m) "Fin height for air side"

F_wid_ref&air=0.55*convert(mm,m) "One fin width for both sides"

F_length_ref=40*convert(mm,m) "Fin flow length for R-134a"

F_length_air=80*convert(mm,m) "Fin flow length for air side"

N_fins_ref=2*convert(mm^-1,m^-1) "51fins/inch""Number of fins per unit length for R-134a side"

N_fins_air=2*convert(mm^-1,m^-1) "51fins/inch""Number of fins per unit length for air side"

N_ch_air=6 "N_ch_air=(m_dot_h)/(G_h*L_2_h*L_3)""Total number of R-134a channels"

N_ch_ref=7 "N_ch_ref=(m_dot_c)/(G_c*L_2_c*L_3)""Total number of air channels"

W_thick=1*convert(mm,m) "Wall thickness between air and R-134a channel"

L_1=85*convert(mm,m) "L_h, Length of heat exchanger in flow direction of R-134a"

L_2_h=37*convert(mm,m) "W_h=L_c, Length of heat exchanger in flow direction of air for R-134a side"

L_2_c=41*convert(mm,m) "W_c, Length of heat exchanger in flow direction of R-134a for air side"

L_3=110*convert(mm,m) "Height of heat exchanger"

"%%%%%%----------Compactness Ratio----------%%%%%%"

F_wid_a=2.05*convert(mm,m) "Width of fin for air side"

F_hei_a=2.05*convert(mm,m) "Height of fin for air side"

F_wid_r=5.05*convert(mm,m) "Width of fin for R-134a side"

F_hei_r=5.05*convert(mm,m) "Height of fin for R-134a side"

Asp_rat_air=1 "Aspect ratio for air channel of square shaped"

Asp_rat_ref=1 "Aspect ratio for R-134a channel of square shaped"

"%%%%%%%----------Surface Geometrical Properties----------%%%%%%%"

"%%%%%%%-------Area Calculation For Air Side--------%%%%%%"

A_ttl_plt_air=2*L_1*L_2_h*N_ch_air "Total area of plate"

A_fin_bs_air=2*F_thick*F_length_air*N_fins_air*L_2_h*N_ch_air "Fin base area covering the plates"

A_hdr_air=2*F_hei_air*L_1*N_ch_air "Area of header bars"

A_hdr&plt_air=2*(F_hei_ref+2*W_thick)*(N_ch_air+1)*L_2_h "Area of header bars and plates of air at R-134a core inlet and outlet faces"

A_ttl_pri_air=(A_ttl_plt_air)-(A_fin_bs_air)+(A_hdr&plt_air)+(A_hdr_air) "The total primary surface area on the air side"

"%%%%%--------Components Of Secondary (Fins) Area For Air Side----------%%%%%"

A_fin_hei_air=2*(F_hei_air-F_thick)*F_length_air*N_fins_air*L_2_h*N_ch_air "Fin height area"

A_fin_edg_hei_air=2*(F_hei_air-F_thick)*F_thick*L_2_h*N_fins_air*N_ch_air "Fin edge height area"

A_fin_edg_wid_air=2*F_wid_ref&air*F_thick*L_2_h*N_fins_air*N_ch_air "Fin edge width area"

A_ttl_fin_air=(A_fin_hei_air)+(A_fin_edg_hei_air)+(A_fin_edg_wid_air) "Total secondary area on air side"

A_ttl_airside=A_ttl_pri_air+A_ttl_fin_air "Total surface area on air side"

A_freeflow_air=F_hei_air*L_2_h*N_ch_air-((F_hei_air-F_thick)+F_wid_ref&air)*F_thick*L_2_h*N_fins_air*N_ch_air "Free flow area on air side"

D_hyd_air=(4*A_freeflow_air*L_1)/A_ttl_airside "Hydraulic diameter of air side"

"%%%%%%%----------Area Calculation For R-134a Side----------%%%%%%%"

A_ttl_plt_ref=2*L_2_c*L_1*(N_ch_air+1) "Total plate area"

A_fin_bs_ref=2*F_thick*F_length_ref*N_fins_ref*L_1*(N_ch_air+1)"Fin base area covering plates"

A_hdr_ref=2*F_hei_ref*L_2_c*N_ch_ref "Area of header bars on the side for R-134a"

A_hdr&plt_ref=2*(F_hei_air+2*W_thick)*N_ch_air*L_1 "Area of header bars and plates of R-134a at air core inlet and outlet faces"

A_ttl_pri_ref=(A_ttl_plt_ref)-(A_fin_bs_ref)+(A_hdr&plt_ref)+(A_hdr_ref) "Total primary surface area on the R-134a side"

"%%%%--------Components Of Secondary (Fins) Area For R-134a Side---------%%%%"

A_fin_hei_ref=2*(F_hei_ref-F_thick)*F_length_ref*N_fins_ref*L_1*N_ch_ref "Fin height area"

A_fin_edg_hei_ref=2*(F_hei_ref-F_thick)*F_thick*N_ch_ref*L_1*N_fins_ref "Fin edge height area"

A_fin_edg_wid_ref=2*F_wid_ref&air*F_thick*N_ch_ref*N_fins_ref*L_1"Fin edge width area"

A_ttl_fin_ref=(A_fin_hei_ref)+(A_fin_edg_hei_ref)+(A_fin_edg_wid_ref) "Total secondary area on R-134a side"

A_ttl_refside=A_ttl_pri_ref+A_ttl_fin_ref "Total surface area on R-134a side"

A_freeflow_ref=F_hei_ref*L_1*(N_ch_ref)-((F_hei_ref-F_thick)+F_wid_ref&air)*F_thick*N_ch_ref*L_1*N_fins_ref"The free flow area on R-134a side"

D_hyd_ref=(4*A_freeflow_ref*L_2_c)/A_ttl_refside "Hydraulic diameter of R-134a side"

"%%%%%%%----------Compactness Of Heat Exchanger----------%%%%%%%"

A_ttl_HEX=A_ttl_airside+A_ttl_refside "Total area of the heat exchanger"

L_HEX=105.1*convert(mm,m) "Total length of heat exchanger"

W_HEX=56.1*convert(mm,m) "Total width of heat exchanger"

H_HEX=109.4*convert(mm,m) "Total height of heat exchanger"

V_ttl_HEX=L_HEX*W_HEX*H_HEX "Total volume of the heat exchanger"

Srf_Dnsty_HEX=A_ttl_HEX/V_ttl_HEX "Surface density of the heat exchanger"

R=287 "Gas

P_atm=91270 [pa] "Pressure at atm level"

rho_ref=P_atm/(R*T_c1) "Density of R-134a"

rho_air=P_atm/(R*T_h1) "Density of Air"

m_dot_air=0.012 [kg/s] "Mass flow rate of air"

m_dot_air=rho_air*A_freeflow_air*u_w

u_ref=3.25 [m/s] "Velocity of air at inlet"

m_dot_ref=rho_ref*A_freeflow_ref*u_ref "Mass flow rate of R-134a"

G_air=m_dot_air/(A_freeflow_air) "Mass flux for air side"

G_ref=m_dot_ref/(A_freeflow_ref) "Mass flux for R-134a side"

T_avg_air=(T_h1+T_h2)/2 "Average temperature of air"

mu_air=viscosity(Water,T=T_avg_air,P=P_atm) "Viscosity for air at avg temperature"

T_avg_ref=(T_c1+T_c2)/2 "Average temperature of R-134a"

mu_ref=viscosity(R-134a,T=T_avg_ref,P=P_atm) "Viscosity for R-134a at avg temperature"

"%%%%%%%----------Reynolds Number----------%%%%%%%"

Re_air=G_air*D_hyd_air/mu_air "Reynold number for air side"

Re_ref=G_ref*D_hyd_ref/mu_ref "Reynold number for R-134a side"

"%%%----Nusselt Number For Fully Developed Laminar Flow In Square Channel-----%%%"

Nu_air=8.235*(1-1.883*(Asp_rat_air)+3.767*(Asp_rat_air^2)-5.814*(Asp_rat_air^3)+5.361*(Asp_rat_air^4)-2*(Asp_rat_air^5))*(mu_air/mu_w)^(-0.14)"Nusselt number correlation from Kays and Crawford for square fully developed flow for air side"

Nu_ref=8.235*(1-1.883*(Asp_rat_ref)+3.767*(Asp_rat_ref^2)-5.814*(Asp_rat_ref^3)+5.361*(Asp_rat_ref^4)-2*(Asp_rat_ref^5))"Nusselt number correlation for R-134a side"

"%%%%%%----------Convection Heat Transfer Coefficient----------%%%%%%"

K_air=conductivity(Water,T=T_avg_air,P=P_atm) "Conductivity for air side"

h_air=Nu_air*K_air/D_hyd_air "Heat transfer coefficient for air"

K_ref=conductivity(R-134a,T=T_avg_ref,P=P_atm) "Conductivity for R-134a side"

h_ref=Nu_ref*K_ref/D_hyd_ref "Heat transfer coefficient for R-134a"

"%%%%%%----------Stanton Number----------%%%%%%"

St_air=h_air/(G_air*cp_h) "Stanton number for air side"

St_ref=h_ref/(G_ref*cp_c) "Stanton number for R-134a side"

"%%%%%%----------Colburn Factor----------%%%%%%"

Pr_air=Prandtl(Air_ha,T=T_avg_air,P=P_atm) "Prandtl number for air"

Pr_ref=Prandtl(R-134a,T=T_avg_ref,P=P_atm) "Prandtl number forR-134a"

j_air=St_air*Pr_air^2/3 "Colburn factor for air"

j_ref=St_ref*Pr_ref^2/3 "Colburn factor for R-134a"

"%%%%%----------Fin Efficiency Calculations----------%%%%%%"

"%%%%%%----------For Air side----------%%%%%%"

"As the Materials of fin at both sides are Aluminum 3003-O"

K_mtl=193 [W/m*K] "Conductivity of Al material"

m_air=(2*h_air/(K_mtl*F_thick)*(1+(F_thick/F_length_air)))^(1/2)

m_ref=(2*h_ref/(K_mtl*F_thick)*(1+(F_thick/F_length_ref)))^(1/2)

"%%%%------Overall Extended Surface Efficiency Adiabatic Fin Lengths------%%%"

l_air=(F_hei_air/2)-F_thick "Overall extended surface efficiency adiabatic fin lengths for air"

l_ref=(F_hei_ref/2)-F_thick "Overall extended surface efficiency adiabatic fin lengths for R-134a"

"%%%%%%----------Fin Efficiency----------%%%%%%"

```
eta_fin_air=(tanh(m_air*l_air))/(m_air*l_air)          "Fin effeiciency for air side"
eta_fin_ref=(tanh(m_ref*l_ref))/(m_ref*l_ref)          "Fin effeiciency for R-134a side"
"%%%%%%----------The Overall Surface Efficiency of Fin----------%%%%%%"
eta_ovr_fin_air=(1-(1-eta_fin_air)*(A_ttl_fin_air/A_ttl_airside))"Overall fin effeiciency for Air side"
eta_ovr_fin_ref=(1-(1-eta_fin_ref)*(A_ttl_fin_ref/A_ttl_refside))"Overall fin effeiciency for R-134a side"
"%%%%%%----------Total Thermal Resistance---------%%%%%%"
R_t=R_h+R_c+R_w+R_fh_bs+R_fc_bs                        "Total convection resistance"
R_h=1/(eta_ovr_fin_air*h_air*A_ttl_airside)            "Convection resistance of air side"
R_c=1/(eta_ovr_fin_ref*h_ref*A_ttl_refside)            "Convection resistance of R-134a side"
A_w=L_1*L_2_c*(2*N_ch_air+2)                           "Area of wall"
k_w=167 [W/K-m]                                        "Conductivity of wall"
R_w=W_thick/(k_w*A_w)                                  "Resistance of wall"
R_fh=0.00018                                           "Fouling resistance of air"
R_fh_bs=R_fh/(eta_ovr_fin_air*A_ttl_airside)
R_fc=0.00567                                           "Fouling resistance of R-134a"
R_fc_bs=R_fc/(eta_ovr_fin_ref*A_ttl_refside)
"%%%%%%----------Heat Transfer From Air----------%%%%%%"
T_h1=converttemp(C,K,150)                              "Inlet temperature of air"
T_h2=converttemp(C,K,90)                               "Outlet temperature of air"
cp_h=SpecHeat(Air_ha,T=T_avg_air,P=P_atm)              "Specific heat value of air"
Q_dot_air=m_dot_air*cp_h*(T_h1-T_h2)                    "Heat transfer from air"
"%%%%%%----------Heat Transfer To R-134a----------%%%%%%"
T_c1=converttemp(C,K,20)                               "Inlet temperature of R-134a"
T_c2= converttemp(C,K,95)                              "Outlet temperature of R-134a"
cp_c=SpecHeat(R-134a,T=T_avg_ref,P=P_atm)              "Specific heat value of R-134a"
Q_dot_ref=m_dot_ref*cp_c*(T_c2-T_c1)                   "Heat transfer to R-134a"
"%%%%%%----------Average Heat Transfer----------%%%%%%"
Q_avg=(Q_dot_air+Q_dot_ref)/2                          "Average heat transfer"
Q_max=m_dot_ref*cp_c*(T_h1-T_c1)                       " (if C_c<C_h)""Maximum heat transfer"
dt_1=T_h1-T_c2
dt_2=T_h2-T_c1
DELTA_T_lm=((dt_2)-(dt_1))/(ln(dt_2/dt_1))             "Log mean temperature difference"
UA=Q_avg/(DELTA_T_lm)                                  "Overall heat transfer coefficient"
```

T_wall=T_avg_ref "Temperature of wall"

mu_w=viscosity(Air_ha,T=T_avg_ref,P=P_atm)

P=(T_c2-T_c1)/(T_h1-T_c1) "Temperature effectiveness"

R_heat_capacity=(T_h1-T_h2)/(T_c2-T_c1) "Heat capacity rate ratio"

"%%%%%%---------Heat Capacity Rates----------%%%%%%"

C_air=m_dot_air*cp_h "Heat capacity rate of air"

C_ref=m_dot_ref*cp_c "Heat capacity rate of ref"

C_min=min(C_ref,C_air) "Minimum heat capacity rate"

C_max=max(C_ref,C_air) "Maximum heat capacity rate"

C.R=C_min/C_max "Capacity rate ratio"

"%%%%%%----------Number Of Transfer Units----------%%%%%%"

NTU=UA/C_min

"%%%%%%----------Effectiveness Of Heat Exchanger----------%%%%%%"

E_HEX=Q_avg/Q_max

"%%%%%%----------Pressure Drop ----------%%%%%%"

f=24/(Re_air*(1-1.3553*Asp_rat_air+1.9467*Asp_rat_air^2-1.7012*Asp_rat_air^3+0.9564*Asp_rat_air^4-0.2537*Asp_rat_air^5)) "For square channel,aspect ratio a < 1Guyer (1989) Shah and London (1979)"

Delta_P_air=(4*f*L_HEX/D_hyd_air)*(1/2*rho_air*u_w^2) "Pressure drop for air"

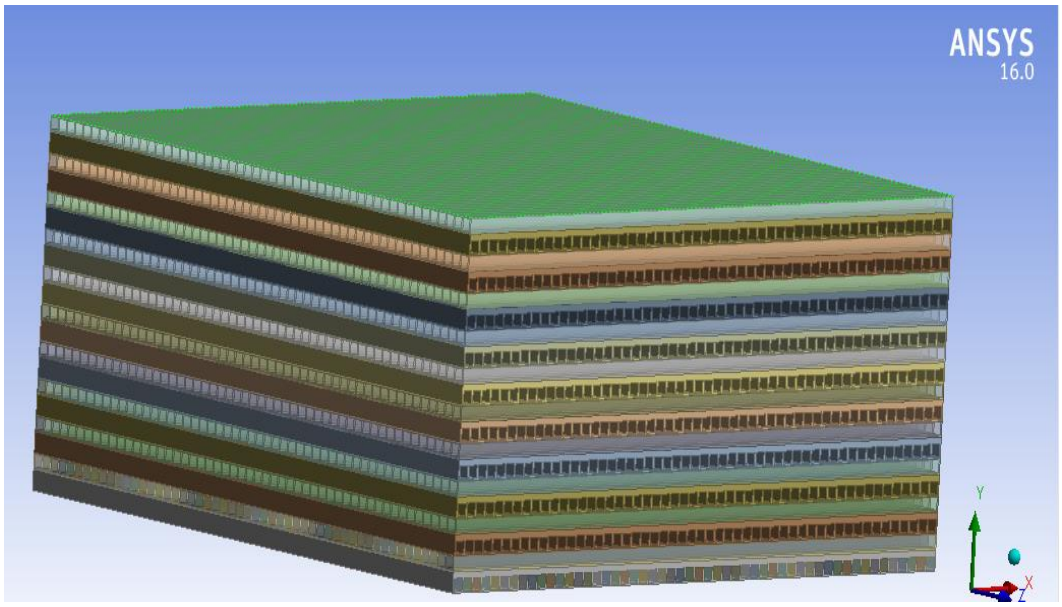

Figure 7.1: Actual diagram drawn on Ansys 16.0 representing square microchannel heat exchanger based on EES code

"%_DESIGNING OF TRIANGULAR MICROCHANNEL HEAT EXCHANGER_%"

"%%%%%----------Geometrical Parameters----------%%%%%"

F_thick=0.2*convert(mm,m) "Fin thickness for both R-134a and air side"

F_hei_ref=7*convert(mm,m) "Fin height for R-134a side"

F_hei_air=4*convert(mm,m) "Fin height for air side"

F_wid_ref&air=0.5*convert(mm,m) "One fin width for both sides"

F_length_ref=40*convert(mm,m) "Fin flow length for R-134a side"

F_length_air=80*convert(mm,m) "Fin flow length for air side"

N_fins_ref=1.5*convert(mm^-1,m^-1) "38fins/inch""Number of fins per unit length for R-134a side"

N_fins_air=1.5*convert(mm^-1,m^-1) "38fins/inch""Number of fins per unit length for air side"

N_ch_air=6"N_ch_ref=(m_dot_c)/(G_c*L_2_c*L_3)""Total number of air channels"

N_ch_ref=7"N_ch_air=(m_dot_h)/(G_h*L_2_h*L_3)""Total number of R-134a channels"

W_thick=1*convert(mm,m) "Wall thickness between R-134a and air channels"

L_1=85*convert(mm,m) "L_h Length of heat exchanger in flow direction of air"

L_2_h=37*convert(mm,m) "W_h=L_c Length of heat exchanger in flow direction of R-134a for air side"

L_2_c=41*convert(mm,m) "W_c Length of heat exchanger in flow direction of air for R-134a side"

L_3=110*convert(mm,m) "Height of heat exchanger"

"%%%%%%----------Compactness Ratio----------%%%%%%"

F_wid_a=0.35*convert(mm,m) "Width of fin for air side"

F_hei_a=3.75*convert(mm,m) "Height of fin for air side"

F_wid_r=0.35*convert(mm,m) "Width of fin for R-134a side"

F_hei_r=9.75*convert(mm,m) "Height of fin for R-134a side"

Asp_rat_air=0.0933 "Aspect ratio for air channel"

Asp_rat_ref=0.0359 "Aspect ratio for R-134a channel"

"%%%%%%%%----------Surface Geometrical Properties----------%%%%%%%%"

"%%%%%%%--------Area Calculation For Air Side---------%%%%%%"

A_ttl_plt_air=2*L_1*L_2_h*N_ch_air "Total area of plate"

A_fin_bs_air=2*F_thick*F_length_air*N_fins_air*L_2_h*N_ch_air"Fin base area covering the plates"

A_hdr_air=2*F_hei_air*L_1*N_ch_air "Area of header bars"

A_hdr&plt_air=2*(F_hei_ref+2*W_thick)*(N_ch_air+1)*L_2_h"Area of header bars and plates of R-134a at air core inlet and outlet faces"

A_ttl_pri_air=(A_ttl_plt_air)-(A_fin_bs_air)+(A_hdr&plt_air)+(A_hdr_air)"The total primary surface area on the air side"

A_freeflow_air=F_hei_air*L_2_h*N_ch_air-((F_hei_air-F_thick)+F_wid_ref&air)*F_thick*L_2_h*N_fins_air*N_ch_air "Free flow area on air side"

"%%%%%--------Components Of Secondary (Fins) Area For Air Side----------%%%%%"

A_unit_cell_a=2*((F_wid_ref&air/2)+x_1)*F_length_air "Unit area of triangle fin"

x_1=(F_wid_ref&air/2)/0.7071 "0.7071=cos60""side length of triangle fin"

A_f_a=N_ch_air*A_unit_cell_a*N_fins_air "Total secondary area on air side"

A_ttl_airside=A_ttl_pri_air+A_f_a "The total surface area on air side"

D_hyd_air=(4*(F_wid_ref&air/2)*F_hei_air)/((F_wid_ref&air/2)+((F_wid_ref&air/2)^2+2*(F_hei_air)^2)^(1/2))"Hydraulic diameter of air side"

"%%%%%%%----------Area Calculation For R-134a Side----------%%%%%%"

A_ttl_plt_ref=2*L_2_c*L_1*(N_ch_air+1) "Total plate area"

A_fin_bs_ref=2*F_thick*F_length_ref*N_fins_ref*L_1*(N_ch_air+1)"Fin base area covering plates"

A_hdr_ref=2*F_hei_ref*L_2_c*N_ch_ref"Area of header bars on the side for R-134a"

A_hdr&plt_ref=2*(F_hei_air+2*W_thick)*N_ch_air*L_1 "Area of header bars and plates of Air_ha at R-134a core inlet and outlet faces"

A_ttl_pri_ref=(A_ttl_plt_ref)-(A_fin_bs_ref)+(A_hdr&plt_ref)+(A_hdr_ref) "The total primary surface area on the R-134a side"

A_freeflow_ref=F_hei_ref*L_1*(N_ch_ref)-((F_hei_ref-F_thick)+F_wid_ref&air)*F_thick*N_ch_ref*L_1*N_fins_ref "The free flow area on R-134a side"

"%%%%-------Components Of Secondary (Fins) Area For R-134a Side--------%%%%"

A_unit_cell_r=2*((F_wid_ref&air/2)+x_2)*F_length_ref "Unit area of triangular fin for R-134a"

x_2=(F_wid_ref&air/2)/0.7071 "Side length of triangular fin"

A_f_r=N_ch_ref*A_unit_cell_r*N_fins_ref "Fin sided total area"

A_ttl_refside=A_ttl_pri_ref+A_f_r "The total surface area on air side"

D_hyd_ref=(4*(F_wid_ref&air/2)*(F_hei_ref))/((F_wid_ref&air/2)+((F_wid_ref&air/2)^2+2*(F_hei_ref)^2)^(1/2)) "Hydraulic diameter of Air_ha side"

"%%%%%%%----------Compactness Of Heat Exchanger----------%%%%%%%"

A_ttl_HEX=A_ttl_airside+A_ttl_refside "Total area of the heat exchanger"

L_HEX=105.1*convert(mm,m) "Total length of heat exchanger"

W_HEX=56.1*convert(mm,m) "Total width of heat exchanger"

H_HEX=109.4*convert(mm,m) "Total height of heat exchanger"

V_ttl_HEX=L_HEX*W_HEX*H_HEX "Total volume of the heat exchanger"

Srf_Dnsty_HEX=A_ttl_HEX/V_ttl_HEX "Surface density of the heat exchanger"

R=287 "Gas constant"

P_atm=91270 [pa] "Pressure at atm level"

rho_ref=P_atm/(R*T_c1) "Density of R-134a"

rho_air=P_atm/(R*T_h1) "Density of air"

m_dot_air=0.012 [kg/s] "Mass flow rate of air"

m_dot_air=rho_air*A_f_a*u_w

u_air=3.25 [m/s] "Velocity of R-134a at inlet"

m_dot_ref=rho_ref*A_freeflow_ref*u_air "Mass flow rate of R-134a"

G_air=m_dot_air/(A_freeflow_air) "Mass flux for air side"

G_ref=m_dot_ref/(A_freeflow_ref) "Mass flux for R-134a side"

T_avg_air=(T_h1+T_h2)/2 "Average temperature of air"

mu_air=viscosity(Air_ha,T=T_avg_air,P=P_atm) "Viscosity for air at avg temperature"

T_avg_ref=(T_c1+T_c2)/2 "Average temperature of R-134a"

mu_ref=viscosity(R-134a,T=T_avg_ref,P=P_atm) "Viscosity of R-134a at avg temperature"

"%%%%%%%----------Reynolds Number----------%%%%%%%"

Re_air=G_air*D_hyd_air/mu_air "Reynold number for air side"

Re_ref=G_ref*D_hyd_ref/mu_ref "Reynold number for R-134a side"

"%%-----Nusselt Number For Fully Developed Laminar Flow In Square Channel------%%"

Nu_air=0.943*(F_wid_a^5+5.35*F_wid_a^4-9.25*F_wid_a^3+11.931*F_wid_a^2-9.8035*F_wid_a^1+3.375) "Nusselt number for fully developed flow inside triangular channel for air side"

Nu_ref=0.943*(F_wid_r^5+5.35*F_wid_r^4-9.25*F_wid_r^3+11.931*F_wid_r^2-9.8035*F_wid_r^1+3.375) "Nusselt number for fully developed flow inside triangular channel for air side"

"%%%%%%%----------Convection Heat Transfer Coefficient----------%%%%%%%"

K_air=conductivity(Air_ha,T=T_avg_air,P=P_atm) "Conductivity For air side"

h_air=Nu_air*K_air/D_hyd_air

K_ref=conductivity(R-134a,T=T_avg_ref,P=P_atm) "Conductivity For R-134a side"

h_ref=Nu_ref*K_ref/D_hyd_ref

"%%%%%%%----------Stanton Number----------%%%%%%%"

St_air=h_air/(G_air*cp_h) "For air side"

St_ref=h_ref/(G_ref*cp_c) "For R-134a side"

"%%%%%%%----------Colburn Factor----------%%%%%%%"

Pr_air=Prandtl(Air_ha,T=T_avg_air,P=P_atm) "Prandtl number of air"

Pr_ref=Prandtl(R-134a,T=T_avg_ref,P=P_atm) "Prandtl number of R-134a"

j_air=St_air*Pr_air^2/3 "Colburn factor for air"

j_ref=St_ref*Pr_ref^2/3 "Colburn factor for R-134a"

"%%%%%%----------Fin Efficiency Calculations----------%%%%%%%"

"%%%%%%%----------For Air side----------%%%%%%%"

"As the Materials of fin at both sides are Aluminum 3003-O"

K_mtl=193 [W/m*K] "Conductivity of Al material"

m_air=(2*h_air/(K_mtl*F_thick)*(1+(F_thick/F_length_air)))^(1/2)

m_ref=(2*h_ref/(K_mtl*F_thick)*(1+(F_thick/F_length_ref)))^(1/2)

"%%%%-------Overall Extended Surface Efficiency Adiabatic Fin Lengths---------%%%%%%"

l_air=(F_hei_air/2)-F_thick "Overall extended surface efficiency adiabatic fin lengths for air"

l_ref=(F_hei_ref/2)-F_thick "Overall extended surface efficiency adiabatic fin lengths for R-134a"

"%%%%%%%----------Fin Efficiency----------%%%%%%%"

eta_fin_air=(tanh(m_air*l_air))/(m_air*l_air) "Fin effeiciency for Air side"

eta_fin_ref=(tanh(m_ref*l_ref))/(m_ref*l_ref) "Fin effeiciency for R-134a side"

"%%%%%%%----------The Overall Surface Efficiency of Fin----------%%%%%%%"

eta_ovr_fin_air=(1-(1-eta_fin_air)*(A_f_a/A_ttl_airside)) "Overall fin effeiciency for Air side"

eta_ovr_fin_ref=(1-(1-eta_fin_ref)*(A_f_r/A_ttl_refside)) "Overall fin effeiciency for R-134a side"

"%%%%%%%----------Total Thermal Resistance---------%%%%%%%"

R_t=R_h+R_c+R_w+R_fh_bs+R_fc_bs "Total convection resistance"

R_h=1/(eta_ovr_fin_air*h_air*A_ttl_airside) "Convection resistance of air side"

R_c=1/(eta_ovr_fin_ref*h_ref*A_ttl_refside) "Convection resistance of R-134a side"

A_w=L_1*L_2_c*(2*N_ch_air+2) "Area of wall"

k_w=167 [W/K-m] "Conductivity of wall"

R_w=W_thick/(k_w*A_w) "Resistance of wall"

R_fh=0.00018 "Fouling resistance of air"

R_fh_bs=R_fh/(eta_ovr_fin_air*A_ttl_airside)

R_fc=0.00567 "Fouling resistance of R-134a"

R_fc_bs=R_fc/(eta_ovr_fin_ref*A_ttl_refside)

"%%%%%%%----------Heat Transfer From Air----------%%%%%%%"

T_h1=converttemp(C,K,150) "Inlet temperature of air"

T_h2=converttemp(C,K,90) "Outlet temperature of air"

cp_h=SpecHeat(Air_ha,T=T_avg_air,P=P_atm) "Specific heat value of air"

Q_dot_air=m_dot_air*cp_h*(T_h1-T_h2) "Heat transfer from air"

"%%%%%%%----------Heat Transfer To R-134a----------%%%%%%%"

T_c1=converttemp(C,K,20) "Inlet temperature of R-134a"

T_c2= converttemp(C,K,95) "Outlet temperature of R-134a"

cp_c=SpecHeat(R-134a,T=T_avg_ref,P=P_atm) "Specific heat value of R-134a"

Q_dot_ref=m_dot_ref*cp_c*(T_c2-T_c1) "Heat transfer to R-134a"

"%%%%%%%----------Average Heat Transfer----------%%%%%%%"

Q_avg=(Q_dot_air+Q_dot_ref)/2 "Average heat transfer"

Q_max=m_dot_ref*cp_c*(T_h1-T_c1) "(if C_c<C_h)""Maximum heat transfer"

dt_1=T_h1-T_c2

dt_2=T_h2-T_c1

DELTA_T_lm=((dt_2)-(dt_1))/(ln(dt_2/dt_1)) "Log mean temperature difference"

UA=Q_avg/(DELTA_T_lm) "Overall heat transfer coefficient"

T_w=T_avg_ref "Temperature of wall"

mu_w=viscosity(Air_ha,T=T_avg_ref,P=P_atm)

P=(T_c2-T_c1)/(T_h1-T_c1) "Temperature effectiveness"

R_heat_capacity=(T_h1-T_h2)/(T_c2-T_c1) "Heat capacity rate ratio"

"%%%%%%%---------Heat Capacity Rates----------%%%%%%%"

C_air=m_dot_air*cp_h "Heat capacity rate of air"

C_ref=m_dot_ref*cp_c "Heat capacity rate of ref"

C_min=min(C_ref,C_air) "Minimum heat capacity rate"

C_max=max(C_ref,C_air) "Maximum heat capacity rate"

C.R=C_min/C_max "Capacity rate ratio"

"%%%%%%%----------Number Of Transfer Units----------%%%%%%%"

NTU=UA/C_min

"%%%%%%----------Effectiveness Of Heat Exchanger----------%%%%%%"

E_HEX=Q_avg/Q_max

"%%%%%%----------Pressure Drop ----------%%%%%%"

f=64/Re_ref"If Re<2300 for laminar case Hagen-Poiseuille equation"

DELTA_P_ref=(f*L_HEX*rho_ref*u_air^2)/(D_hyd_ref*2) "Pressure drop for R-134a"

"DELTA_P_h=(f*L_HEX*rho_air*m_dot_air^2)/(D_hyd_air*2)" "Pressure drop for air"

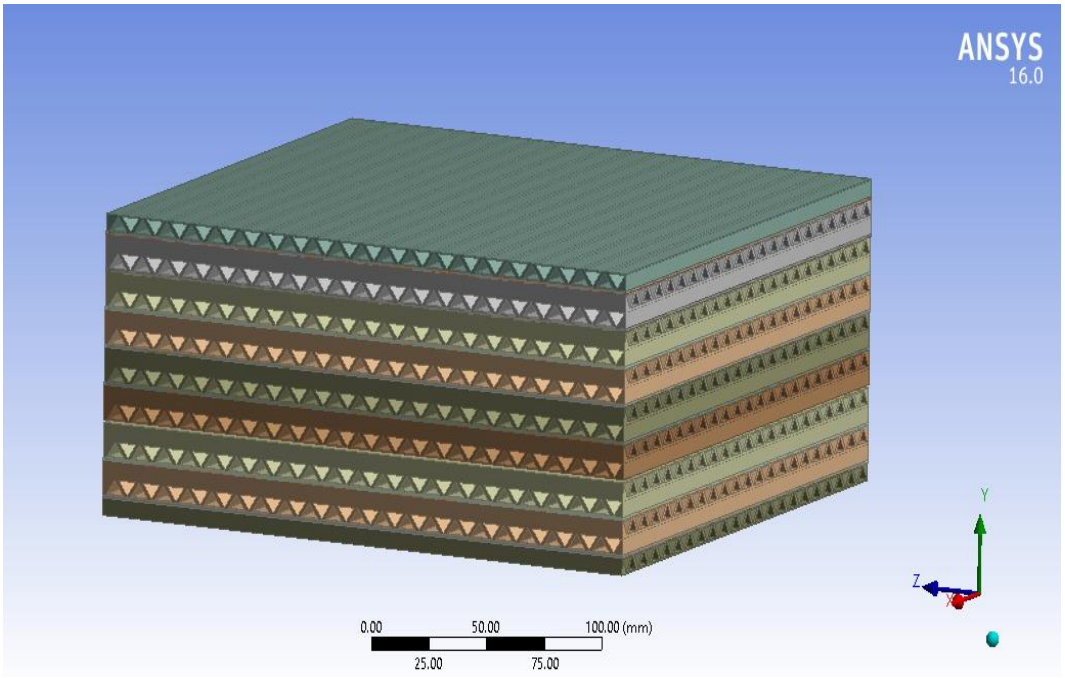

Figure 7.2: Actual diagram drawn on Ansys 16.0 representing triangular microchannel heat exchanger based on EES code

"%%%DESIGNING OF CIRCULAR MICROCHANNEL HEAT EXCHANGER%%%"

"%%%%%----------Geometrical Parameters----------%%%%%%"

F_thick=0.1*convert(mm,m) "Thickness of circular channel for both R-134a and air side"

D_ref=0.00065[m] "Diameter of channel for R-134a side"

D_air=0.00068[m] "Diameter of channel for air side"

F_length_ref=40*convert(mm,m) "Fin flow length for R-134a side"

F_length_air=80*convert(mm,m) "Fin flow length for air side"

N_fins_ref=1.7*convert(mm^-1,m^-1) "44fins/inch""Number of fins per unit length for R-134a side"

N_fins_air=1.7*convert(mm^-1,m^-1) "44fins/inch""Number of fins per unit length for Air side"

N_ch_air=6 "Total number of air channels"

N_ch_ref=7 "Total number of R-134a channels"

W_thick=0.5*convert(mm,m) "Wall thickness between R-134a and air channels"

L_1=70*convert(mm,m) "L_h, Length of heat exchanger in flow direction of air"

L_2_h=30*convert(mm,m) "W_h=L_c Length of heat exchanger in flow direction of R-134a for air side"

L_2_c=86*convert(mm,m) "W_c Length of heat exchanger in flow direction of Air for R-134a side"

L_3=110*convert(mm,m) "Height of heat exchanger"

"%%%%%%%----------Surface Geometrical Properties----------%%%%%%%"

"%%%%%%--------Area Calculation For Air Side---------%%%%%%"

A_ttl_plt_air=2*L_1*L_2_h*N_ch_air "Total area of plate"

A_fin_bs_air=2*F_thick*F_length_air*N_fins_air*L_2_h*N_ch_air"Fin base area covering the plates"

A_hdr_air=2*L_1*N_ch_air*(D_air+2*F_thick+2*W_thick)"Area of header bars"

A_ttl_pri_air=(A_ttl_plt_air)-(A_fin_bs_air)+(A_hdr_air) "Total primary surface area on the air side"

A_ttl_airside=A_ttl_pri_air+A_f_1 "Total area on area side"

A_freeflow_air=0.000539 "Free frontal flow area for air side"

A_f_1=0.25

{A_freeflow_air=pi*D_air^2/4*N_ch_air*N_fins_air "Free flow area on Air side"}

"D_air=(4*A_freeflow_air*L_1)/A_ttl_airside" "Hydraulic diameter of Air side"

"%%%%%%%----------Area Calculation For R-134a Side----------%%%%%%%"

A_ttl_plt_ref=2*L_2_c*L_1*(N_ch_air+1) "Total plate area"

A_fin_bs_ref=2*F_thick*F_length_ref*N_fins_ref*L_1*(N_ch_air+1)"Fin base area covering plates"

A_hdr_ref=2*L_2_c*N_ch_air*(D_ref+2*F_thick+2*W_thick)"Area of header bars on the side for R-134a"

A_ttl_pri_ref=(A_ttl_plt_ref)-(A_fin_bs_ref)+(A_hdr_ref) "Total surface area on the R-134a side"

A_ttl_refside=A_ttl_pri_ref+A_f_2 "Total surface area on R-134a side"

"Free Frontal flow area for R-134a side"

A_freeflow_ref=pi*D_ref^2/4*N_ch_ref*N_fins_ref "Free flow area on R-134a side"

"D_ref=(4*A_freeflow_ref*L_2_c)/A_ttl_pri_ref" "Hydraulic diameter of R-134a side"

A_f_2=0.840

"%%%%%%%----------Compactness Of Heat Exchanger----------%%%%%%%"

A_ttl_HEX=A_ttl_airside+A_ttl_refside "Total area of the heat exchanger"

L_HEX=105.1*convert(mm,m) "Total length of heat exchanger"

W_HEX=56.1*convert(mm,m) "Total width of heat exchanger"

H_HEX=109.4*convert(mm,m) "Total height of heat exchanger"

V_ttl_HEX=L_HEX*W_HEX*H_HEX "Total volume of the heat exchanger"

Srf_Dnsty_HEX=A_ttl_HEX/V_ttl_HEX "Surface density of the heat exchanger"

R=287 "Gas constant"

P_atm=91270 [pa] "Pressure at atm level"

rho_ref=P_atm/(R*T_c1) "Density of ref"

rho_air=P_atm/(R*T_h1) "Density of air"

m_dot_air=0.012 [kg/s] "Mass flow rate of air"

m_dot_air=rho_air*A_freeflow_air*u_h

u_ref=3.25 [m/s] "Velocity of R-134a at inlet"

m_dot_ref=rho_ref*A_freeflow_ref*u_ref "Mass flow rate of R-134a"

G_air=m_dot_air/(A_freeflow_air) "Mass flux for air side"

G_ref=m_dot_ref/(A_freeflow_ref) "Mass flux for R-134a side"

T_avg_h=(T_h1+T_h2)/2 "Average temperature of air"

mu_air=viscosity(Air_ha,T=T_avg_h,P=P_atm) "Viscosity for Air at avg temperature"

T_avg_ref=(T_c1+T_c2)/2 "Average temperature of R-134a"

mu_c=viscosity(R-134a,T=T_avg_ref,P=P_atm) "Viscosity for R-134a at avg temperature"

"%%%%%%%----------Reynolds Number----------%%%%%%%"

Re_air=G_air*D_air/mu_air "Reynold number for air side"

Re_ref=G_ref*D_ref/mu_c "Reynold number for R-134a side"

"%%-----Nusselt Number For Fully Developed Laminar Flow In Circular Channel------%%"

Nu_air=1.86*Re_air^(1/3)*Pr_h^(1/3)*(D_air/L_1)^(1/3)*(mu_air/mu_c)^(0.14) "For air side, Nusselt number correlation of Sieder and Tate for fully developed flow inside circular channel"

Nu_ref=1.86*Re_ref^(1/3)*Pr_c^(1/3)*(D_ref/L_2_h)^(1/3)*(mu_air/mu_c)^(0.14) "For R-134a side, Nusselt number correlation of Sieder and Tate for fully developed flow inside circular channel"

"%%%%%%%----------Convection Heat Transfer Coefficient----------%%%%%%%"

K_air=conductivity(Air_ha,T=T_avg_h,P=P_atm) "Conductivity of air at avg temperature"

h_air=Nu_air*K_air/D_air "Heat transfer coefficient of air"

K_ref=conductivity(R-134a,T=T_avg_ref,P=P_atm) "Conductivity of R-134a at avg temperature"

h_ref=Nu_ref*K_ref/D_ref "Heat transfer coefficient of R-134a"

"%%%%%%%----------Stanton Number----------%%%%%%%"

St_air=h_air/(G_air*cp_h) "Stanton number for air side"

St_ref=h_ref/(G_ref*cp_c) "Stanton number for R-134a side"

"%%%%%%%----------Colburn Factor----------%%%%%%%"

Pr_h=Prandtl(Air_ha,T=T_avg_h,P=P_atm) "Prandtl number for air"

Pr_c=Prandtl(R-134a,T=T_avg_ref,P=P_atm) "Prandtl number for R-134a"

j_h=St_air*Pr_h^2/3 "Colburn factor for air"

j_c=St_ref*Pr_c^2/3 "Colburn factor for Ref"

"%%%%%%----------Fin Efficiency Calculations----------%%%%%%%"

"As the Materials of fin at both sides are Aluminum 3003-O"

K_mtl=193 [W/m*K] "Conductivity of Al material"

m_h=(2*h_air/(K_mtl*F_thick)*(1+(F_thick/F_length_air)))^(1/2)

m_c=(2*h_ref/(K_mtl*F_thick)*(1+(F_thick/F_length_ref)))^(1/2)

"%%%%----Overall Extended Surface Efficiency Adiabatic Fin Lengths------%%%%"

I_1h=(D_air+2*F_thick+2*W_thick/2)-F_thick "Overall extended surface efficiency adiabatic fin lengths for air"

l_1c=(D_ref+2*F_thick+2*W_thick/2)-F_thick "Overall extended surface efficiency adiabatic fin lengths for R-134a"

"%%%%%%%----------Fin Efficiency----------%%%%%%%"

eta_fin_air=(tanh(m_h*l_1h))/(m_h*l_1h) "Fin effeiciency for air side"

eta_fin_ref=(tanh(m_c*l_1c))/(m_c*l_1c) "Fin effeiciency for R-134a side"

"%%%%%%%----------The Overall Surface Efficiency of Fin----------%%%%%%%"

eta_ovr_fin_air=(1-(1-eta_fin_air)*(A_fin_bs_air/A_ttl_pri_air))"Overall fin effeiciency for air side"

eta_ovr_fin_ref=(1-(1-eta_fin_ref)*(A_fin_bs_ref/A_ttl_pri_ref)) "Overall fin effeiciency for R-134a side"

"%%%%%%%----------Total Thermal Resistance----------%%%%%%%"

R_t=R_h+R_c+R_w+R_fh_bs+R_fc_bs "Total convection resistance"

R_h=1/(eta_ovr_fin_air*h_air*A_ttl_pri_air) "Convection resistance of air side"

R_c=1/(eta_ovr_fin_ref*h_ref*A_ttl_pri_ref) "Convection resistance of R-134a side"

A_w=L_1*L_2_c*(2*N_ch_air+2) "Area of wall"

k_w=167 [W/K-m] "Conductivity of wall"

R_w=W_thick/(k_w*A_w) "Resistance of wall"

R_fh=0.00018

R_fh_bs=R_fh/(eta_ovr_fin_air*A_ttl_pri_air) "Fouling resistance of air"

R_fc=0.00567

R_fc_bs=R_fc/(eta_ovr_fin_ref*A_ttl_pri_ref) "Fouling resistance of R-134a"

"%%%%%%%----------Heat Transfer From Air----------%%%%%%%"

T_h1=converttemp(C,K,150) "Inlet temperature of air"

T_h2=converttemp(C,K,90) "Outlet temperature of air"

cp_h=SpecHeat(Air_ha,T=T_avg_h,P=P_atm) "Specific heat value of air"

Q_dot_air=m_dot_air*cp_h*(T_h1-T_h2) "Heat Transfer from R-134a"

"%%%%%%%----------Heat Transfer To R-134a----------%%%%%%%"

T_c1=converttemp(C,K,20) "Inlet temperature of R-134a"

T_c2= converttemp(C,K,95) "Outlet temperature of R-134a"

cp_c=SpecHeat(R-134a,T=T_avg_ref,P=P_atm) "Specific heat value of R-134a"

Q_dot_ref=m_dot_ref*cp_c*(T_c2-T_c1) "Heat transfer to R-134a"

"%%%%%%%----------Average Heat Transfer----------%%%%%%%"

Q_avg=(Q_dot_air+Q_dot_ref)/2 "Average heat transfer"

Q_max=m_dot_ref*cp_c*(T_h1-T_c1) "(if C_c<C_h)""Maximum heat transfer"

dt_1=T_h1-T_c2

```
dt_2=T_h2-T_c1
DELTA_T_lm=((dt_2)-(dt_1))/(ln(dt_2/dt_1))        "Log mean temperature difference"
UA=Q_avg/(DELTA_T_lm)                             "Overall heat transfer coefficient"
P=(T_c2-T_c1)/(T_h1-T_c1)                         "Temperature effectiveness"
R_heat_capacity=(T_h1-T_h2)/(T_c2-T_c1)           "Heat capacity rate ratio"
                "%%%%%%%---------Heat Capacity Rates-----------%%%%%%%"
C_air=m_dot_air*cp_h                              "Heat capacity rate of air"
C_ref=m_dot_ref*cp_c                              "Heat capacity rate of ref"
C_min=min(C_ref,C_air)                            "Minimum heat capacity rate"
C_max=max(C_ref,C_air)                            "Maximum heat capacity rate"
C.R=C_min/C_max                                   "Capacity rate ratio"

              "%%%%%%%-----------Number Of Transfer Units-----------%%%%%%%"
NTU=UA/C_min
           "%%%%%%%-----------Effectiveness Of Heat Exchanger------------%%%%%%%"
E_HEX=Q_avg/Q_max
                "%%%%%%%------------Pressure Drop ----------------%%%%%%%"
f=64/Re_ref  "if Re<2300 for laminar case Hagen-Poiseuille equation"
DELTA_P_ref=(f*L_HEX*rho_ref*u_ref^2)/(D_ref*2) "Pressure drop for R-134a"
"DELTA_P_air=(f*L_HEX*rho_air*u_h^2)/(D_air*2)" "Pressure drop for air"
```

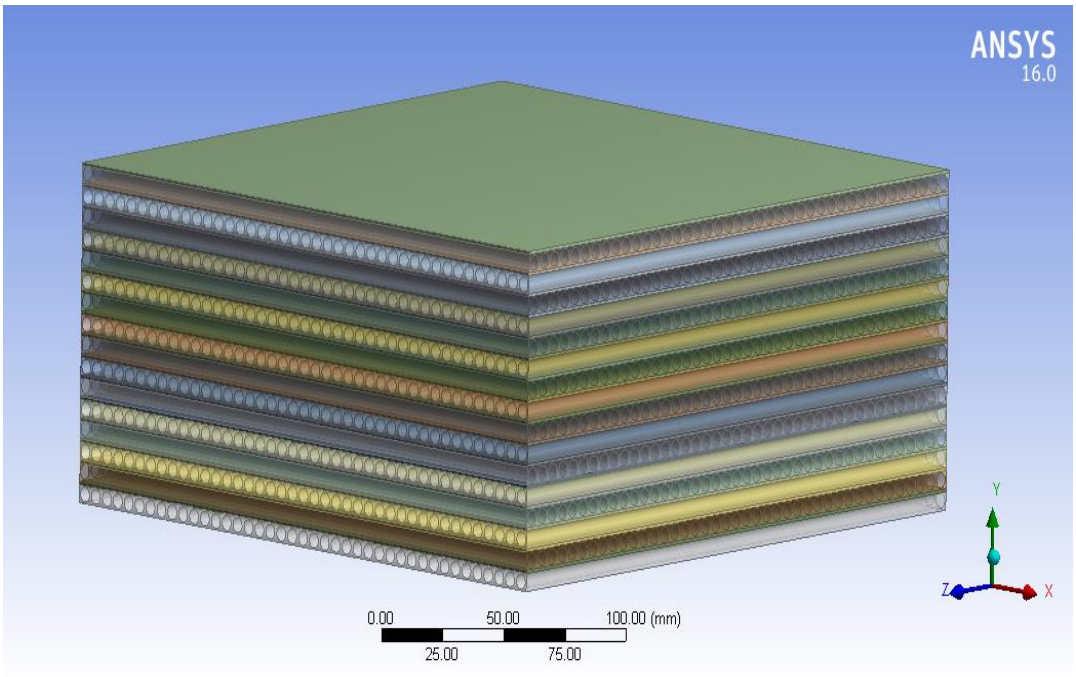

Figure 7.3: Actual diagram drawn on Ansys 16.0 representing circular microchannel heat exchanger based on EES code

"%%DESIGNING OF RECTANGULAR MICROCHANNEL HEAT EXCHANGER%%"

"%%%%%------Geometrical Parameters-------%%%%%"

F_thick=0.2*convert(mm,m) "Fin thickness for both R-134a and air side"

F_hei_ref=10*convert(mm,m) "Fin height for R-134a"

F_hei_air=4*convert(mm,m) "Fin height for air side"

F_wid_ref&air=0.55*convert(mm,m) "One fin width for both sides"

F_length_ref=40*convert(mm,m) "Fin flow length for R-134a"

F_length_air=80*convert(mm,m) "Fin flow length for air side"

N_fins_ref=1.8*convert(mm^-1,m^-1) "46fins/inch""Number of fins per unit length for R-134a side"

N_fins_air=1.8*convert(mm^-1,m^-1) "46fins/inch""Number of fins per unit length for air side"

N_channels_air=6 "N_channels_ref=(m_dot_c)/(G_c*L_2_c*L_3)""Total number of air channels"

N_channels_ref=7 "N_channels_air=(m_dot_h)/(G_h*L_2_h*L_3)""Total number of R-134a channels"

W_thick=1*convert(mm,m) "Wall thickness between R-134a and air channels"

L_1=85*convert(mm,m) "L_h, Length of heat exchanger in flow direction of Air"

L_2_h=37*convert(mm,m) "W_h=L_c Length of heat exchanger in flow direction of R-134a for Air side"

L_2_c=41*convert(mm,m) "W_c Length of heat exchanger in flow direction of water for R-134a side"

L_3=110*convert(mm,m) "Height of heat exchanger"

"%%%%%--------Compactness Ratios------%%%%%"

F_wid_a=0.35*convert(mm,m) "Width of fin for air side"

F_hei_a=3.75*convert(mm,m) "Height of fin for air side"

F_wid_r=0.35*convert(mm,m) "Width of fin for R-134a side"

F_hei_r=9.75*convert(mm,m) "Height of fin for R-134a side"

Asp_rat_air=0.0933 "Aspect ratio for air channel"

Asp_rat_ref=0.0359 "Aspect ratio for R-134a channel"

"%%%%%%----------Surface Geometrical Properties----------%%%%%%"

"%%%%%%-----------Area calculation for Air side----------%%%%%%"

A_ttl_plt_air=2*L_1*L_2_h*N_channels_air "Total area of plate"

A_fin_bs_air=2*F_thick*F_length_air*N_fins_air*L_2_h*N_channels_air "Fin

A_hdr_air=2*F_hei_air*L_1*N_channels_air "Area of header bars"

A_hdr&plt_air=2*(F_hei_ref+2*W_thick)*(N_channels_air+1)*L_2_h"Area of header bars and plates of R-134a at air core inlet and outlet faces"

A_ttl_pri_air=(A_ttl_plt_air)-(A_fin_bs_air)+(A_hdr&plt_air)+(A_hdr_air)"The total primary surface area on the air side"

"%%%%%--------Three components of the secondary (fins) area of Air side---------%%%%"

A_fin_hei_air=2*(F_hei_air-F_thick)*F_length_air*N_fins_air*L_2_h*N_channels_air "Fin

A_fin_edg_hei_air=2*(F_hei_air-F_thick)*F_thick*L_2_h*N_fins_air*N_channels_air "Fin

A_fin_edg_wid_air=2*F_wid_ref&air*F_thick*L_2_h*N_fins_air*N_channels_air"Fin edge width area"

A_ttl_fin_air=(A_fin_hei_air)+(A_fin_edg_hei_air)+(A_fin_edg_wid_air)"Total secondary area on air side"

A_ttl_airside=A_ttl_pri_air+A_ttl_fin_air "The total surface area on air side"

A_freeflow_air=F_hei_air*L_2_h*N_channels_air-((F_hei_air-F_thick)+F_wid_ref&air)*F_thick*L_2_h*N_fins_air*N_channels_air"Free flow area on air side"

D_hyd_air=(4*A_freeflow_air*L_1)/A_ttl_airside "Hydraulic diameter of air side"

"%%%%%------Area calculation for R-134a side---------%%%%%%%"

A_ttl_plt_ref=2*L_2_c*L_1*(N_channels_air+1) "Total plate area"

A_fin_bs_ref=2*F_thick*F_length_ref*N_fins_ref*L_1*(N_channels_air+1)"Fin base area covering plates"

A_hdr_ref=2*F_hei_ref*L_2_c*N_channels_ref "Area of header bars on the side for R-134a"

A_hdr&plt_ref=2*(F_hei_air+2*W_thick)*N_channels_air*L_1"Area of header bars and plates of air at R-134a core inlet and outlet faces"

A_ttl_pri_ref=(A_ttl_plt_ref)-(A_fin_bs_ref)+(A_hdr&plt_ref)+(A_hdr_ref)"The total primary surface area on the R-134a side"

"%%%-------Three components of the secondary (fins) area of R-134a side----------%%%"

A_fin_hei_ref=2*(F_hei_ref-F_thick)*F_length_ref*N_fins_ref*L_1*N_channels_ref "Fin

A_fin_edg_hei_ref=2*(F_hei_ref-F_thick)*F_thick*N_channels_ref*L_1*N_fins_ref "Fin

A_fin_edg_wid_ref=2*F_wid_ref&air*F_thick*N_channels_ref*N_fins_ref*L_1"Fin edge width area"

A_ttl_fin_ref=(A_fin_hei_ref)+(A_fin_edg_hei_ref)+(A_fin_edg_wid_ref)"The total secondary area on R-134a side"

A_ttl_refside=A_ttl_pri_ref+A_ttl_fin_ref "The total surface area on R-134a side"

A_freeflow_ref=F_hei_ref*L_1*(N_channels_ref)-((F_hei_ref-F_thick)+F_wid_ref&air)*F_thick*N_channels_ref*L_1*N_fins_ref"The free flow area on R-134a side"

D_hyd_ref=(4*A_freeflow_ref*L_2_c)/A_ttl_refside "Hydraulic diameter of R-134a side"

"%%%%%%--------Compactness of heat exchanger---------%%%%%%%"

A_ttl_HEX=A_ttl_airside+A_ttl_refside "Total area of the heat exchanger"

L_HEX=105.1*convert(mm,m) "Total length of heat exchanger"

W_HEX=56.1*convert(mm,m) "Total width of heat exchanger"

H_HEX=109.4*convert(mm,m) "Total height of heat exchanger"

V_ttl_HEX=L_HEX*W_HEX*H_HEX "Total volume of the heat exchanger"

Srf_Dnsty_HEX=A_ttl_HEX/V_ttl_HEX "Surface density of the heat exchanger"

R=287 "Gas constant"

P_atm=91270 [pa] "Pressure at atm level"

rho_ref=P_atm/(R*T_c1) "Density of R-134a"

rho_air=P_atm/(R*T_h1) "Density of air"

m_dot_air=0.012 [kg/s] "Mass flow rate of air"

m_dot_air=rho_air*A_freeflow_air*u_w

u_ref=3.25 [m/s] "Velocity of R-134a at inlet"

m_dot_ref=rho_ref*A_freeflow_ref*u_ref "Mass flow rate of R-134a"

G_air=m_dot_air/(A_freeflow_air) "Mass flux for air side"

G_ref=m_dot_ref/(A_freeflow_ref) "Mass flux for R-134a side"

T_avg_air=(T_h1+T_h2)/2 "Average temperature of air"

mu_air=viscosity(Air_ha,T=T_avg_air,P=P_atm) "Viscosity for Air at avg temperature"

T_avg_ref=(T_c1+T_c2)/2 "Average temperature of R-134a"

mu_ref=viscosity(R-134a,T=T_avg_ref,P=P_atm) "Viscosity for R-134a at avg temperature"

"%%%%%%----------Reynolds Number----------%%%%%%"

Re_air=G_air*D_hyd_air/mu_air "Reynold number for air side"

Re_ref=G_ref*D_hyd_ref/mu_ref "Reynold number for R-134a side"

"%%%------Nusselt Number For fully developed laminar flow in rectangular flow-------%%%"

Nu_air=8.235*(1-1.883*(Asp_rat_air)+3.767*(Asp_rat_air^2)-5.814*(Asp_rat_air^3)+5.361*(Asp_rat_air^4)-2*(Asp_rat_air^5))*(mu_air/mu_w)^(-0.14)"Nusselt

number for air side" "Nusselt no. Correlation from Kays and Crawford for rectangular channel for fully developed flow"

Nu_ref=8.235*(1-1.883*(Asp_rat_ref)+3.767*(Asp_rat_ref^2)-5.814*(Asp_rat_ref^3)+5.361*(Asp_rat_ref^4)-2*(Asp_rat_ref^5) "Nusselt number for R-134a side"

"%%%%----------Convection Heat Transfer Coefficient----------%%%%"

K_air=conductivity(Air_ha,T=T_avg_air,P=P_atm) "Conductivity for air side"

h_air=Nu_air*K_air/D_hyd_air "Heat transfer coefficient for air"

K_ref=conductivity(R-134a,T=T_avg_ref,P=P_atm) "Conductivity for R-134a side"

h_ref=Nu_ref*K_ref/D_hyd_ref "Heat transfer coefficient for R-134a"

"%%%%----------Stanton Number----------%%%%"

St_air=h_air/(G_air*cp_h) "Stanton number for air side"

St_ref=h_ref/(G_ref*cp_c) "Stanton number for R-134a side"

"%%%%----------Colburn Factor----------%%%%"

Pr_air=Prandtl(Air_ha,T=T_avg_air,P=P_atm) "Prandtl number for air"

Pr_ref=Prandtl(R-134a,T=T_avg_ref,P=P_atm) "Prandtl number for R-134a"

j_air=St_air*Pr_air^2/3 "Colburn factor for air"

j_ref=St_ref*Pr_ref^2/3 "Colburn factor for ref"

"%%%%%%----------Fin Efficiency Calculations----------%%%%%%"

"%%%%%---------For Air side----------%%%%%%"

"As the Materials of fin at both sides are Aluminum 3003-O"

K_mtl=193 [W/m*K] "Conductivity of Al material"

m_air=(2*h_air/(K_mtl*F_thick)*(1+(F_thick/F_length_air)))^(1/2)

m_ref=(2*h_ref/(K_mtl*F_thick)*(1+(F_thick/F_length_ref)))^(1/2)

"%%%-------Overall extended surface efficiency adiabatic fin lengths----------%%%%"

l_1air=(F_hei_air/2)-F_thick "Overall extended surface efficiency adiabatic fin lengths for air"

l_1ref=(F_hei_ref/2)-F_thick "Overall extended surface efficiency adiabatic fin lengths for R-134a"

"%%%%%%----------Fin Efficiency----------%%%%%%"

eta_fin_air=(tanh(m_air*l_1air))/(m_air*l_1air) "Fin efficiency for air side"

eta_fin_ref=(tanh(m_ref*l_1ref))/(m_ref*l_1ref) "Fin efficiency for R-134a side"

"%%%%%%----------The Overall Surface Efficiency of Fin----------%%%%%%"

eta_ovr_fin_air=(1-(1-eta_fin_air)*(A_ttl_fin_air/A_ttl_airside)) "Fin overall efficiency for air side"

eta_ovr_fin_ref=(1-(1-eta_fin_ref)*(A_ttl_fin_ref/A_ttl_refside)) "Fin overall efficiency for R-134a side"

"%%%%%%%----------Total Thermal Resistance----------%%%%%%%"

R_t=R_h+R_c+R_w+R_fh_bs+R_fc_bs "Total convection resistance"

R_h=1/(eta_ovr_fin_air*h_air*A_ttl_airside) "Convection resistance of air side"

R_c=1/(eta_ovr_fin_ref*h_ref*A_ttl_refside) "Convection resistance of R-134a side"

A_w=L_1*L_2_c*(2*N_fins_air+2) "Area of wall"

K_wall=167 [W/K-m] "Conductivity of wall"

R_w=W_thick/(K_wall*A_w) "Resistance of wall"

R_f_h=0.00018 "Fouling resistance of air"

R_fh_bs=R_f_h/(eta_ovr_fin_air*A_ttl_airside)

R_f_c=0.00567 "Fouling resistance of R-134a"

R_fc_bs=R_f_c/(eta_ovr_fin_ref*A_ttl_refside)

"%%%%%%%----------Heat Transfer From Air----------%%%%%%%"

T_h1=converttemp(C,K,150) "Inlet temperature of R-134a"

T_h2=converttemp(C,K,90) "Outlet temperature of R-134a"

cp_h=SpecHeat(Air_ha,T=T_avg_air,P=P_atm) "Specific heat value of R-134a"

Q_dot_air=m_dot_air*cp_h*(T_h1-T_h2) "R-134a heat transfer"

"%%%%%%%---------Heat Transfer To R-134a----------%%%%%%%"

T_c1=converttemp(C,K,20) "Inlet temperature of air"

T_c2= converttemp(C,K,95) "Outlet temperature of air"

cp_c=SpecHeat(R-134a,T=T_avg_ref,P=P_atm) "Specific heat value of air"

Q_dot_ref=m_dot_ref*cp_c*(T_c2-T_c1) "Air heat transfer"

"%%%%%%%----------Average Heat Transfer----------%%%%%%%"

Q_avg=(Q_dot_air+Q_dot_ref)/2 "Average heat transfer"

Q_max=m_dot_ref*cp_c*(T_h1-T_c1) "(if C_c<C_h)" "Maximum heat transfer"

dt_1=T_h1-T_c2

dt_2=T_h2-T_c1

DELTA_T_lm=((dt_2)-(dt_1))/(ln(dt_2/dt_1)) "Log mean temperature difference"

UA=Q_avg/(DELTA_T_lm) "Overall heat transfer coefficient"

T_wall=T_avg_ref "Temperature of wall"

mu_w=viscosity(Air_ha,T=T_avg_ref,P=P_atm) "Average viscosity"

P=(T_c2-T_c1)/(T_h1-T_c1) "Temperature effectiveness"

R_heat_capacity=(T_h1-T_h2)/(T_c2-T_c1) "Heat capacity rate ratio"

"%%%%%%%----------Heat Capacity Rates----------%%%%%%%"

C_h=m_dot_air*cp_h "Heat capacity rate of air"

C_c=m_dot_ref*cp_c "Heat capacity rate of R-134a"

C_min=min(C_c,C_h) "Minimum heat capacity rate"

C_max=max(C_c,C_h) "Maximum heat capacity rate"

C.R=C_min/C_max "Capacity rate ratio"

"%%%%%%----------Number Of Transfer Units----------%%%%%%"

NTU=UA/C_min

"%%%%%%----------Effectiveness Of Heat Transfer----------%%%%%%"

E=Q_avg/Q_max

"%%%%%----------Pressure Drop----------%%%%%%%"

f=64/Re_ref "If Re<2300 for laminar case Hagen-Poiseuille equation"

DELTA_P_ref=(f*L_HEX*rho_ref*u_ref^2)/(D_hyd_ref*2) "Pressure drop of R-134a"

DELTA_P_air=(f*L_HEX*rho_air*m_dot_air^2)/(D_hyd_air*2) "Pressure drop of Air"

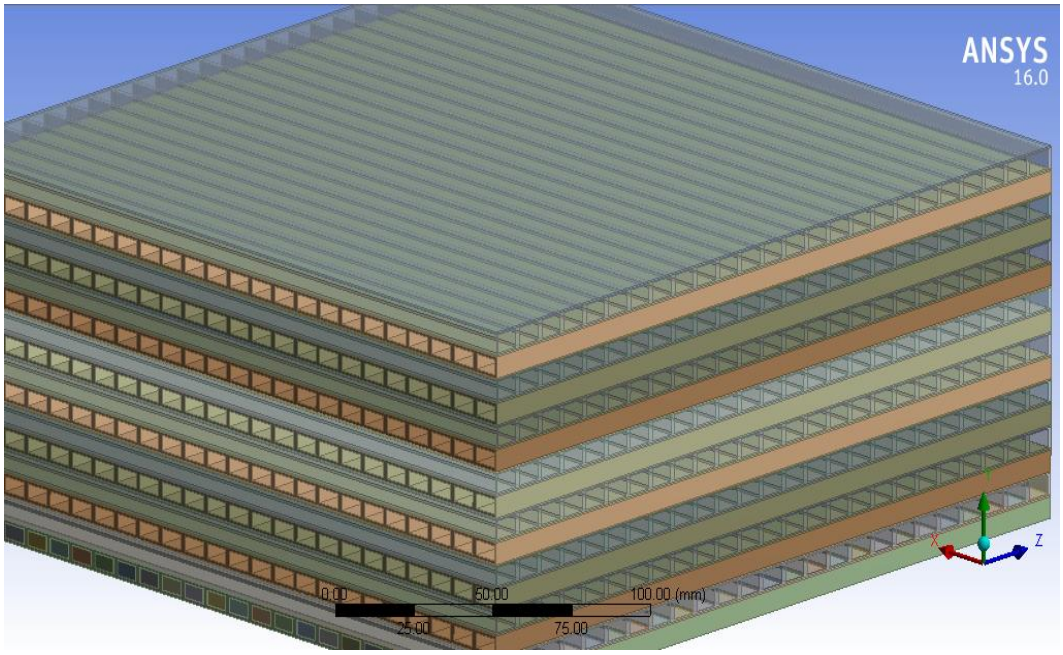

Figure 7.4: Actual diagram drawn on Ansys 16.0 representing rectangular microchannel heat exchanger based on EES code

Table 7.1: Collected data from EES coded for rectangular microchannel geometry

Delta_P	eta_f_h	G_c	G_h	h_c	h_h	NU_c	NU_h	Q_avg	Q_max	Re_c	Re_h	T_c1	T_c2	T_h1	T_h2	UA	E
232	0.9804	3.48	30.04	172.5	185.8	7.716	6.828	627.8	1624	190.3	834.6	297	339	439	392	6.21	0.3735
232.5	0.9803	3.468	30.04	174.1	186.4	7.716	6.828	647.6	1625	188.5	830.9	298	342	442	394	6.609	0.3801
232.3	0.9802	3.445	30.04	176	186.8	7.716	6.831	652.9	1610	185.8	828	300	345	444	396	6.697	0.3841
232.9	0.9802	3.434	30.04	177.2	187.2	7.716	6.831	675	1620	184.4	825.1	301	347	447	397	6.889	0.3918
243	0.9803	3.457	50.06	174.1	221.1	7.716	6.827	885.7	1630	187.9	1384	299	341	442	395	8.69	0.5216
243.5	0.9802	3.422	50.06	176	221.6	7.716	6.83	851.3	1631	184.6	1379	302	343	443	398	8.688	0.5114
243.1	0.9801	3.4	50.06	178.4	222.2	7.716	6.832	903.9	1625	181.8	1373	304	347	447	399	9.272	0.5359
243.5	0.98	3.378	50.06	180.7	223.1	7.716	6.833	928.9	1628	179	1365	306	351	451	402	9.48	0.544
253	0.9803	3.457	70.01	174.8	248	7.716	6.828	1125	1633	187.3	1951	299	343	442	397	11.12	0.6571
253.84	0.9802	3.434	70.33	176.8	248.9	7.716	6.829	1165	1631	184.7	1930	301	346	446	399	11.77	0.6749
253.4	0.98	3.389	70.33	178.8	250.3	7.716	6.827	1165	1635	180.9	1915	305	347	451	403	11.54	0.676
253.1	0.9799	3.345	70.33	182.2	250.6	7.716	6.834	1131	1632	176.2	1909	309	352	452	406	11.49	0.6738
265	0.9802	3.4	89.76	178.4	269.5	7.716	6.834	1378	1652	181.8	2466	304	347	445	399	14.02	0.78
265.1	0.98	3.356	89.76	184.1	270.8	7.716	6.843	1369	1653	175.5	2445	308	358	449	405	14.57	0.8203

Table 7.2: Collected data from EES coded for circular microchannel geometry

Delta_P	eta_f_h	G_c	G_h	h_c	h_h	Q_avg	m_dot_ma	Re_c	Re_h	T_c1	T_c2	T_h1	T_h2	UA	E
195	0.9896	3.48	30.11	67.91	220	641.6	1718	179.3	863.7	297	339	439	392	6.582	0.55
195.78	0.9896	3.468	30.11	68.31	220.4	662.2	1742	177.6	859.9	298	342	442	394	6.758	0.4693
195.35	0.9895	3.445	30.11	68.74	221	667.7	1738	175.1	856.9	300	345	444	396	6.849	0.4693
195.25	0.9895	3.434	30.11	69.02	221.21	690.2	1761	173.8	853.9	301	347	447	397	7.044	0.4765
210.02	0.9877	3.457	50.19	68.25	250	899.5	1724	177	1432	299	341	442	395	9.134	0.6971
210.25	0.9876	3.422	50.19	68.6	250.25	864.8	1691	174	1427	302	343	443	398	8.825	0.7137
210.521	0.9876	3.4	50.19	69.13	250.36	888	1713	171.3	1421	304	347	447	399	9.417	0.6806
210.85	0.9875	3.378	50.19	69.67	251.02	898	1734	168.7	1412	306	351	451	402	9.63	0.6667
223.7	0.9862	3.457	70.5	68.48	274	1135	1727	176.5	2008	299	343	442	397	11.52	0.82
223.5	0.9861	3.434	70.5	68.92	274.56	1180	1748	174	1998	301	346	446	399	11.92	0.742
223.8	0.9861	3.389	70.5	69.22	274	1179	1744	170.5	1982	305	347	451	403	11.68	0.75
223.52	0.986	3.345	70.5	69.89	274.65	1145	1700	166.1	1976	309	352	452	406	11.63	0.756
232.5	0.985	3.4	89.98	69.11	294	1392	1740	171.3	2552	304	347	445	399	14.43	0.95
232.1	0.9849	3.356	89.98	70.45	295.2	1385	1689	165.4	2530	308	358	449	405	14.74	0.953

Table 7.3: Collected data from EES coded for square microchannel geometry

Delta_P	eta_f_h	G_c	G_h	h_c	h_h	NU_c	NU_h	Q_avg	Q_max	Re_c	Re_h	T_c1	T_c2	T_h1	T_h2	UA	E
171	0.9874	3.48	29.24	94.75	164.6	3.549	3.719	566	1475	159.3	859	297	339	439	392	5.71	0.34
171.5	0.9874	3.48	29.24	94.75	164.8	3.549	3.719	566	1478	159.3	868	297	339	439	392	5.806	0.3932
171.9	0.9874	3.48	29.24	94.75	165	3.549	3.719	566	1471	159.3	888	297	339	439	392	5.806	0.3973
171.89	0.9873	3.468	29.24	95.62	165.7	3.549	3.718	582.9	1475	157.8	895	298	342	442	394	5.949	0.4054
190.2	0.9873	3.445	49.78	96.71	212	3.549	3.718	850.9	1483	155.6	1606	300	345	444	396	8.35	0.452
190.1	0.9872	3.434	48.74	97.35	212.05	3.549	3.717	882.7	1485	154.4	1620	301	347	447	397	9.008	0.5326
190.8	0.9873	3.457	48.74	95.62	212.5	3.549	3.717	824.1	1481	157.3	1660	299	341	442	395	8.368	0.5582
190.4	0.9872	3.422	48.74	96.71	212.8	3.549	3.717	791.6	1489	154.6	1690	302	343	443	398	8.078	0.5665
204	0.9872	3.4	69.45	97.99	235	3.549	3.718	1098	1495	152.2	2105	304	347	447	399	10.74	0.59
204.1	0.987	3.378	68.47	99.26	236.5	3.549	3.716	1078	1498	149.9	2125	306	351	451	402	11.6	0.7049
204.6	0.9873	3.457	68.47	96.06	236.4	3.549	3.717	1056	1495	156.8	2168	299	343	442	397	10.72	0.7067
204.9	0.9872	3.434	68.47	97.14	237.05	3.549	3.716	1099	1494	154.6	2198	301	346	446	399	11.1	0.7041
215.3	0.987	3.389	90.2	98.2	254	3.549	3.712	1361	1521	151.5	2601	305	347	451	403	13.35	0.71
215.4	0.9869	3.345	87.39	100.1	254.52	3.549	3.715	1315	1523	147.6	2621	309	352	452	406	13.35	0.8575

Table 7.4: Collected data from EES coded for triangular microchannel geometry

Delta_T	eta_f_h	G_c	G_h	h_c	h_h	NU_c	NU_h	Q_avg	Q_max	Re_c	Re_h	T_c1	T_c2	T_h1	T_h2	UA	E
97.48	0.991	3.48	29.25	71.09	140	3.179	3.179	530	1345	190.2	769.9	297	339	439	392	5.12	0.21
97.48	0.991	3.48	26.98	71.09	140.5	3.179	3.179	527	1346	190.2	769.9	297	339	439	392	5.865	0.4592
97.48	0.991	3.48	26.98	71.09	140.58	3.179	3.179	521	1348	190.2	769.9	297	339	439	392	5.865	0.4592
97.99	0.991	3.468	26.98	71.74	140.65	3.179	3.179	523	1347	188.4	766.5	298	342	442	394	6.01	0.4664
97.49	0.9909	3.445	49.2	72.56	170	3.179	3.179	810	1365	185.8	1273	300	345	444	396	8.021	0.29
97.99	0.9909	3.434	44.96	73.04	170.2	3.179	3.179	811	1335	184.3	1269	301	347	447	397	9.072	0.6963
98.48	0.991	3.457	44.96	71.74	170.5	3.179	3.179	812	1350	187.8	1276	299	341	442	395	8.426	0.664
97.99	0.9909	3.422	44.96	72.56	170.36	3.179	3.179	817	1361	184.5	1272	302	343	443	398	8.135	0.6504
97.48	0.9909	3.4	69.52	73.52	200.52	3.179	3.179	1070	1378	181.7	1788	304	347	447	399	10.25	0.41
97.99	0.9908	3.378	63.16	74.47	200.8	3.179	3.179	1071	1375	178.9	1768	306	351	451	402	11.66	0
98.5	0.9909	3.457	63.16	72.07	200.89	3.179	3.179	1075	1380	187.2	1790	299	343	442	397	10.78	0.8482
99	0.9909	3.434	63.16	72.88	200.98	3.179	3.179	1078	1379	184.6	1781	301	346	446	399	11.16	0.8723
101	0.9908	3.389	89.9	73.68	239	3.179	3.179	1341	1402	180.8	2710	305	347	451	403	12.85	0.54
98.49	0.9908	3.345	80.62	75.1	239.8	3.179	3.179	1351	1405	176.2	2726	309	352	452	406	13.41	0.975